

SHORTER TITLE

FULL LENGTH THESIS TITLE

BY

KYLE O'SHAUGHNESSY,

A THESIS

SUBMITTED TO THE DEPARTMENT OF ELECTRICAL & COMPUTER ENGINEERING

AND THE SCHOOL OF GRADUATE STUDIES

OF MCMASTER UNIVERSITY

IN PARTIAL FULFILMENT OF THE REQUIREMENTS

FOR THE DEGREE OF

MASTER OF APPLIED SCIENCE

© Copyright by Kyle O'Shaughnessy, June 2025

All Rights Reserved

Master of Applied Science (2025)  
(Electrical & Computer Engineering)

McMaster University  
Hamilton, Ontario, Canada

TITLE: Full Length Thesis Title

AUTHOR: Kyle O'Shaughnessy  
Bachelor of Applied Science (Queen's University)

SUPERVISOR: Ian C. Bruce, PhD

NUMBER OF PAGES: xxv, 164

*Dedication*

# **Lay Abstract**

# **Abstract**

# Acknowledgements

# Notation and abbreviations

**Notation1** Definition

**Notation2** Definition

# Contents

<b>Lay Abstract</b>	<b>iv</b>
<b>Abstract</b>	<b>v</b>
<b>Acknowledgements</b>	<b>vi</b>
<b>Notation and abbreviations</b>	<b>vii</b>
<b>1 Introduction and Background</b>	<b>1</b>
1.1 Acoustics of Reverberation . . . . .	1
1.1.1 Sound . . . . .	1
1.1.2 Room Acoustics . . . . .	5
1.1.3 Early and Late Reflections . . . . .	7
1.1.4 Numerical Properties of Room Impulse Reponses . . . . .	10
1.2 The Auditory System . . . . .	11
1.2.1 The Outer and Middle Ear . . . . .	11
1.2.2 The Inner Ear . . . . .	12
1.2.3 Tuning, Non-Linearities and Active Amplification in the Cochlea	14
1.2.4 Sound Localization . . . . .	16

1.3	Hearing Loss . . . . .	19
1.3.1	Overview of Hearing Loss . . . . .	19
1.3.2	Perceptual Impacts of Sensorineural Hearing Loss . . . . .	21
1.4	Speech Production . . . . .	22
1.4.1	Anatomy of Speech Production . . . . .	22
1.4.2	Classification of Speech Sounds . . . . .	24
1.4.3	Discrete-Time Speech Production Model . . . . .	25
1.5	Linear Prediction . . . . .	28
1.5.1	Signal Prediction Perspective . . . . .	29
1.5.2	System Identification / Inverse Filtering Perspective . . . . .	31
1.5.2.1	Autocorrelation Method . . . . .	34
1.5.2.2	Covariance Method . . . . .	38
1.5.3	Spectral Estimation / Spectral Whitening Perspective . . . . .	41
1.6	Speech Perception in Adverse Conditions . . . . .	42
1.6.1	Characterizing Speech Perception . . . . .	42
1.6.2	Impact of Reverberation on Speech Cues . . . . .	44
1.6.3	Impact of Reverberation on Speech Intelligibility and Listening Effort . . . . .	45
1.6.4	Impact of Reverberation on Spatial Cues . . . . .	47
1.6.5	Perceptual Adaptation to Reverberation and Noise . . . . .	47
1.6.5.1	The Precedence Effect . . . . .	47
1.6.5.2	Spatial Release From Masking . . . . .	50
1.7	Hearing Aids . . . . .	51
1.8	Metrics of Speech Perception . . . . .	52

1.8.1	Objective Predictors of Speech Intelligibility . . . . .	53
1.8.1.1	Neurologically-Motivated Objective Predictors of Speech Intelligibility . . . . .	57
1.8.2	Objective Predictors of Listening Effort . . . . .	60
1.8.3	Objective Predictors of Speech Quality . . . . .	61
1.9	Summary and Motivation . . . . .	61
<b>2</b>	<b>De-Reverberation Literature Review</b>	<b>62</b>
2.1	Reverberation Suppression . . . . .	63
2.1.1	Beamforming . . . . .	63
2.1.2	Linear Prediction Residual Enhancement . . . . .	63
2.1.3	Statistical Methods . . . . .	63
2.2	Reverberation Cancellation . . . . .	63
2.2.1	Invertibility of Room Impulse Response . . . . .	63
2.2.2	Single Channel Room Response Equalization . . . . .	67
2.2.2.1	Homomorphic Approaches to Room Response Equal- ization . . . . .	67
2.2.2.2	Linear Prediction Approaches to Room Response Equal- ization . . . . .	69
2.2.2.3	Frequency Domain Approaches to Room Response Equal- ization . . . . .	70
2.2.2.4	Least Squares Optimization Approaches to Room Re- sponse Equalization . . . . .	71
2.2.3	Multiple Input-Output Inverse Theorem (MINT) . . . . .	73
2.2.4	Blind Deconvolution Problem . . . . .	78

2.2.4.1	The Wiener Filter (Supervised Optimal Filtering) . . . . .	79
2.2.4.2	Supervised Adaptive Filtering . . . . .	82
2.2.4.3	Blind Deconvolution . . . . .	85
2.2.4.4	Practical Blind Deconvolution in Wireless Systems . . . . .	87
2.2.5	HOS Methods for Blind Deconvolution . . . . .	88
2.2.6	SOS Methods for Blind Deconvolution . . . . .	88
2.2.6.1	Subspace Methods . . . . .	88
2.2.6.2	MC-LPC-based approaches . . . . .	88
2.2.6.3	STFT Spectrum Estimation (Furuya 2007) . . . . .	88
2.2.6.4	Estimation Theory Approaches (BSI using estimation theory)— . . . . .	88
2.2.7	Adaptive Implementations . . . . .	88
2.2.8	Subband Implementations . . . . .	88
<b>3</b>	<b>Delay and Predict Dereverberation Parameters</b>	<b>89</b>
3.1	Multi-channel Linear Prediction Order . . . . .	89
3.2	Source Whitening Linear Prediction Order . . . . .	94
3.3	Blind Deconvolution Performance . . . . .	97
3.4	Source Properties . . . . .	98
3.4.1	Source Data Length . . . . .	98
3.4.2	Source Spectrum . . . . .	100
3.5	Time Alignment of RIRs and Linear Combiner . . . . .	103
3.6	Algorithmic Complexity Analysis . . . . .	105
3.7	Conclusions . . . . .	106
3.8	Appendices . . . . .	106

3.8.1	MC-LP Order . . . . .	106
3.8.2	Source Whitening Order . . . . .	108
3.8.3	Source Properties: Data Length . . . . .	111
3.8.4	Source Properties: Spectrum . . . . .	115
<b>4</b>	<b>Methods and Results</b>	<b>120</b>
4.1	Evaluation of Proposed Speech Intelligibility Prediction Method for Reverberation . . . . .	120
4.1.1	Proposed Method . . . . .	120
4.1.2	Analysis of RIR Databases . . . . .	122
4.1.3	Evaluation of Equalization-Cancellation Front-End . . . . .	124
4.1.4	Hearing Aid Gain Comparison . . . . .	131
4.1.5	Evaluation of Monaural Speech Intelligibility Metrics In Context of Reverberation . . . . .	134
4.2	Final Method Used . . . . .	140
4.3	Delay-and-Predict Dereverberation Evaluation with Synthetic Reverberation . . . . .	140
4.4	Delay-and-Predict Dereverberation Evaluation with Realistic Reverberation . . . . .	143
4.5	Impact of Noise on Performance . . . . .	145
4.6	Impact of an Interfering Talker on Performance . . . . .	151
<b>5</b>	<b>Conclusions and Future Work</b>	<b>153</b>

# List of Figures

2.1	Block diagram for supervised optimal filtering, which attempts to produce a desired output, $d(n)$ , from a known input, $x(n)$ . . . . .	79
2.2	Block diagram for supervised inverse filtering / equalization, which attempts to produce reproduce the known input, $s(n)$ , to an unknown system $G(z)$ , from the measured system output, $m(n)$ , using a filter, $H(z)$ . . . . .	80
2.3	Block diagram for supervised blind deconvolution, which attempts to produce reproduce the unknown input, $s(n)$ , to an unknown system $G(z)$ , from the measured system output, $m(n)$ , including additive noise $v(n)$ , using a filter, $H(z)$ . . . . .	85
3.1	MINT equalizer performance for various equalizer orders relative to the actual length of the FIR channel (L) and the number of samples corresponding to the T60 of the channel ( $N60 = T60 * \text{sample rate}$ )	90
3.2	Source whitening results using a $p1 = 4000$ order linear predictor. The prediction error filter coefficients were computed based on clean speech and the same filter was used in all tests in this section to assess the multichannel prediction stage of the delay-and-predict algorithm in isolation. . . . .	91

3.3	Delay-and-Predict dereverberation performance with multichannel linear prediction order $p2 = L / (M-1)$ , where L is the FIR RIR length and M is the number of channels. Figure 3.2 shows the common source whitening filter used. . . . .	92
3.4	Delay-and-Predict dereverberation performance with various multichannel linear prediction orders ( $p2$ ) relative to the actual length of the FIR channel (L) and the number of samples corresponding to the T60 of the channel ( $N60$ ). Figure 3.2 shows the common source whitening filter used. . . . .	93
3.5	Delay-and-Predict dereverberation performance with source whitening prediction order $p1 = 200$ and multichannel linear prediction order $p2 = N60 / (M-1)$ . . . . .	95
3.6	Delay-and-Predict dereverberation performance with various source whitening prediction orders ( $p1$ ) relative to the multichannel linear prediction order $p2 = N60 / (M-1)$ . . . . .	96
3.7	MINT Equalizer performance (EDC and Spectrogram) . . . . .	97
3.8	Delay-and-Predict Equalizer performance (EDC and Spectrogram) with the source-whitening filter computed using clean speech (i.e., not blind)	97
3.9	Delay-and-Predict Equalizer performance (EDC and Spectrogram) with the source-whitening filter computed using reverberant speech (i.e., blind)	98

3.10 Delay-and-Predict dereverberation performance with the same speech sample (SA1.WAV, 58061 samples) looped to various data lengths to preserve the same spectrum. Source whitening prediction order was $p1 = 2 * p2 * (M-1)$ and multichannel linear prediction order was $p2 = N60 / (M-1)$ . Source Whitening stage was performed on reverberant speech (i.e., blind). . . . .	99
3.11 Delay-and-Predict dereverberation performance with the source signal generated by looping various length white noise sequences looped the same data length (i.e., same data length, different spectra). Source whitening prediction order was $p1 = 2 * p2 * (M-1)$ and multichannel linear prediction order was $p2 = N60 / (M-1)$ . Source Whitening stage was performed on reverberant speech (i.e., blind). . . . .	101
3.12 Delay-and-Predict dereverberation performance with the source signal generated by filtering 60 msec of speech with filters of various peakiness. Source whitening prediction order was $p1 = 2 * p2 * (M-1)$ and multichannel linear prediction order was $p2 = N60 / (M-1)$ . Source Whitening stage was performed on reverberant speech (i.e., blind). . .	102
3.13 Showing the impact of RIR time alignment on multichannel linear prediction performance. The RIRs (left column) were synthetically generated exponentially decaying gaussians and an incremental delay of 2 samples was added to each channel. The right column shows the result of each individual prediction error filter (i.e., the top-most one is the result of predicting the current sample of microphone 1 from the past samples of microphones 1-4) . . . . .	103

3.14 Delay-and-Predict dereverberation performance an incremental 2 sample delay added to each channel. . . . .	104
3.15 Repeating with no time delay . . . . .	104
3.16 Delay-and-Predict dereverberation performance for perfectly time-aligned RIRs . . . . .	105
3.17 Analysis of the computational complexities of Least Squares solution and Inverse filter implementations as a function of T60, For M=4 microphones, $p2 = N60/(M-1)$ and $p1 = 1.25*p2*(M-1)$ . Complexity of LMS Solution also shown for comparison. . . . .	105
3.18 Analysis of the algorithmic memory requirements of Least Squares solution (could be temporary memory) and Inverse filter implementations (persistent memory) as a function of T60, For M=4 microphones, $p2 = N60/(M-1)$ and $p1 = 1.25*p2*(M-1)$ . Memory requirements of LMS Solution also shown for comparison. . . . .	106
3.19 Delay-and-Predict dereverberation performance with multichannel linear prediction order $p2 = N60 / (M-1)$ , where N60 is the number of samples corresponding to the T60 and M is the number of channels (i.e., the MINT condition based on T60 rather than the FIR RIR length). Figure 3.2 shows the common source whitening filter used. . . . .	107

3.20 Delay-and-Predict dereverberation performance with multichannel linear prediction order $p2 = 0.75 * N60 / (M-1)$ , where $N60$ is the number of samples corresponding to the $T60$ and $M$ is the number of channels (i.e., suboptimal with respect to the MINT condition based on $T60$ rather than the FIR RIR length). Figure 3.2 shows the common source whitening filter used. . . . .	107
3.21 Delay-and-Predict dereverberation performance with multichannel linear prediction order $p2 = 0.5 * N60 / (M-1)$ , where $N60$ is the number of samples corresponding to the $T60$ and $M$ is the number of channels (i.e., More suboptimal with respect to the MINT condition based on $T60$ rather than the FIR RIR length). Figure 3.2 shows the common source whitening filter used. . . . .	108
3.22 Delay-and-Predict dereverberation performance with source whitening prediction order $p1 = 1000$ and multichannel linear prediction order $p2 = N60 / (M-1)$ . . . . .	109
3.23 Delay-and-Predict dereverberation performance with source whitening prediction order $p1 = p2 * (M-1)$ and multichannel linear prediction order $p2 = N60 / (M-1)$ . I.e., The source whitening filter order is the same as the effective MINT filter order. . . . .	110
3.24 Delay-and-Predict dereverberation performance with source whitening prediction order $p1 = 2 * p2 * (M-1)$ and multichannel linear prediction order $p2 = N60 / (M-1)$ . I.e., The source whitening filter order is twice the effective MINT filter order. . . . .	111

3.25 Delay-and-Predict dereverberation performance for a 3.6 second speech source (58061 samples). Source whitening prediction order was $p1 = 2 * p2 * (M-1)$ and multichannel linear prediction order was $p2 = N60 / (M-1)$ . Source whitening filter was estimated using clean speech. . .	112
3.26 Delay-and-Predict dereverberation performance for a 3.6 second speech source (58061 samples). Source whitening prediction order was $p1 = 2 * p2 * (M-1)$ and multichannel linear prediction order was $p2 = N60 / (M-1)$ . Source whitening filter was estimated using reverberant speech (blind estimation). . . . .	113
3.27 Delay-and-Predict dereverberation performance for a 10.9 second speech source (174183 samples). The source was generated by looping the same 3.6 secound source 3 times to maintain the same spectrum. Source whitening prediction order was $p1 = 2 * p2 * (M-1)$ and multichannel linear prediction order was $p2 = N60 / (M-1)$ . Source whitening filter was estimated using clean speech. . . . .	114
3.28 Delay-and-Predict dereverberation performance for a 10.9 second speech source (174183 samples). The source was generated by looping the same 3.6 secound source 3 times to maintain the same spectrum. Source whitening prediction order was $p1 = 2 * p2 * (M-1)$ and multichannel linear prediction order was $p2 = N60 / (M-1)$ . Source whitening filter was estimated using revererant speech (blind estimation). . . . .	115

3.29 Delay-and-Predict dereverberation performance with source being 1 second of white noise looped to 60 sec. Source whitening prediction order was $p1 = 2 * p2 * (M-1)$ and multichannel linear prediction order was $p2 = N60 / (M-1)$ . Source whitening filter was estimated using clean speech. . . . .	116
3.30 Delay-and-Predict dereverberation performance with source being 1 second of white noise looped to 60 sec. Source whitening prediction order was $p1 = 2 * p2 * (M-1)$ and multichannel linear prediction order was $p2 = N60 / (M-1)$ . Source whitening filter was estimated using revererant speech (blind estimation). . . . .	117
3.31 Delay-and-Predict dereverberation performance with source being 10 second of white noise looped to 60 sec (i.e., source is less peaky than the previous case). Source whitening prediction order was $p1 = 2 * p2 * (M-1)$ and multichannel linear prediction order was $p2 = N60 / (M-1)$ . Source whitening filter was estimated using clean speech. . . .	118
3.32 Delay-and-Predict dereverberation performance with source being 10 second of white noise looped to 60 sec (i.e., source is less peaky than the previous case). Source whitening prediction order was $p1 = 2 * p2 * (M-1)$ and multichannel linear prediction order was $p2 = N60 / (M-1)$ . Source whitening filter was estimated using revererant speech (blind estimation). . . . .	119
4.1 HRIR database office II room . . . . .	122
4.2 HRIR database courtyard room . . . . .	122
4.3 HRIR database cafeteria room . . . . .	123

4.4	MYRiAD database SAL room . . . . .	124
4.5	Impact of EC algorithm on speech intelligibility (using HASPI) as a function of noise direction, anechoic directional speech and noise . . .	125
4.6	Impact of EC algorithm on speech intelligibility (using HASPI) as a function of SNR, for anechoic directional speech and various noise types (anechoic directional, reverberant, spatial recording, diffuse) . . . . .	126
4.7	Impact of EC algorithm on speech intelligibility (using HASPI) as a function of SNR, for reverberant speech and various noise types (anechoic directional, reverberant, spatial recording, diffuse) . . . . .	127
4.8	Impact of EC algorithm on speech intelligibility (using HASPI) as a function of SNR, for diffuse speech and various noise types (anechoic directional, reverberant, spatial recording, diffuse) . . . . .	128
4.9	Impact of EC algorithm on speech intelligibility (using HASPI) as a function of varying amounts of synthetic reverb, for spatial noise recording with $\text{SNR} = -12 \text{ dB}$ and $\text{SNR} = 0 \text{ dB}$ . . . . .	129
4.10	Impact of EC algorithm on speech intelligibility (using HASPI) as a function of varying amounts of synthetic reverb, for spatial noise recording with $\text{SNR} = -12 \text{ dB}$ . . . . .	130
4.11	Impact of EC algorithm on speech intelligibility (using HASPI) as a function of varying amounts of synthetic reverb, noise-free . . . . .	131
4.12	Hearing aid gains to be used in evaluation . . . . .	132

4.13 Comparison of perceptual benefit of four different linear hearing aid gains in the presence of reverb. Moderate high frequency hearing loss used in the perceptual models (IEC 60118-15 Moderate HL, Moderately Sloping Group), and RIRs were generated synthetically . . . . .	133
4.14 Impact of synthetic reverberation (exponentially decaying gaussian RIRs) on SI predictors with and without hearing loss. NAL-R linear hearing aid amplification included in hearing loss case for metrics that including modeling of hearing loss . . . . .	134
4.15 Impact of synthetic reverberation (exponentially decaying gaussian RIRs) with added real early reflections generated by truncating a real RIR (Office II RIR from the HRIR database) on SI predictors with and without hearing loss. NAL-R linear hearing aid amplification included in hearing loss case for metrics that including modeling of hearing loss	135
4.16 Impact of practical reverberation (several real measured RIRs) on SI predictors with and without hearing loss. NAL-R linear hearing aid amplification included in hearing loss case for metrics that including modeling of hearing loss . . . . .	135
4.17 TODO: REPLOT THIS WITH SAME X-AXIS USED IN ALL PLOTS FOR EDC. Example of how SAL was truncated by applying additional exponential decay as a window to manipulate T60 synthetically . . .	136
4.18 Impact of practical reverberation (SAL room from MYRiAD database exponentially truncated to control T60) on SI predictors with and without hearing loss. NAL-R linear hearing aid amplification included in hearing loss case for metrics that including modeling of hearing loss .	136

4.19 Example of how early reflections of SAL RIR were reduced in magnitude (by 6 dB) to make reverberation effect stronger . . . . .	137
4.20 Impact of reducing early reflections of SAL RIR (i.e., Figure 4.19). SI shown before RIR processing (left) and after RIR processing (right) for comparison . . . . .	137
4.21 Impact of synthetic reverberation (exponentially decaying gaussian RIRs) on SI predictors with and without hearing loss. NAL-R linear hearing aid amplification included in hearing loss case for metrics that including modeling of hearing loss. Scaling applied to NSIM and STMI values to better view all metrics on the same plot. . . . .	138
4.22 Impact of synthetic reverberation (exponentially decaying gaussian RIRs) with added real early reflections generated by truncating a real RIR (Office II RIR from the HRIR database) on SI predictors with and without hearing loss. NAL-R linear hearing aid amplification included in hearing loss case for metrics that including modeling of hearing loss. Scaling applied to NSIM and STMI values to better view all metrics on the same plot. . . . .	139
4.23 Impact of practical reverberation (several real measured RIRs) on SI predictors with and without hearing loss. NAL-R linear hearing aid amplification included in hearing loss case for metrics that including modeling of hearing loss. Scaling applied to NSIM and STMI values to better view all metrics on the same plot. . . . .	139

4.24 Impact of practical reverberation (SAL room from MYRiAD database exponentially truncated to control T60) on SI predictors with and without hearing loss. NAL-R linear hearing aid amplification included in hearing loss case for metrics that including modeling of hearing loss. Scaling applied to NSIM and STMI values to better view all metrics on the same plot. . . . .	140
4.25 Block diagram for method used in evaluating dereverberation algorithm performance. Microphone signals include reverberant speech (MYRiAD SAL RIR windowed exponentially to control T60) with added noise signal (real multichannel noise recordings) and added reverberant interference signal. All SI and SQ predictors were computed for the unprocessed microphone signals and the dereverberation output both with and without hearing loss included in all models of speech perception. . . . .	141
4.26 Evaluation of delay-and-predict dereverberation performance as a function of T60. RIRs were synthetically generated by applying a variable decay-rate exponential window to sequences of uncorrelated Gaussian white noise. . . . .	142
4.27 Evaluation of delay-and-predict dereverberation performance as a function of T60. RIRs were generated by applying a variable decay-rate exponential window to a measured RIR (The SAL room from the MYRiAD database, T60 = 2.2 sec) to control T60. . . . .	144

4.28 Evaluation of delay-and-predict dereverberation performance in the presence of noise as a function of T60. RIRs were generated by applying a variable decay-rate exponential window to a measured RIR (The SAL room from the MYRiAD database, T60 = 2.2 sec) to control T60. Noise was a multichannel recording of approximately stationary noise (Office ventilation noise from the HRIR database), and SNR was set to 12 dB. . . . .	146
4.29 Evaluation of delay-and-predict dereverberation performance in the presence of noise as a function of SNR. RIRs were generated by applying a variable decay-rate exponential window to a measured RIR (The SAL room from the MYRiAD database, T60 = 2.2 sec) to set T60 = 1 second. Noise was a multichannel recording of approximately stationary noise (Office ventilation noise from the HRIR database). . .	148
4.30 Evaluation of delay-and-predict dereverberation performance in the presence of noise as a function of SNR. RIRs were generated by applying a variable decay-rate exponential window to a measured RIR (The SAL room from the MYRiAD database, T60 = 2.2 sec) to set T60 = 1 second. Noise was a multichannel recording of non-stationary noise (Cafeteria babble noise from the HRIR database). . . . .	150

4.31 Evaluation of delay-and-predict dereverberation performance in the presence of an interfering talker, as a function of T60. RIRs were generated by applying a variable decay-rate exponential window to a measured RIR (The SAL room from the MYRiAD database,  $T60 = 2.2$  sec) to control  $T60$ . Similarly, a measured RIR from a different location in the room was exponentially windowed and used for the interfering talker. The primary-to-interfering talker ratio, i.e., signal-to-interference ratio, was set to SIR = 12 dB. . . . . . . . . . . . . . . . . . 152

# Chapter 1

## Introduction and Background

### 1.1 Acoustics of Reverberation

This overview of acoustics was based on Beranek and Mellow (2012) and Kuttruff (2016).

#### 1.1.1 Sound

Earths atmosphere is full of air particles of varying densities depending on altitude. Random motion of air particles gives rise to a static air pressure (i.e., atmospheric pressure,  $p_0 = 101.3 \text{ kPa}$  at  $15^\circ\text{C}$  at sea level). When air is moved by a surface such as the diaphragm of a loudspeaker, this compresses or rarefacts air generating a pressure differential which is termed sound pressure. The total air pressure ( $p_{\text{total}}$ ) is thus made up of static pressure ( $p_0$ ) and sound pressure ( $p$ ):

$$p_{\text{total}} = p_0 + p$$

This change to air pressure is also accompanied by a displacement of particles and a corresponding particle velocity ( $\mathbf{u}$  [m/s]). Due to the flow of particles from regions of high pressure to regions of low pressure, sound pressure propagates through air at a speed that depends on the elasticity of air ( $c = 343 \text{ m/s}$  on earth at  $20^\circ\text{C}$ ). When air is compressed and rarefacted in a periodic manner, this gives rise to a periodic sound pressure wave that oscillates in time and space. As shown in (Figure), the resulting pressure wave oscillates relative to the ambient pressure, is accompanied by a synchronized particle velocity wave, and a particle displacement wave which is delayed by a quarter wavelength.

(figure: Pressure, Velocity and displacement)

As a result, sound source such as a loudspeaker or human speech production system vibrates air particles generating a sound pressure wave which propagates through air and vibrates other surfaces such as a microphone diaphragm or a human ear drum.

Sound Intensity is calculated as the sound pressure and particle velocity,  $\mathbf{I} = p\mathbf{u}$  [ $\text{W/m}^2$ ]), and represents the power carried by a sound pressure wave per unit area. More commonly, sound magnitude is described in terms of its sound pressure level ( $L_p$ , i.e., SPL), which is a logarithmic metric of the effective RMS sound pressure relative to the ambient air pressure.

$$L_p = 20 \log_{10} \left( \frac{p_{\text{rms}}}{p_0} \right) \text{ [dBSPL]}$$

As will be discussed in more detail later, the human auditory system does not perceive all frequencies equally. This phenomenon is often described using equal loudness contours (figure), where each contour represents the levels across frequency which would be perceived by the average human listeners as having the same loudness.

To account for this, loudness is often modeled using frequency weighting function that approximates equal loudness contours, such as A-weighting or dBA.

(figure equal loudness contours)

The ideal sound source is often modeled as a point source that vibrates radially outward, i.e., a monopole, generating a spherical sound wave that propagates outward in all directions symmetrically. Although a monopole is a theoretical construct which would not be found in nature, it has proven to be a useful building block in modeling more realistic sound sources. The sound intensity of a spherical wavefront spreads out geometrically over a larger surface area, decreasing in magnitude as it propagates. In the far field (i.e., a distance greater than several wavelengths) the wavefront is highly symmetrical and becomes approximately planar. This results in the so-called inverse square law whereby the sound intensity is proportional to the inverse of the square of the radius from the source in free space (i.e., an anechoic environment, without reflections). More intuitively, for each doubling of distance, sound intensity decreases by 12 dB, and equivalently the sound pressure decreases by 6 dB. In the near field, complex particle interactions result in propagation and circulation of air, and sound intensity cannot be modeled as a simple function of distance.

More practical sound sources such as loudspeakers can be modeled by integration point sources over the surface of the sound producing object. Typically practical sound sources have some degree of directivity which focuses propagation towards a particular direction and reduces propagation loss to other directions. Additionally air absorption due to particle interactions and refraction resulting from wind and temperature gradients provide additional losses in free space. Air absorption tends to affect high frequencies more than low frequencies resulting in loss of high frequencies

at far distances. Mathematically, in free space the sound pressure level ( $L_p$ ) at a distance  $r$  can be modeled as

$$L_p = L_w - 10 \log_{10}(4\pi) - 20 \log_{10}(r) + 10 \log_{10}(Q) - A_E$$

Where  $L_w$  is the source power,  $Q$  is the directivity of the sound source (e.g.,  $Q = 1$  implies omnidirectional), and  $A_E$  represents additional attenuation due to air absorption, wind and temperature gradients.

Different fluid media have different resistances to propagation of sound due to density and compressibility. This is termed acoustic impedance and is mathematically defined as the ratio of effective sound pressure to effective volume velocity of air particles.

$$Z_A = \frac{\tilde{P}}{\tilde{U}}$$

Where  $\tilde{P}$  is the phasor representation of sound pressure, and  $\tilde{U}$  is the phasor representation of volume velocity. The phase between sound pressure and volume velocity, as well as the frequency dependency of acoustic impedance is represented through it's complex representation.

When a sound pressure wave reaches a boundary between two media with different acoustic impedances (i.e., an impedance mismatch), some of the energy is transmitted through the boundary, some is absorbed by the boundary and some is reflected backwards. The proportion of energy transmitted, absorbed and reflected is defined by the reflection and transmission coefficients which are a result of the impedance mismatch. In the extreme case where impedance mismatches are very high, this can

produce an acoustic shadow behind the object or boundary.

When sound passes through a boundary at a non-normal angle, its direction is changed (i.e., refraction) by an amount defined by the angle of incidence and the impedance mismatch across the boundary. Additionally, when sound passes around an object or through an opening in an object, its direction bends around the object (i.e., defraction).

### 1.1.2 Room Acoustics

When sound is produced in a practical room, it interacts with many physical surfaces such as walls, ceilings, floor and objects, resulting in a wide array of reflections and defraction/refraction effects. Surfaces that are smooth and large relative to the wavelength cause the effective plane wave front to be reflected off in an individual direction (i.e., specular reflection). When surfaces are smaller or highly uneven, sound is reflected in many directions (i.e., scattering) resulting in a spreading of energy (i.e., diffuse reflection). Curved surfaces cause sound to be focused for concave curves, or dispersed for convex curves. When reflections are sparse, they are perceived as distinct echoes, while dense concentrations of reflections are perceived as persistence of the direct sound (i.e., reverberation).

Reflected sound results in a series of wavefronts reaching the listener with different amplitudes and phases, which can be modeled as a sequence of impulses called the room impulse response (RIR). Similarly, the transfer function corresponding to the RIR (i.e., its Z-Transform) is referred to as the room transfer function (RTF). Like any impulse response, the RIR can be convolved with a theoretical source signal to compute the (noise-free) soundfield that would be perceived at the listener. The

sound that arrives at the listener via line-of-sight is called the direct sound, which is typically the first impulse in the RIR.

Symmetric acoustic spaces such as rectangular rooms tend to produce consistent reflection patterns which results in concentration of reflections from particular directions and patterns of constructive and destructive interference throughout the room (i.e., room modes). Irregular room shapes, and the presence of objects in the space result in more scattering of waves, resulting in a sound field that is more symmetric in the dispersion of energy (i.e., more diffuse). In the extreme case, a diffuse sound field is generated whereby the direct sound is the same level as the reflections, sound appears to arrive from all directions equally, sound pressure is distributed evenly throughout the room, and phase relationships between waves can be considered uncorrelated.

Reflection is not uniform over frequency, so reflected sound waves have different spectrum from their corresponding incident waves. Common surfaces such as walls and fabric tend to have a lowpass response. This effect is particularly pronounced in the presence of multiple reflections, giving typical room frequency responses some roll-off at high frequencies. Room frequency response can be divided into three primary regions: a low frequency "mode-dominated" region, a mid frequency "transition" region, and a high frequency "diffuse field dominated" region. At low frequencies, where wavelengths are similar to room dimensions, standing waves give rise to strong room modes (i.e., room resonances), which results in a frequency response with a smoother pattern of spectral peaks and notches. As frequency increases through the transition zone, these spectral peaks and notches become more dense. Above a frequency threshold called the Shroeder Frequency (Schroeder and Kuttruff, 1962), the reverberant sound field is highly diffuse and the frequency response becomes highly

irregular. At frequencies below the transition zone, room modes are predictable, therefore most acoustic measures of reverberation (e.g., RT60 described in the next section) generally only apply above the low frequency modal region. These frequency response effects can be seen in (figure).

### 1.1.3 Early and Late Reflections

RIRs are often divided conceptually into three temporal sections: direct sound, early reflections and late reflections (Figure). The direct sound is an acoustically attenuated version of the transmitted sound, delayed by the time of flight between the sound source and the listening location. Early reflections are generally considered to be the reflections which arrive within 50 - 100 ms of the direct sound, and late reflections represent the rest of the reflections that follow. Early reflections are generally not perceived as distinct reflections, instead being integrated with the direct sound by perceptual adaptations which will be discussed later. This results in a perceptual SNR boost of up to approximately 9 dB, which aids in speech perception. Conversely, late reflections are perceived as distinct sounds and collectively create a dense decaying sound “tail” after the perceived direct and early sound. This produces the characteristic decaying sustained sound of reverberation (i.e., the reverberant tail), which has a negative impact on speech perception. As such, in the design of an acoustic space for speech perception, the goal is not to minimize reverberation, but rather it is often to minimize late reflections and maximize early reflections. It should be noted however, that for in certain acoustic spaces (e.g., music performance halls), some late reflections are also subjectively preferable.

(Figure showing direct sound ER and LR and ITDG, and Frequency response

showing Frequency zones)

In simple room geometries and diffuse field conditions, late reflection sound pressure decays exponentially. Early reflections primarily consist of the first reflections off the walls, floor and ceiling of the room. These reflections off a small number of large discrete surfaces result in highly non-diffuse field making the RIR sporadic and non-exponential. Since late reflections involve many wavefronts produced by repeated reflections around the room, they are much more dense and diffuse in nature. The initial time delay gap (ITDG) between the direct sound and the first early reflection, as well as the duration of these first reflections increases with room size. Although early reflections are not perceptually distinct, they still provide a perceptual sense of room size.

The perceptual distinction between early and late reflections has led to a number of useful metrics which describe amount of reverberation in terms of their relative energies. The direct-to-reverberant ratio (DRR) which is the ratio of direct sound to all reverberant energy expressed in dB, i.e.,

$$DRR = 10 \log_{10} \left( \frac{\int_{t_d-t_0}^{t_d+t_0} h^2(t) dt}{\int_{t_d+t_0}^{\infty} h^2(t) dt} \right) \text{ dB}$$

Where  $h(t)$  is the RIR,  $t_d$  is the time of the direct sound, and  $t_0$  represents a small window around the direct sound. Typically  $t_0$  is approximately 1.0 to 2.5 ms, not the early reflection window. A more perceptually relevant metric is clarity ( $C_{t_e}$ , commonly  $C50$ ) which is the ratio of direct and early energy to late energy expressed in dB, i.e.,

$$C_{t_e} = 10 \log_{10} \left( \frac{\int_{t_d}^{t_d+t_e} h^2(t) dt}{\int_{t_d+t_e}^{\infty} h^2(t) dt} \right) \text{ dB}$$

Where  $t_d$  is the time of the direct sound, and  $t_e$  is the duration after the direct sound defined as early reflections (i.e., around 50 ms for speech). Another related metric is definition ( $D_{t_e}$ , commonly  $D50$ ) which is the ratio of direct and early energy to total RIR energy, i.e.,

$$D_{t_e} = 10 \log_{10} \left( \frac{\int_{t_d}^{t_d+t_e} h^2(t) dt}{\int_0^\infty h^2(t) dt} \right) \text{ dB}$$

Another common way of analyzing reverberation is using the energy decay curve (EDC), which is a metric of the amount of energy remaining in the RIR  $h(n)$  at time  $t$ .

$$\text{EDC}(t) = \int_t^\infty h^2(\tau) d\tau$$

(figure EDC example)

Note in (figure) how the EDC decays linearly in the log domain (i.e., exponentially in the linear domain) during late reflections, but is more step-like during early reflections. The EDC is much smoother than the RIR, making it much more useful for analyzing the decay rate of reverberation.

An extention of the EDC is the energy decay relief (EDR), which uses the short-time fourier transform (STFT) to represent the EDC per frequency band.

$$\text{EDR}(t_n, f_k) = \sum_{m=n}^M |H(m, k)|^2$$

Where  $H(m, n)$  is the STFT at time window  $m$  and frequency bin  $k$ , and  $M$  is the total number of time windows in the RIR.  $t_n$  and  $f_k$  represent the equivalent physical times and frequencies.

The most common objective metric of reverberation is reverberation time (RT60) which describes the time required for the reverberant energy to decay by 60 dB, becoming effectively inaudible. Sabine (1922) proposed a closed-form calculation for RT60 from the volume  $V$  in  $\text{m}^3$  of the room, the surface area  $S$  in  $\text{m}^2$  of the room boundary surfaces and the average absorption  $\alpha$  of the surfaces.

$$\text{RT}_{60} = \frac{0.161V}{S\alpha} \text{ s}$$

Alternatives to RT60 are RT30 and RT20, both of which attempt to estimate RT60 from the more exponentially decaying parts of the RIR. RT30 performs linear interpolation of the log-domain EDC from -5 dB to -35 dB down to -60 dB. i.e., RT30 is an estimate of RT60 based on the first 30 dB of the EDC. Similarly, RT20 estimates RT60 based on the first 20 dB of the EDC.

#### 1.1.4 Numerical Properties of Room Impulse Responses

- \* Typically non-minimum phase (Not all poles/zeros in U.C.), making them non-invertible (no causal stable inverse exists)
- \* May have many perfect zeros (leading to completely unrecoverable content) or near-perfect/strong zeros (leading to effectively unrecoverable content in the presence of noise – severe noise amplification)
- \* Very long (multiple seconds, 1000s of samples)

## 1.2 The Auditory System

The human auditory system is a complex biological system which has evolved to optimally transform acoustical stimulus into neurological excitations that can be understood by the brain and interpreted as sound. It is made up of many acoustical, mechanical, fluid dynamic, chemical and neurological subsystems, each of which plays a key role in this process.

A complete discussion of the auditory system can be found in Pickles (2013), but the important details for this thesis have been reviewed here.

### 1.2.1 The Outer and Middle Ear

(figure auditory system showing outer ear, ossicles and cochlea)

The outer ear is an acoustical/mechanical system which transfroms and transfers acoustical signals to the middle ear. When air is pushed and pulled by a sound source (e.g., a loudspeaker or glottal pulsing in human speech production), this gives rise to a pattern of compression and rarefaction in the volume of air particles, which propagates away from the sound source as a pressure wave (i.e., an acoustical signal). Acoustical signals in the vicinity of the human ear are collected by the pinna which consists of an exposed cartilage structure (i.e., the flange) and a resonant cavity (i.e., the concha). The sound propagates through the external auditory meatus (i.e., the ear canal) and excites the tympanic membrane (i.e., the ear drum). The shape of the pinna and ear canal maximize transfer of acoustical energy to the ear drum. Additionally, the complex shape of the flange gives rise to a frequency-selective directional response known as a head-related tranfer function (HRTF), which plays an important

role in sound localization.

The middle ear transfers the mechanical energy from the vibration of the tympanic membrane to the inner ear via a collection of bones called the ossicles. The three osiccles are the malleus, incus and stapes, and together their rotation/motion performs a lever-like action which trasfers energy from the tympanic membrane to a much smaller flexible membrane-covered opening into the cochlea of the inner ear known as the oval window. The middle ear ossicles act as an impedance-matching mechanical transformer, maximizing energy transfer from the outer ear to the cochlea and minimizing the reflection of energy back into the outer ear.

### 1.2.2 The Inner Ear

(figure cochlea showing basilar membrane and stereocilia)

The inner ear consists of two complex fluid-filled bone structures: the vestibular system which is responsible for balance and the cochlea which is responsible for hearing. The cochlea is a spiral-shaped structure made up of three separate bone cavities (i.e., scalae) which extend its full length: the scala vestibuli, scala tympani and scala media. The scala vestibuli and scala tympani share the same cochlear fluid (perilymph) and are connected at the apex of the cochlea by a narrow opening called the helicotrema. The scala media sits between the other two scalae and is filled with a separate cochlear fluid called endolymph. The scala media is separated from the scala tympani by the basilar membrane.

Inside the scala media, the organ of corti sits on top of the basilar membrane, and is the primary organ involved in transduction of auditory signals. It's base holds thousands of hair cells, each of which have clusters of hair called stereocilia. The

stereocilia connect hair cells on the base of the organ of corti to the upper part of it's structure which is called the tectorial membrane. The hair cells are innervated by auditory nerve fibres (ANFs) which carry messages to and from the brain. Inner hair cells (IHCs) are primarily innervated by afferent ANFs which carry auditory sensory information to the brain, whereas outer hair cells (OHCs) are mostly innervated by efferent ANFs which provide a mechanism for active amplification (discussed later).

When the middle ear ossicles push the oval window in response to an acoustic stimulus, a pressure wave is induced inside the cochlear fluids. The pressure wave propagates from the oval window at the base of the cochlea, through the scala vestibuli to the apex of the cochlea, and then returns to the base via the scala tympani, reaching the round window. The basilar membrane moves in response to the pressure wave, which in turn moves the organ of corti. The base of the organ of corti moves relative to the more rigid tectorial membrane, causing the stereocilia to flex. This results in the opening/closing of transduction channels which modulate the flow of positively charged ions from the cochlear fluid in the scala media into the hair cells. This modulation to the electrical potential in the hair cells induces an electrical signal into the ANFs via neurotransmitter release.

To summarize, acoustic stimulus propagates through the pinna and ear canal, vibrating the ear drum. The signal is transferred from the ear drum to the oval window of the cochlea by the ossicles in the middle ear. A fluid pressure wave is generated in the cochlear fluids which flexes the stereocilia, modulating current flow into the hair cells and generating an electrical signal in the auditory nerve.

The electrical signal generated in the ANFs consists of a sequence of "spike rate".

These impulses represent depolarization (i.e., rising phase) and subsequent repolarization (i.e., falling phase) of a neuron cell membrane during exchange of neurotransmitter across the inter-neuron gap (i.e., the synapse). In the absence of auditory stimulation, action potentials firing continues at a rate called the spontaneous firing rate. At the onset of auditory stimulation, the firing rate increases above the spontaneous rate if the intensity of auditory stimulation is above a certain threshold. Auditory stimuli below this threshold will not produce any detectable change to electrical activity in the auditory nerve, and therefore will not be detected by the brain. This threshold therefore results in a minimum acoustic level that can be detected by the auditory system (i.e., the threshold of hearing).

(figures action potential and spontaneous firing rate ADSR)

### 1.2.3 Tuning, Non-Linearities and Active Amplification in the Cochlea

At the base of the cochlea, the basilar membrane is narrow and rigid making it sensitive to high frequencies. The basilar membrane becomes progressively wider and less rigid towards the apex, making it more sensitive to low frequencies. This frequency selectivity is responsible for a frequency decomposition whereby each ANF responds electrically to a certain range of frequencies. As such, each point along the basilar membrane (or similarly each ANF) is described as having a characteristic frequency (CF) to which it is most sensitive, and a tuning curve that describes its frequency response as a whole. The frequency mapping as a function of displacement along the basilar membrane is more linear at low frequencies, and more logarithmic at high frequencies. The bandwidth of the tuning increases as CF increases (**note this**

might be wrong, my notes say the opposite but this doesn't make sense to me) which gives the time-frequency analysis of the cochlea better frequency resolution at low frequencies, and better time resolution at high frequencies. It has been shown that this is similar to a gammatone filterbank (Lewicki, 2002) and it is believed to have evolved this way as an optimization for classification of the sounds experienced in nature. This frequency tuning is a key part of the neurological encoding of sounds and is fundamental to speech perception.

At low frequencies the tuning curves are reasonably symmetric about the CF. For higher CFs, the tuning curve is increasingly broader on the low-frequency side, generating more of a low-pass response. This results in effect known as upward spread of masking, whereby low frequency signals have a tendency to activate higher frequency ANFs, perceptually interfering with (i.e., masking) high frequency content. The hair cells also provide some additional tuning which slightly shifts the effective lowpass cutoff of the basilar membrane at that point.

Additionally, the basilar membrane responds non-linearly to higher intensity signals, resulting in a broadening of tuning curves. Due to this loss of frequency resolution, it is often easier to understand speech at lower levels (i.e., conversational speech levels). This results in a worsening of the effects of upward spread of masking.

The efferent innervation of OHCs provides non-linear amplification by means of an active mechanical process (i.e., feeding energy back into the cochlea) which produces a sharp tuning in the vicinity of the CF (figure) for lower input levels. In this way, the OHCs provide dynamic range compression on a per-hair cell basis. The hair cells also have some non-linearities which introduces additional compression.

Although ANFs have a flat threshold relative to the frequency of their input, they

inherit the tuning of the basilar membrane and hair cells. The frequency tuning of the entire auditory system up to each ANF is thus collectively described as the frequency tuning curve (FTC) of the ANFs.

(FTC figure)

The combined FTCs of all the ANFs innervating the cochlea results in frequency-dependent minimum acoustic level that can be detected by the auditory system. A typical curve for the absolute threshold of hearing is shown in (figure).

(figure absolute threshold of hearing)

In the presence of background noise, the activation of the cochlea and subsequent firing of the corresponding ANFs due to the interfering noise obscures the firing due to the desired signal (i.e., spectral masking). This perceptual masking effect reduces audibility at the frequencies where noise is present, and raises the effective threshold of hearing. The resulting threshold depends on noise type, and increases with noise level as shown for white noise in (figure)

(figure absolute threshold of hearing with spectral masking)

#### 1.2.4 Sound Localization

The detection of the direction of arrival (DOA) and distance of sound sources plays an important role in everyday life. Not only is sound localization useful for spatial awareness, but there are several auditory mechanisms by which spatial information is used help with speech perception when in adverse listening conditions (e.g., the cocktail party effect, reviewed by Bronkhorst (2000)). A detailed review of the sound localization cues and physiology was provided by Risoud *et al.* (2018), but has been summarized below.

Acoustic properties of the human auditory system enable sound localization by means of a number of binaural and monaural spatial cues. Firstly, when sound originates from the side of the head, the acoustic level is attenuated on the other side of the head due to reduction in direct line-of-sight propagation. This is referred to as the head-shadow effect and produces a difference in acoustic level between the ears called an interaural level difference (ILD). This effect is less pronounced at low frequencies (approximately below 1960 Hz) where diffraction around the head is less efficient, and most pronounced above approximately 3 kHz. ILD magnitude varies depending on individual head acoustics and horizontal angle of arrival (i.e., azimuth angle), and is one of the two spatial cues decoded by the brain to estimate azimuth DOA. The smallest perceiveable ILD has been shown to be approximately 0.5 - 1 dB.

Sound arriving from an off-axis azimuth angle will also arrive at the closer ear first, resulting in an interaural time delay (ITD). The auditory system estimates DOA from ITDs by analyzing phase differences between the ears. For wavelengths less than the distance between the two ears, multiple periods can occur within the time difference, resulting in an ambiguous mapping between phase difference and DOA. For this reason, ITDs become less reliable for frequencies above approximately 1500 Hz. In the case of complex amplitude modulation waveforms such as speech, the auditory system can use some higher frequency ITD information by tracking delays in the temporal envelope rather than the high frequency carrier. The shortest perceivable ITD has been shown to be around 10  $\mu$ s.

For vertical location finding (i.e., sound localization on the elevation angle), the auditory system takes advantage of the acoustic characteristics provided by the shape of the outer ear. The exposed flange of the pinna has a complex shape with many

different ridges which introduce acoustic reflections in the vicinity of the ear canal. These reflections and those provided by the head and upper body result in a DOA-dependent spectral coloration which is referred to as a head-related transfer function (HRTF). Spectral notches produced by destructive interference of head-related reflections are particularly used by the auditory system in estimation of the elevation angle. HRTF have been shown to be most reliable for frequencies above approximately 7 kHz

To estimate the distance of a sound source, the auditory system takes advantage of spectral cues and reverberation-related cues. In the presence of reverberant reflections, the listener first detects the direct sound (i.e., not reflected), and then directs a number of reflections dependent on the room acoustics. Due to the inherent attenuation of acoustic signals as they propagate, as the separation between the sound source and the listener increases, the direct sound is attenuated and becomes increasingly dominated by the reflections. In this way, the auditory system is able to use an estimate of the direct-to-reverberant ratio to detect the distance of the sound source. Similarly, the time delay between the direct sound and the first reflections (i.e., the initial time delay gap, ITDG) decreases with distance, and can be used to estimate distance. Additionally, since higher frequency acoustic signals decay more rapidly over distance, the auditory system is able to use the lowpass-filtered quality of signal spectrum to estimate distance.

There are also several dynamic methods by which humans reinforce the spatial information decoded from the above described cues. Head turning is often performed instinctively to manually adjust spatial cues and confirm the changes that occur. Visual information is also incorporated both as a means of detecting and maintaining

location estimates.

## 1.3 Hearing Loss

A detailed discussion of this topic can be found in Pickles (2013) and the review by Shapiro *et al.* (2021), but I have summarized the important concepts.

### 1.3.1 Overview of Hearing Loss

Hearing loss has many causes and impacts, which are broadly grouped into three categories: Conductive, Sensorineural and mixed hearing loss. Conductive hearing loss describes any damage to the structures of the outer and/or middle ear. Sensorineural hearing loss describes any damage to the inner ear organs and auditory nerve, and is the most common type. Mixed hearing loss represents any combination of conductive and sensorineural hearing loss. Hearing loss can be in a single ear or in both ears (i.e., unilateral or bilateral), and can be symmetric or asymmetric between the two ears. Impairment may be present since birth (i.e., congenital hearing loss), or may accumulate over time (i.e., progressive hearing loss).

Conductive hearing loss includes blockages of the ear canal (e.g., due to ear wax build up), infections in the outer/middle ear, fixation of the ossicles, and damage to the tympanic membrane or oval/round windows. The general result of these issues is reduced energy transfer to the inner ear. Conductive damage can often be treated by medication or surgery, and otherwise is still easily treated by hearing aids since the inner ear is not affected and therefore the mapping/encoding of frequencies is not changed.

Sensorineural hearing loss can be caused by infection, aging, genetics, noise exposure, and most commonly results in damage or loss of stereocilia and hair cells in the cochlea. Hair cells and stereocilia are fragile and irreplaceable, and as will be described in the next section, loss of these structures significantly changes the neural encoding of sounds making it very hard to treat effectively. Age-induced sensorineural hearing loss (i.e., presbycusis) is thought to be caused by a combination of genetics and environmental factors. It is typically symmetric and bilateral, and primarily occurs at high frequencies. Chronic loud noise exposure primarily impacts frequencies in the 3 kHz to 6 kHz range, and is usually bilateral and symmetric, but may be asymmetric if the exposure is asymmetric. Individual acoustic events of substantial loudness may also cause temporary or permanent damage to stereocilia (i.e., acute acoustic trauma). Mild trauma may only result in temporary damage, while more severe trauma are more likely to permanently bend or break stereocilia resulting in complete loss of transduction. The stereocilia of OHCs are more likely to be lost completely, while IHCs tend to only lose some stereocilia resulting in some transduction remaining with weaker sensitivity. Since sensorineural hearing loss largely impacts the auditory system on a per-hair cell basis and hearing aids process the acoustic signal before transmission into the cochlea, the efficacy of hearing aids at compensating these impairments is somewhat limited.

Hearing loss may also be induced by medications with ototoxic effects, which describe a wide range of biochemical reactions with various parts of the auditory system. Most often this begins with fusion or loss of stereocilia, eventually resulting in loss of hair cells. Examples of ototoxic medications include many chemotherapies and antibiotics.

### 1.3.2 Perceptual Impacts of Sensorineural Hearing Loss

Since sensorineural hearing loss primarily impacts OHC function, this usually results in loss of the active amplification mechanism provided by efferent innervation of the OHCs. This and the reduction of IHC sensitivity produces lower stimulus levels at the auditory nerve. This results increase in threshold of hearing, which can have a significant impact on audibility at conversational speech levels.

Additionally the loss of OHC function results in loss of the sharp tuning of the auditory ANFs. This results in a broadening of the ANF tuning and reduces the frequency resolution of the cochlea.

A reduction in temporal sensitivity has also been correlated to both aging and sensorineural hearing loss. The physiological explanations for these effects are complex and still under study, but it is generally explained by reduced ability to track the temporal fine structure (TFS) in complex broadband stimuli, especially in the presence of noise (Xia *et al.*, 2018). There are a number of proposed physiological explanations for this including a reduced number of ANFs, reductions to phase locking of neurons with periodic waveforms, the broadening of cochlear tuning resulting in more complex waveforms arriving at each ANF, and distorted basilar membrane phase response (Tsironis *et al.*, 2024).

The reduction of spectral and temporal resolution results in a coarse and distorted neurological encoding of sound, which significantly impacts speech perception (i.e., impairs the classification of phonemes described in the next section). In addition, loss of temporal resolution impairs the ability of the auditory system to track ITDs which has a significant impact on sound localization.

## 1.4 Speech Production

The ability of humans to generate speech sounds is central to our social communication and societal organization. Speech communication is facilitated by manipulating the body to generate audible sounds from the mouth and/or nose. A specific configuration of the speech-related physiology (to be discussed below) produces a specific sound which is referred to as a phoneme. Phonemes are produced together to form words, which are spoken in sequence to form sentences. By inversely mapping acoustic signal properties to the speech-related configuration used to produce them, listeners are able to decode the intended sentence and perceive its meaning.

A detailed discussion of this topic can be found in Quatieri (2002), but the important details have been summarized here.

### 1.4.1 Anatomy of Speech Production

(figure 3.2 from quatieri)

The physiology underlying speech production can be broadly broken down into three sections: The lungs, the larynx and the vocal tract. The lungs act as a power supply, contracting and expanding to provide air pressure to the larynx. The larynx uses the power from the lungs to generate a specific acoustic waveform. The vocal tract shapes the acoustic waveform before its emission from the mouth and/or nasal passage.

Inside the larynx, air flow is controlled into the vocal tract by opening and closing three separate muscle-controlled barriers, namely the false vocal folds (i.e., false vocal cords), the true vocal folds, and the epiglottis. The vocal folds are composed of

two masses of flesh which can be pulled towards the sides of the larynx revealing a opening known as a glottis (i.e., glottal slit). Muscles-activated control over both the size glottis and the tension in the vocal folds give rise to three different modes of operation: breathing, voicing and unvoicing. When the glottis is fully open, the lungs push air into the vocal tract with minimal resistance (i.e., breathing). The glottis is closed slightly and pulled tight, the applied air pressure initiates an periodic pattern of glottal opening and closing (i.e., glottal pulsing). When air is pushed through the open glottis, it causes the pressure to decrease within the opening (Bernoulli's Principle). The increased tension in the vocal folds then forces the glottis shut, causing the pressure to build up behind the vocal folds until they forced open restarting the process. This process releases a periodic acoustic waveform into the vocal tract (i.e., voicing). An example of a typical waveform generated by glottal pulsing and its correspond spectrum is shown in (figure). The pitch period of voiced speech is controled by tightening and loosening the vocal folds. During unvoicing, the glottis is left open similar to breathing, but the folds are pulled tighter generating audible turbulence. Unvoicing is used in the speech sounds such as the "h" in "house"

(Glottal pulse waveform/spectrum figure)

The vocal tract is an oral cavity extending from the larynx to the lips and nasal passage. Manipulation of the position of the tongue, lips and mouth changes the acoustic resonances of the cavity to modulate the spectra shape of the emitted acoustic waveform. These resonances, called formants, emphasize certain harmonics of the glottal pulse waveform. The relative positioning of formants is central to the classification of different voiced phonemes (e.g., "a", "e", "o"). When the lips or tongue are used to seal the mouth during voiced speech, the glottal pulsing waveform is

forced through the nose generating nasal phonemes (e.g., "ng" in "sing", or "m" in "mother"). Applying pressure behind the lip or tongue seal before releasing it produces a sudden burst of air from the mouth, generating an impulsive sound known as a plosive phoneme (e.g., "p" in "pop", "t" in "train" or "c" in "cane"). When the lips or tongue are positioned to provide a partial seal of the mouth, an audible turbulence is produced which is classified as a fricative phoneme (e.g., "sh" in "she" or "s" in "snake").

### 1.4.2 Classification of Speech Sounds

Together the voicing state of the glottis (i.e., voiced, unvoiced or breathed) and the vocal tract configuration (i.e., formant ratios, fricatives, plosives, nasals) form a collection of acoustic cues which are used by the listener to interpret what is being said. The interaction between each of these speech parameters forms a much wider set of phonemes. Vowels are voiced phonemes with no frication or obstruction of the vocal tract (e.g., "a" in "apple"). Fricatives can be unvoiced (e.g., "f" in "flake") or voiced (e.g., "v" in "van"). Plosives can be unvoiced (e.g., "p" in "pop") or voiced (e.g., "b" in "boot"). Whispers are breathed (e.g., "h" in "have"). Diphthongs, Liquids and Glides are all characterized by a time-varying vocal tract between vowels (e.g., "y" in "boy"). Affricatives are describe the time-varying transition between plosives and fricatives (e.g., "ch" in "chew"). A full breakdown of the categorization of phonemes is shown in (figure).

(figure 3.17 from quatieri)

or

(spectrogram figure)

### 1.4.3 Discrete-Time Speech Production Model

The process of speech production can largely be described with a source-filter model, the acoustic waveform generated by the lungs and larynx are modeled as a source, which is processed by a filter which models the vocal tract and acoustic radiation from the lips.

(figure: my source-filter block diagram)

In this paradigm, lungs and larynx are grouped into an idealized source model which generates a linear combination of an impulse train sequence, an impulse, sequence and a white noise sequence depending on the voicing mode. I.e., the source signal is a linear combination of

$$u_g(n) = \sum_{k=-\infty}^{\infty} \delta(n - kP)$$

$$u_i(n) = \delta(n)$$

$$u_n(n) \sim \mathcal{N}(0, 1)$$

Where  $u_g(n)$  represents idealized glottal pulsing during voiced phonemes,  $u_i(n)$  represents idealized impulsive bursts during plosive phonemes, and  $u_n(n)$  represents idealized turbulence during fricative phonemes.

To obtain an accurate model of the glottal pulse train waveform, the idealized impulse train  $u_g(n)$  is convolved with an individual cycle of glottal pulsing. It has been shown that the Z-transform of a typical glottal flow waveform can be modeled by two identical poles outside the unit circle (ref) (i.e., two maximum phase poles representing a left sided sequence)

$$G(z) = \frac{1}{(1 - \beta z)^2} \quad \beta < 1 \quad (1.1)$$

Therefore the Z-transform of the glottal pulse train modeled is  $U_g(z)G(z)$ , and the Z-transform of the overall source model is

$$U(z) = A_g U_g(z)G(z) + A_i U_i(z) + A_n U_n(z)$$

During oral voiced speech, it has been shown that the vocal tract effect can be modeled by a minimum-phase all-pole filter (Atal and Hanauer, 1971). However, when the oral tract is sealed by the tongue or lips (e.g., during nasalized phonemes) and during unvoiced speech, the effective filter has been shown to have some mixed-phase zeros. Therefore a complete model for the vocal tract is a mixed-phase filter with poles and zeros. i.e.,

$$V(z) = \frac{\prod_{k=1}^{M_{min}} (1 - \tilde{b}_{min,k}z^{-1}) \prod_{k=1}^{M_{max}} (1 - \tilde{b}_{max,k}z^{-1})}{\prod_{k=1}^{N_{min}} (1 - \tilde{a}_{min,k}z^{-1})}$$

The acoustic radiation from the lips (i.e., the radiation impedance) has been shown to impart a highpass response which can be approximately modeled by a single zero just inside the unit circle (ref), i.e.,

$$R(z) \approx 1 - \alpha z^{-1} \quad \alpha < 1$$

Therefore the complete filter model is  $H(z) = V(z)R(z)$ , and the complete source-filter model of speech production is

$$S(z) = U(z)H(z)$$

It is also common to group the Z-transform of the glottal pulse waveform,  $G(z)$ , into the filter model so the source can always be treated as an idealized uncorrelated excitation (i.e., impulse train, impulse or white noise). In this case the speech production filter,  $H(z)$ , has mixed-phase poles and zeros.

$$H(z) = G(z)V(z)R(z) = \frac{\prod_{k=1}^{M_{min}}(1 - \tilde{b}_{min,k}z^{-1})\prod_{k=1}^{M_{max}}(1 - \tilde{b}_{max,k}z^{-1})}{\prod_{k=1}^{N_{min}}(1 - \tilde{a}_{min,k}z^{-1})\prod_{k=1}^{N_{max}}(1 - \tilde{a}_{max,k}z^{-1})} \quad (1.2)$$

From the geometric series expansion, it can be shown that a single zero inside the unit circle can be represented by a set of infinite poles inside the unit circle, i.e.,

$$1 - \tilde{b}z^{-1} = \frac{1}{\prod_{k=0}^{\infty}(1 - \tilde{a}_kz^{-1})}, \quad |z| > |\tilde{a}| \quad (1.3)$$

and in practice, a sufficiently large finite number of poles works with reasonable accuracy. Therefore an all-pole, i.e., autoregressive (AR), model of speech production is often used.

$$H(z) = \frac{A}{\prod_{k=1}^p(1 - \tilde{a}_kz^{-1})} = \frac{A}{1 - \sum_{k=1}^p a_k z^{-k}} \quad (1.4)$$

$$S(z) = U(z)H(z) \quad (1.5)$$

$$s(n) = \sum_{k=1}^p a_k s(n-k) + Au(n) \quad (1.6)$$

It is important to note that this stationary model of the speech production system is incomplete when it comes to modeling full utterances that span multiple phonemes, or even phonemes that involve time variance in the vocal tract (e.g., diphthongs). To

address this, the source weights ( $A_g$ ,  $A_i$  and  $A_n$ ) and the filter parameters must all be made time-varying.

## 1.5 Linear Prediction

The concept of linear prediction was originally proposed by Wiener (1949) in his seminal contributions on modeling discrete time signals as stochastic processes, and equivalently modeling filtering and prediction as a statistical problem. The first formal discussions of linear prediction in the context of speech signals were presented concurrently by Saito *et al.* (1967) and Atal and Schroeder (1970). Linear prediction for speech analysis was proposed as an efficient method for encoding speech signals by estimating and storing the poles of the speech production filter, and later using them to re-synthesize the original speech waveform.

As described in the previous section, speech production can be roughly modeled as the excitation of time-varying all-pole filter with a source signal made up of a combination of ideal impulse trains, white noise and individual impulse spikes. Motivated by this source-filter/AR model of speech (equation 1.6), linear prediction was proposed as an efficient method for encoding speech by estimating and storing the poles of the effective all-pole vocal tract filter, and later using them to re-synthesize the original speech waveform. This is commonly used in speech codecs where the speech is broken into frames and the parameters of the source/filter model can be encoded at a lower bit rate than the raw PCM waveform.

The process of linear prediction can be viewed from three separate but related perspectives, namely as a method prediction a signal, identifying/inverting a system (i.e., the speech production filter), and estimating/whitening signal spectrum. Each

of these perspectives presents important insights..

### 1.5.1 Signal Prediction Perspective

Posed as a prediction problem, the approximately AR model of speech motivates the prediction,  $\hat{s}(n)$ , of a speech signal,  $s(n)$ , from only its previous samples. I.e.,

$$\hat{s}(n) = \sum_{k=1}^p \alpha_k s(n-k) \quad (1.7)$$

Where  $\{\alpha_k, k = 1, \dots, p\}$  are referred to as the prediction coefficients. The corresponding prediction error (i.e., the prediction residual) is

$$e(n) = \hat{s}(n) - s(n) = \hat{s}(n) - \sum_{k=1}^p \alpha_k s(n-k) \quad (1.8)$$

If the original speech signal is indeed an autoregressive process, if the prediction order is sufficiently high, and if the poles of the effective speech production filter are correctly estimated (i.e.,  $\alpha_k = a_k$ ,  $k = 1, \dots, p$ ), Equation 1.7 exactly matches the equation for the AR model of speech (Equation 1.6) and therefore the residual will be equal to the idealized excitation sequence. I.e.,

$$e(n) \Big|_{\alpha_k = a_k, \forall k=1, \dots, p} = u(n) = \begin{cases} u_g(n) & \text{during voiced speech} \\ u_i(n) & \text{during unvoiced plosive speech} \\ u_n(n) & \text{during unvoiced fricative speech} \end{cases} \quad (1.9)$$

In estimation of the coefficients of the all-pole model, the optimal prediction coefficients are found by minimizing prediction error in a total squared-error sense, i.e.,

$$E = \sum_{n=-\infty}^{\infty} e(n) \quad (1.10)$$

$$\{\alpha_k\} = \arg \min_{\{\alpha_k\}} E \quad (1.11)$$

It turns out that prediction error metric  $E$  forms a  $(p + 1)$ -dimensional error surface which is a quadradic function of the prediction coefficients, with exactly one global minimum corresponding to the optimal set of coefficients (i.e., a quadratic bowl).

**TBD Explain if needed:** This can be shown by vector expansion, . . . , Leading to quadratic form, . . . Positive (semi?)definite implying a minimum. Therefore the optimal solution can be found by taking the partial derivative of the total squared error with respect to each prediction coefficient, and setting them equal to zero.

$$\frac{\partial E}{\partial \alpha_k} = 0 \quad (1.12)$$

The total squared error above is computed over all time, which is theoretically ideal. However, in practice minimization is done for a short-term signal frame (i.e., prediction error interval) due to availability of a finite amount of data, and/or due to time-varying nature of speech which makes it only short-time stationary. The specific definition of short-term total squared error in the vicinity of time  $n$ , denoted  $E_n$ , differs for the autocorrelation method and covariance method which will be discussed in the next section.

From the orthogonality principle, the optimal solution will produce an error signal that is orthogonal to, and therefore uncorrelated with, the input signal except at a lag of zero (i.e., uncorrelated with a unit-delayed version of the speech signal). Since

any autocorrelation in the residual also implies correlation between the residual and the input, the optimal prediction residual is also uncorrelated with itself except at a lag of zero. I.e.,

$$r_{es}(\tau) = E[e(n)s(n - \tau)] = \delta(\tau) \quad \tau = 0, \dots, p \quad (1.13)$$

$$r_{ee}(\tau) = E[e(n)e(n - \tau)] = \delta(\tau) \quad \tau = 0, \dots, p \quad (1.14)$$

This makes intuitive sense because by optimally predicting and subtracting the part of the speech signal that can be predicted from its past samples, linear prediction exploits and removes all temporal correlation from the signal. Since this is also the autocorrelation function of the idealized excitation sequence (impulse, pulse train or white noise), this reinforces that the optimal prediction residual will be the idealized excitation sequence and therefore the prediction coefficients will correspond to the AR parameters of the underlying process.

It is important to note that Equations 1.13 and 1.14 only hold for certain lags, which is dictated by the prediction order,  $p$ . This will be discussed more later.

### 1.5.2 System Identification / Inverse Filtering Perspective

In describing speech as the excitation of an all-pole filter with an idealized uncorrelated excitation sequence, we can also describe linear prediction as identification of the corresponding all-pole filter (i.e., system identification).

In this context, prediction (Equation 1.7) can be described by a  $p^{\text{th}}$  order FIR prediction filter  $P(z)$ . I.e.,

$$P(z) = \sum_{k=1}^p \alpha_k z^{-k} \quad (1.15)$$

$$\hat{S}(z) = P(z)S(z) \quad (1.16)$$

And a corresponding  $p^{\text{th}}$  order FIR prediction error filter,  $A(z)$ .

$$A(z) = 1 - P(z) = 1 - \sum_{k=1}^p \alpha_k z^{-k} \quad (1.17)$$

$$E(z) = A(z)S(z) = S(z) - P(z)S(z) = S(z) - \hat{S}(z) \quad (1.18)$$

where  $S(z)$ ,  $\hat{S}(z)$  and  $E(z)$  are the Z-transforms of the speech signal,  $s(n)$ ,  $\hat{s}(n)$ , and  $e(n)$  respectively.

The inverse of prediction error filter (i.e., the inverse filter in linear prediction theory), which is a  $p^{\text{th}}$  order all-pole filter, produces the original speech signal when excited with the prediction residual. I.e.,

$$\frac{1}{A(z)} = \frac{1}{1 - P(z)} = \frac{1}{1 - \sum_{k=1}^p \alpha_k z^{-k}} \quad (1.19)$$

$$S(z) = \frac{1}{A(z)} E(z) \quad (1.20)$$

The block diagrams corresponding to these three filters are shown in (figure)  
(figure block diagrams)

If the  $s(n)$  truly represents an the excitation of an all-pole system,

$$H(z) = \frac{A}{1 - \sum_{k=1}^p a_k z^{-k}} \quad (1.21)$$

and if the prediction coefficients are correctly estimated (i.e.,  $\alpha_k = a_k$ ,  $k = 1, \dots, p$ ), the inverse filter will be identical to the actual all-pole system. Consequently, the prediction error filter will be the exact inverse of the all-pole system. I.e.,

$$\frac{1}{A(z)} \Big|_{\{\alpha_k\}=\{a_k\}} = H(z) \quad (1.22)$$

$$A(z) = \frac{1}{H(z)} \quad (1.23)$$

If however the system has zeros, the linear prediction solution will be forced approximate these zeros with a finite number of poles in the inverse filter. As previously explained, an infinite number of poles are required to perfectly model a zero (Equation 1.3), so the inverse filter will always be approximate when the true system has zeros.

When the all-pole inverse filter,  $1/A(z)$ , is used for resynthesis of the speech signal, careful attention must be given to ensure that it is stable (i.e., all poles must be inside the unit circle). This implies that the prediction error filter, generated by the optimization solution, must have all zeros inside the unit circle. If the real system is truly a physical all-pole system, it will be inherently causal and stable, and therefore the optimization process will be able to achieve perfect prediction with a minimum phase prediction error filter. However, if the system has zeros, the all-pole model will be approximate, and in some cases it may be optimal to incorporate some maximum

phase zeros into the prediction error filter. Additionally, if the underlying process has acausal maximum phase poles (e.g., the left-sided glottal pulse shape in speech production, Equation 1.1), the optimal prediction error filter would include zeros at these locations, even though the inverse filter would be unstable.

To handle the issue of inverse filter stability, two different formulations of the optimization problem have been developed: the autocorrelation method and the covariance method. These two methods differ in their definition of the short-term total squared error metric,  $E_n(n)$ , to be minimized.

### 1.5.2.1 Autocorrelation Method

In the autocorrelation method, the speech signal is windowed to the prediction error interval  $n \in [n, n + N_w - 1]$  and the total squared error is computed using error samples over all time. I.e.,

$$s_n(m) = s(m + n)w(m) \quad (1.24)$$

$$e_n(m) = s_n(m) - \hat{s}_n(m) = s_n(m) - \sum_{k=1}^p \alpha_k s(m - k) \quad (1.25)$$

$$E_n = \sum_{m=-\infty}^{\infty} e_n^2(m) = \sum_{m=0}^{N_w+p-1} e_n^2(m) \quad (1.26)$$

where the subscript  $n$  implies "in the vicinity of time  $n$ ", and  $w(n)$  is the length- $N_w$  window function, which is non-zero only in the range  $n \in [0, N_w - 1]$ . The window function could be rectangular, or some other non-uniform window (e.g., hamming). Note that the reduction of the summation range in 1.26 is a result of the limited range of non-zero elements in  $e_n(n)$  due to the windowing of  $s(n)$ .

Minimization of  $E_n$  with respect to the prediction coefficients (i.e., setting  $\partial E / \partial \alpha_k = 0$ ) results in the so-called Yule-Walker equations.

$$\sum_{k=1}^p \alpha_k r_n(i-k) = r_n(i), \quad i = 1, \dots, p \quad (1.27)$$

Where  $r_n(\tau) = \sum_{m=0}^{N_w-1-\tau} s_n(m)s_n(m-\tau)$  is the short-term autocorrelation function of  $s(n)$ . This is simply the least-squares normal equations applied to linear prediction. The autocorrelation function appears due to the infinite summation over the error signal, and implies an inherit assumption of stationary speech.

The Yule-Walker equations can be restated in matrix form as

$$R_n \boldsymbol{\alpha} = \mathbf{r}_n \quad (1.28)$$

$$\begin{bmatrix} r_n(0) & r_n(1) & r_n(2) & \dots & r_n(p-1) \\ r_n(1) & r_n(0) & r_n(1) & \dots & r_n(p-2) \\ r_n(2) & r_n(1) & r_n(0) & \dots & r_n(p-3) \\ \vdots & \vdots & \vdots & \ddots & \vdots \\ r_n(p-1) & r_n(p-2) & r_n(p-3) & \dots & r_n(0) \end{bmatrix} \begin{bmatrix} \alpha_1 \\ \alpha_2 \\ \alpha_3 \\ \vdots \\ \alpha_p \end{bmatrix} = \begin{bmatrix} r_n(1) \\ r_n(2) \\ r_n(3) \\ \vdots \\ r_n(p) \end{bmatrix} \quad (1.29)$$

This problem is overdetermined and thus must be solved by least-squares using the pseudo-inverse.

$$\boldsymbol{\alpha} = R_n^+ \mathbf{r}_n = (R_n^T R_n)^{-1} R_n^T \mathbf{r}_n \quad (1.30)$$

The Toeplitz nature of the autocorrelation matrix additionally enables usage of the recursive Levinson-Durbin algorithm. This algorithm is highly efficient compared

to other methods of solving systems of linear equations, but is known to be prone to numerical instability due to its inherit recursion when the autocorrelation matrix is ill-conditioned.

It has been shown that due to the Toeplitz nature of the autocorrelation matrix  $R_n$ , the autocorrelation method produces a minimum phase prediction error filter. Therefore the resulting inverse filter used for speech resynthesis is a stable all-pole filter. It has also been shown that the autocorrelation method ( $p^{\text{th}}$  order LPC) produces a filter (i.e., the inverse filter) for which the first  $p + 1$  values of the autocorrelation function of the system impulse response,  $h(n) = Z^{-1}\{H(z)\}$ , is identical to the first  $p + 1$  autocorrelation values of the signal, i.e.,

$$r_h(\tau) = r_s(\tau) \quad \tau = 0, \dots, p \quad (1.31)$$

Since the autocorrelation function completely defines the power spectral density (i.e., PSD is the fourier transform of the autocorrelation function), it can be concluded that the magnitude response of the resulting filter is identical to that of the true system up to a spectral resolution defined by the prediction order. Therefore, for large enough prediction orders, the inverse filter resulting from the autocorrelation method represents the equivalent minimum phase representation of the true system. I.e., if real system,  $H(z)$  is non-minimum phase and we decompose it into it's equivalent minimum phase and all-pass components,

$$H(z) = H_{\min}(z)H_{\text{allpass}}(z) \quad (1.32)$$

$$\|H_{\min}(z)\| = \|H(z)\| \quad (1.33)$$

$$(1.34)$$

Then as  $p \rightarrow \infty$ ,  $\frac{1}{A(z)} \rightarrow H_{\min}(z)$ , and

$$H(z)A(z) = H_{\text{allpass}}(z) \quad (1.35)$$

However the windowing of the speech signal prior to error calculation means that only part of the infinite-length system impulse response will be captured in the autocorrelation function. This can result in distortion of the estimated all-pole inverse filter, an effect that can be minimized but never avoided entirely by using a longer window. When attempting to model the vocal tract as an all-pole filter, the window must also be short enough that the signal is considered short-time stationary, otherwise the analyzed spectrum will be smoothed by the time-varying nature of speech. The window size thus represents a trade off between capturing short-time spectra and capturing the IIR system impulse response.

The effect of windowing the speech signal in the autocorrelation method can therefore be described as biasing the solution, the result being a potentially sub-optimal (in a total squared error sense) prediction error filter which is guaranteed to be minimum phase, and a stable minimum-phase inverse filter that matches the magnitude response of the true system up to a spectral resolution defined by the prediction order.

### 1.5.2.2 Covariance Method

In the covariance method, the speech signal is not windowed, but the prediction error is computed using error samples only within the prediction error interval  $n \in [n, n + N_w - 1]$ . This means that the error samples are computed using samples outside of the prediction error interval, and thus represent the true error signal over the entire interval. I.e.,

$$s_n(m) = s(m + n) \quad (1.36)$$

$$e_n(m) = s_n(m) - \hat{s}_n(m) = s_n(m) - \sum_{k=1}^p \alpha_k s(m - k) \quad (1.37)$$

$$E_n = \sum_{m=0}^{N_w-1} e_n^2(m) \quad (1.38)$$

Minimization of short-term total squared error,  $E_n$ , with respect to the prediction coefficients (i.e., setting  $\partial E / \partial \alpha_k = 0$ ) results in a different set of normal equations in terms of the short-term covariance function.

$$\sum_{k=1}^p \alpha_k \phi_n(i, k) = \phi_n(i, 0) \quad (1.39)$$

Where  $\phi_n(i, k) = \sum_{m=0}^{N_w-1} s_n(m - i) s_n(m - k)$  is the short-term covariance. It is important to note that by convention in signal processing theory, short-term covariance is not used to mean the short-term parallel of long-term covariance. While long-term covariance is formally defined as the autocorrelation function with its mean removed, short-term covariance is defined as the short-term parallel of non-stationary correlation. In other words short-term correlation is a function of lag and implies analysis of

stationary processes, while short-term correlation is a function of two time instances and implies analysis of non-stationary processes.

The covariance method normal equations can also be represented in matrix form.

$$\Phi_n \boldsymbol{\alpha} = \boldsymbol{\phi}_n \quad (1.40)$$

$$\begin{bmatrix} \phi_n(1, 1) & \phi_n(1, 2) & \phi_n(1, 3) & \dots & \phi_n(1, p) \\ \phi_n(2, 1) & \phi_n(2, 2) & \phi_n(2, 3) & \dots & \phi_n(2, p) \\ \phi_n(3, 1) & \phi_n(3, 2) & \phi_n(3, 3) & \dots & \phi_n(3, p) \\ \vdots & \vdots & \vdots & \ddots & \vdots \\ \phi_n(p, 1) & \phi_n(p, 2) & \phi_n(p, 3) & \dots & \phi_n(p, p) \end{bmatrix} \begin{bmatrix} \alpha_1 \\ \alpha_2 \\ \alpha_3 \\ \vdots \\ \alpha_p \end{bmatrix} = \begin{bmatrix} \phi_n(1) \\ \phi_n(2) \\ \phi_n(3) \\ \vdots \\ \phi_n(p) \end{bmatrix} \quad (1.41)$$

This problem is overdetermined and thus must be solved by least-squares using the pseudo-inverse.

$$\boldsymbol{\alpha} = \Phi_n^+ \boldsymbol{\phi}_n = (\Phi_n^T \Phi_n)^{-1} \Phi_n^T \boldsymbol{\phi}_n \quad (1.42)$$

The covariance matrix is symmetric but not Toeplitz, therefore more correlation coefficients must be calculated compared to the autocorrelation method, and it cannot be solved efficiently with the Levinson-Durbin. However covariance matrices are usually positive definite allowing use of Cholesky decomposition. Cholesky is less efficient than the Levinson-Durbin algorithm, but is more numerically stable.

Unlike the autocorrelation method where windowing enforces an implicit stationary assumption and derives a minimum phase equivalent system, the covariance method represents an unconstrained/unbiased optimization problem. As such the covariance method tends to perform better when the system/process is known to

be non-stationary, since the time-varying statistics are captured in the covariance matrix and used in the optimization. Being unconstrained, the covariance method may derive a non-minimum phase prediction error filter in cases where such a filter achieves a lower prediction error (e.g., in some cases when the underlying process includes zeros and/or acausal maximum phase poles). The covariance method is only guaranteed to come up with a minimum phase prediction error filter if the underlying process is indeed minimum-phase all-pole. It is important to note however, that the prediction error filter is only required to be minimum-phase if the inverse filter is intended to be used for respeech synthesis (e.g., speech codecs). In some cases, only the prediction error filter is used (e.g., equalizer/whitening filter design), in which case a non-minimum phase solution may be desirable.

Additionally, while the windowing in the autocorrelation method means that the modeling of the true all-pole system is always approximate (except as the window size approaches infinity), the covariance method can perfectly estimate the coefficients of an all-pole system with only a finite number of data points.

To summarize, the covariance method represents an unbiased solution for the optimal prediction error filter (in the least-squares sense) which may outperform the minimum-phase solution produced by the autocorrelation method if the underlying system/process is non-stationary, not all-pole, or has non-minimum phase acausal poles. However, the covariance method is more computationally complex and does not guarantee that the inverse filter used for speech resynthesis will be stable.

### 1.5.3 Spectral Estimation / Spectral Whitening Perspective

The process of linear prediction can also be viewed as an estimation of the speech spectrum or the speech spectrum envelope. In the previous section, speech was modeled as the excitation of an all-pole filter with an uncorrelated input sequence. Under these conditions, it was explained that the autocorrelation method produces an inverse filter with an impulse response that has an autocorrelation function matching that of the signal, up to  $p + 1$  lags. It was explained that the resulting inverse filter exactly matches the magnitude response of the all-pole speech production filter, up to a spectral resolution defined by the prediction order. Identically, if the signal being analyzed is a realization of an AR process (i.e., the output of the system previously described), the autocorrelation method will generate an inverse filter with a magnitude response that exactly matches the signal spectrum up to a spectral resolution defined by the prediction order

Similarly, the prediction error filter represents the inverse of the signal spectrum and therefore flattens it. This explanation aligns with the prediction perspective previously outlined, since the autocorrelation of the optimal solution was found to be an impulse, which corresponds to a flat PSD. It also aligns with the previous inverse filtering perspective where the prediction error filter inverts and therefore equalizes (i.e., whitens) the all-pole speech production filter. For this reason the prediction error filter is commonly referred to as a whitening filter.

In speech spectrum analysis, it may be desirable to use a lower prediction order which underfits the spectrum, so as to only model the vocal tract resonances and spectral tilt (i.e., model the speech spectrum envelope). If the spectral resolution is increased too much, the inverse filter will begin to model not only the spectral

envelope, but also the harmonics of glottal pulsing during voiced speech. This is undesirable in many speech codecs where the goal is to generate a model of the vocal tract and use it to resynthesize the speech signal using synthetically generated impulse trains.

## 1.6 Speech Perception in Adverse Conditions

### 1.6.1 Characterizing Speech Perception

As a whole, speech perception describes a listener's ability to hear and understand what is being said by a talker. This is directly dependent on the listener's ability to detect the presence of the acoustic speech signal, and decode the speech cues to accurately reconstruct the spoken utterances. There are several characteristics of speech perception which are related but distinct: speech audibility, speech intelligibility and listening effort.

Audibility describes the listener's ability to detect the presence of sound. The auditory system is physically capable of detecting any sound that is above the absolute threshold of hearing. As such, speech audibility may be defined as the fraction of speech spectrum over time that is above the listener's threshold of hearing.

Speech intelligibility (SI) represents how accurately the listener is able to identify what is being said, and is usually measured as a fraction of phonemes or words correctly identified. SI is typically evaluated based on objective tests involving human participants. Speech is presented, and the participant attempts to identify what is being spoken. Often nonsense utterances are used to remove mental correction (i.e., post-diction).

$$SI = \frac{\text{Correctly Identified [words/syllables/phonemes]}}{\text{Total Presented [words/syllables/phonemes]}}$$

Listening effort (LE) describes the allocation of mental resources required to understand speech. When speech cues are obscured (e.g., in noisy or reverberant environments), the brain has to apply work harder to fill in missing information (i.e., post-diction). LE is often evaluated by presenting a test signal to participants and asking them to complete an effort-related questionnaire, but in general complex to evaluate in a single test. It has been proposed that a more statistically consistent evaluation of listening effort is based on three separate factors (Shields *et al.*, 2023): self-reported LE, behavioral signs of LE, and physiological signs of LE. Self-reported LE is usually evaluated by having participants complete questionnaires assessing their effort during listening, and fatigue after listening. Behavioral signs of LE describe reduced ability to complete mentally-intensive tasks due to exhaustion, and is assessed by evaluating their performance on a selected test task. Physiological signs of LE are widespread and can be assessed via objective biological measurements such as electroencephalogram analysis (EEG), functional magnetic resonance imaging (fMRI), eye tracking and heart rate tracking. Psychological effects of increased listening effort include distress, fatigue, and has been shown to lead to social withdrawal and to increase with prevalence of stress-related leave from work (Ohlenforst *et al.*, 2017). Although speech intelligibility and listening effort are closely related, an increase listening effort is not always correlated to a decrease in speech intelligibility (Winn and Teece, 2021).

When evaluating the performance of a speech reproduction system such as a hearing aid, speech quality is also an important consideration in the subjective experience

of the user. Speech quality (SQ) is usually evaluated based on subjective ranking of a test/distorted signal on a provided scale. The most common test is the so-called mean opinion score (MOS) test whereby the participants are asked to rank the quality of a test signal on a five point scale (i.e., absolute category rating, ACR).

### (ACR TABLE)

The MOS test procedure consists first of a training phase (i.e., anchoring phase) where the participant is presented with example signals for the low, middle and high quality categories. After the training phase, the evaluation phase is completed using the real test signal. The test is repeated for a group of participants, and the MOS rating is computed as the average ACR across all participants.

An alternative quality test is the comparative mean opinion score (CMOS) whereby the participants are presented with a test signal and a separate clean reference signal, and are asked rank how much better or worse the quality of the test signal is relative to the reference signal.

### 1.6.2 Impact of Reverberation on Speech Cues

As previously discussed, phoneme recognition relies on the identification of spectral acoustic cues. Temporal cues such as periodicity, onsets, offsets and stops are important to detect the boundaries of words and identify phonemes as voiced, fricative and plosive. Spectral cues such as phoneme ratios and spectral tilt are important to differentiate specific voiced phonemes. Accurate phoneme identification therefore is strongly dependent on temporal envelope clarity and spectral contrast.

Reverberation smears energy across time, blurring temporal and spectral cues.

Periods of low energy are filled with reverberant energy, smoothing out temporal envelope. This results in blurring of word onsets, offsets and stops. Phonemes also overlap in time, resulting in a masking effect. Speech perception is particularly impacted during highly time-varying speech segments (e.g., consonants or word boundaries) and following loud bursts which take longer to decay. Formant transitions during diphthongs, liquids and glides are also flattened making them harder to identify.

### **1.6.3 Impact of Reverberation on Speech Intelligibility and Listening Effort**

It has been shown that reverberation and noise both have a negative impact on speech intelligibility and listening effort. However, in most realistic listening environments, where reverberation time is fairly short and SNR is positive, the effects on speech intelligibility are minimal (Schepker *et al.*, 2016).

Normal hearing listeners are generally able maintain good speech understanding even under reasonably severe listening conditions (Schepker *et al.*, 2016) due largely to perceptual adaptations which will be explained in the next section. This is especially true when the listeners has prior exposure to the listening environment (George *et al.*, 2010).

Hearing impaired individuals are more sensitive to the effects of reverb and noise. Even when audibility is good, intelligibility and listening effort tend to be worse due to degraded temporal and spectral resolution from sensorineural hearing loss (Reinhart and Souza, 2018) and reduced perceptual adaptations (explained in next section) (Srinivasan *et al.*, 2017; Roberts *et al.*, 2003). There is a lot of variability in the impact of reverberation for hearing impaired listeners, and the reasons are not

fully understood. However it has generally been shown that more severe impairment equates to more difficulty in reverberant environments (Xia *et al.*, 2018).

The individual and combined impacts of reverberation and noise are often investigated through from the perspective of speech transmission index (STI). This is done by mapping both variables onto a 2D grid showing iso-STI contours (figure). In this way the impacts of reverberation and/or noise can be analyzed through a single variable. STI has been shown to be correlated to speech intelligibility and listening effort regardless of whether changes due to reverberation or noise.

(figure 1 george et al)

George *et al.* (2010) showed that for normal hearing listeners, speech recognition threshold (SRT, i.e., the minimum conditions for 50% speech intelligibility) is approximately an STI of 0.36. This translates to a reverberation time of approximately 2 seconds or a SNR of approximately -4 dB, which are very severe conditions not typically experienced in everyday life. As the conditions improve from this point (i.e., as reverberation time decreases and/or SNR increases), speech intelligibility very rapidly returns to 100%. This shows the insensitivity of speech intelligibility as a measurement of the impacts of reverberation under typical conditions.

Conversely, listening effort has been shown to vary monotonically with reverberation time and noise even under moderate conditions. For this reason, listening effort is generally considered a better metric under typical listening conditions, and a combination of listening effort and speech intelligibility is best for a reliable analysis over a wide range of conditions (Schepker *et al.*, 2016).

Independent of hearing loss, age related neurological and auditory deteriorations and differences in working memory capacity have been shown to impact the extent

to which reverberation inhibits speech perception (Reinhart and Souza, 2018).

#### **1.6.4 Impact of Reverberation on Spatial Cues**

As previously discussed, detection of the directional of arrival (DOA) of sound is important for spatial awareness and speech perception. In anechoic environments, sound arrives from a single distinct direction, making localization a relatively simple task. In reverberant environments, sound arrives from many directions due to reflections, which blurs the spatial cues which are central to sound localization (i.e., ILDs, ITDs and HRTFs).

However, it has been shown that with extended exposure to a reverberant environment, the auditory system's ability to estimate direction and distance improves greatly. This is due to perceptual adaptations which are described in the next section.

#### **1.6.5 Perceptual Adaptation to Reverberation and Noise**

Normal hearing (NH) auditory systems have a strong ability to maintain speech perception in adverse listening conditions due to a number of perceptual adaptations which work to provide phonetic perceptual consistency. A detailed overview of these perceptual adaptations can be found in the review by Tsironis *et al.* (2024), but the key information is summarized below.

##### **1.6.5.1 The Precedence Effect**

The precedence effect (PE) describes a perceptual phenomena whereby delayed repetitions of the same sound are perceived as an individual sound, provided the delay between the sounds is short enough. This effect was originally demonstrated by

Wallach *et al.* (1949) and Haas (1951), and was reviewed by Litovsky *et al.* (1999). Studies of the precedence effect usually involve playing two identical stimuli with a delay between them (i.e., a lead-lag pair). Commonly clicks are used but studies have also been done involving more complex stimuli such as noise and speech. The precedence effect is most pronounced for brief/transient sounds such as clicks but is still reasonably effective for complex stimuli like speech. The effect is much weaker for stationary sounds such as sustained tones.

Under the umbrella of the precedence effect there are three phenomena which are separate but related: Lead-lag fusion, lead-lag localization dominance, lead-lag discrimination suppression.

Lead-lag fusion describes the process whereby lead-lag pairs of stimuli are perceived as a single auditory event provided the delay between the stimuli is less than the so-called echo threshold (i.e., the echo fusion threshold). This results in a sort of echo suppression for reverberation whereby reflections that arrive within the echo threshold are fused with the direct sound and do not affect speech perception. Reflections with delays greater than the echo threshold are perceived as distinct and have an adverse affect on speech perception. Echo thresholds are typically in the range of 5 milliseconds to 30 milliseconds, but can be as low as 2 milliseconds or as high as more than 100 milliseconds. This wide range is dependent on stimulus characteristics (i.e., spatial, spectral and temporal properties) and the listener's age, hearing status and extent of prior exposure to the current room acoustics. Fusion has been shown to occur even when the lagging stimulus is up to 10 to 15 dB louder than the leading stimulus.

Lead-lag localization dominance is a phenomena whereby the fused signal is perceived to arrive from or near the direction of the leading stimulus. Lead-lag discrimination suppression describes the listener's inability perceive the location of the lagging stimulus. Together, localization dominance and discrimination suppression are responsible for reducing disruptions to sound localization due to reflections in reverberant environments. Although fusion occurs for delays lower than the echo threshold, localization dominance and discrimination suppression only occur for shorter delays. Additionally, for very short delays less than approximately 0.5 to 1 milliseconds, localization dominance and discrimination suppression break down, and summation localization occurs. For these delays, sound is perceived to arrive from the average direction between the leading and lagging stimuli (i.e., weak precedence).

The precedence effect also includes an adaptive mechanism called the build-up effect. When lead-lag pairs are repeated, over time the echo threshold has been shown to increase, resulting in fusing of longer and longer delays with the direct sound. As a result, when a listener is exposed to stimuli in a relatively stationary acoustic environment, their ability to perceptually suppress reverberant reflections increases over time. This is an example of how normal hearing individuals benefit from prior exposure to room acoustics. Conversely, when room acoustics change, this can result in a mismatch between the lead-lag relationships mapped by the auditory system and the true characteristics of the acoustic reflections. In this situation, the mechanisms of the precedence effect reset to their base states, and the listeners perceives an increase in amount of echo. This is referred to as the breakdown effect.

Hearing impaired listeners have been shown to experience less of the benefits of the precedence effect (Roberts *et al.*, 2003; Rennies *et al.*, 2022b). Research into the

physiological explanations for this is ongoing, but it is generally thought to be related to reduction of temporal resolution in impaired auditory systems. This contributes to the difficulties hearing impaired listeners experience in reverberant environments.

#### **1.6.5.2 Spatial Release From Masking**

Another key perceptual adaptation involved in handling adverse listening conditions is spatial release from masking (SRM), which was reviewed by Litovsky (2012). This phenomenon encompasses several mechanisms by which the auditory system leverages the spatial diversity between the ears to process spatially separated sound sources. In the presence of many interfering acoustic signals, a normal hearing auditory system has a strong ability to isolate the target talker and maintain speech perception. This phenomena was originally explored by Cherry (1953), who referred to it as the "cocktail party effect", and has since been largely attributed to SRM. Since this effect leverages spatial diversity, speech perception is better in noisy environments if the maskers are separated spatially (i.e., not co-located).

There are three main mechanisms involved in SRM: The better ear effect, the binaural squelch effect and binaural summation. The better ear effect describes how the auditory system will increase focus on a single ear, chosen based on SNR estimated from ILD cues. It is well known that sounds arriving from one side of the head can be attenuated by up to approximately 9 dB on the other side of the head due to the so-called head shadow effect. The binaural squelch effect (i.e., binaural unmasking) describes the auditory systems usage of binaural cues to focus on the target with the better ear effect taken into account. Binaural summation is a mechanism by which speech perception for co-located target and maskers is better for binaural

listening than monaural listening. This is distinct from the binaural squelch effect in that it does not depend on binaural cues, and is more similar to signal averaging for noise reduction in signal processing theory. The better ear effect has been shown to be the most significant contributor to SRM, while the binaural squelch effect is less significant, and binaural summation is the least significant..

In a normal hearing auditory system, SRM has been shown to provide from SNR gains ranging from several dB to upwards of 25 dB. The benefits of SRM are much less for hearing impaired listeners, likely due largely to degraded binaural sensitivity caused by reduced temporal resolution.

In reverberant environments, the binaural cues are distorted, which reduces the effects of SRM. Generally, it has been shown that the benefits of SRM diminish as reverberation time increases. However it has been shown that SRM can also provide a small amount of reverberation suppression by suppressing the spatial directions corresponding to reflections. To explain this Leclerc *et al.* (2015) proposed a distinction between conventional binaural unmasking which reduces the effects of noise maskers and binaural dereverberation which reduces the effects of self-masking due to reverberation. Binaural unmasking has been shown to be negatively impacted by reverberation, and interestingly binaural reverberation has been shown to be negatively impacted by the presence of noise maskers.

## 1.7 Hearing Aids

Maybe later: - Might need to discuss practical requirements (delay etc) - Impact of acoustic design/positioning of hearing aids (BTE, RIC, ITE etc) on spatial cues etc  
-*i* How hearing loss makes cues worse but hearing aids maybe make them doubly

worse (often doesn't compensate spatial cue loss or even makes them worse) - How algorithms don't help the fundamental issues with hearing loss (especially relating to reverb)

## 1.8 Metrics of Speech Perception

As previously discussed, it has been shown that a combination of speech intelligibility and listening effort is best for evaluating the impacts of reverberation on speech perception under a wide range of acoustic conditions. Additionally speech quality an important consideration in the subjective experience of hearing aid users.

While evaluations of SI, LE and SQ involving test participants are the most effective, they are time consuming and often not practical. A number of objective prediction metrics have been developed to estimate SI, LE and SQ by quantitative signal analysis. Although these prediction metrics are only approximations, many of them have proven to be strongly correlated to the true test metrics under certain conditions, and they are easily reproducible and greatly reduce the time required to evaluate speech reproduction systems such as hearing aids.

When selecting a prediction metric for a study, careful attention must be given to ensure that the metric is suitable for the test conditions and the processing performed by the system under test (SUT). Since this thesis is focused on speech perception of hearing aid users in reverberant environments, it is important to include metrics that incorporate some modeling of the auditory system and the impacts of hearing loss (i.e., frequency tuning and non-linearities). If the metric does not include any modeling of the non-linearities in the human auditory system, it will not accurately predict

the target speech perception metric across a wide range of input levels, under non-linear distortions or under non-linear hearing aid processing such as dynamic range compression or statistical time frequency masking. Additionally, it is important to include binaural metrics that are capable of representing the perceptual adaptations that are key to speech perception in reverberant environments (i.e., the precedence effect and SRM).

### 1.8.1 Objective Predictors of Speech Intelligibility

Objective predictors of SI generally consist of a signal analysis procedure which generates an intelligibility-related metric, and often provide a function that maps this objective metric to a prediction of subjective SI. Since the mapping between objective metrics and subjective SI ratings varies depending on the SI metric definition (e.g., phonemes or words identified correctly) and due to other factors such as participant knowledge of context, the map function is usually separate from the objective metric itself. The mapping is often non-linear due to floor and ceiling effects at 0% and 100% intelligibility respectively.

One of the earliest objective predictors is the articulation index (AI) (Kryter, 1962) which estimates intelligibility from audibility by analyzing SNR across frequencies. Under the assumption that speech has a dynamic range of approximately 30 dB, if SNR (plus 15 dB to get maxima of dynamic range) is greater than 30 dB at all frequencies, all speech cues are assumed to be audible, and therefore intelligibility is assumed to be perfect. AI splits the noise and speech spectra into bands that roughly approximate human auditory filters and for each band specifies a lower and upper SNR limit corresponding to 0% and 100% audibility respectively (i.e., the articulation

window). The AI metric is computated as the percentage of the articulation window covered, with frequencies weighted by perceptual importance.

The speech intelligibility index (SII) (ASA/ANSI S3.5-1997, 1997) was provided as an extension of and replacement for AI. SII defines a generic framework for specifying signal spectrum levels, noise spectrum levels, hearing thresholds, and the measurement reference point (e.g., free field or ear drum). Additionally, it includes some simplistic modeling of the non-linearities of the auditory system, namely the upward spread of masking which occurs at higher acoustic levels. SII is calculated as:

$$\text{SII} = \sum_{i=1}^n I_i A_i$$

Where  $i$  is the frequency band index,  $n$  is the number of bands,  $I_i$  is a frequency weighting function and  $A_i$  is an audibility function. The frequency weighting is selected to represent the perceptual importance of different frequencies. The audibility function is calculated as the per-band ratio of SNR to 30 dB, to represent the fraction of speech cues in 30 dB dynamic speech that are audible. Finally the SII is limited to values ranging from 0 to 1. The speech and noise spectra are often A-weighted to better approximate human thresholds of hearing, and can be weighted differently to model hearing loss.

The speech transmission index (STI) (IEC 60268-16:2020, 2003) modified SII to estimate intelligibility by measuring changes to the spectrum of the temporal envelope rather than SNR. STI is based on the concept of the so-called modulation transfer function (MTF) which measures the ratio of temporal envelope per-bin from the input to the output of an acoustic channel. Specific narrowband test signals are used to measure MTF in octave frequency bands for a range of modulation frequencies. The

STI metric is calculated by averaging over modulation frequencies, and performing a perceptually-weighted average over frequency bands. The calculation includes adjustments for auditory thresholds, noise levels and upward spread of masking. STI has been shown to have a strong correlation to speech intelligibility under reverberation (Schepker *et al.*, 2016).

STI, and SII both focus on audibility, and apart from accounting for upward spread of masking, they do not model the non-linearities in the auditory system. Even with hearing thresholds incorporated, they do not take into account the many non-linear complexities of hearing loss which extend beyond audibility. This particularly limits their ability to assess the benefits of non-linear processing in hearing aids such as wide dynamic range compression (WDRC) and speech enhancement techniques for noise reduction. Furthermore, these metrics are all monaural and do not take into account important binaural perceptual adaptations.

To achieve better prediction of SI under non-linear signal processing techniques such as time-frequency masks for noise reduction (i.e., ideal binary masks), the short-time objective intelligibility measure (STOI) was proposed by Taal *et al.* (2010). Unlike STI and SII, which are based on stationary spectra, STOI performs a STFT-based decomposition with short time windows of approximately 400 ms. An intermediate measure of intelligibility is computed for each time-frequency region, using one-third octave bands. The measure is based on correlation of the STFT decomposition of the signal under test to a clean reference signal which has not been distorted or processed. The final STOI metric is computed by averaging the intermediate intelligibility measures across time and frequency. STOI has been shown to outperform STI and SII at

predicting SI for noisy speech with and without ideal binary masking applied. However, it does not include any modeling of the auditory system or hearing loss, and thus its performance is still limited in this regard.

More recently, several objective predictors of SI have been developed which incorporate improved modeling of the auditory system and hearing loss. The hearing aid speech perception index (HASPI), proposed by Kates and Arehart (2022), was specifically developed for evaluating the effects of hearing aid processing. Its auditory periphery model uses a fourth-order gammatone filterbank to approximate the time-frequency decomposition of the cochlea, and modulates the filter bandwidths with signal level to model cochlear non-linearities. The model accounts for upward spread of masking, active amplification by OHCs, and compression provided by the basilar membrane and OHCs. It includes a configurable hearing loss model which increases the threshold of hearing, modifies the filterbank structure to model broadening of cochlear filters, and models changes to cochlear non-linearities. The auditory model outputs a per-band temporal envelope signal (ENV) and temporal fine structure signal (TFS). The test signal is passed through the model with hearing loss configured, and a reference is acquired by passing the clean reference signal (i.e., not degraded or processed) through the model with no hearing loss. The two outputs are compared via correlation of their modulation rates on a MEL-frequency scale. HASPI has been used extensively in hearing aid research, but is still considered somewhat simplistic in the field of auditory modeling.

To take into account the benefits of binaural perceptual adaptations on SI, many monaural predictors have been extended to include a binaural front-end. The most common approach is to use an equalization-cancellation stage (EC) proposed by

Durlach (1960), which is an adaptive strategy of cancelling directional interfering noise that emulates how the brain exploits ILDs and ITDs. The EC front-end combines the binaural inputs, generating a monaural output which is then processed by a monaural predictor of SI. While an EC can be used as a binaural front-end for any monaural predictor of SI, it should be noted however that it does not model any of the reductions to binaural processing which have been shown to occur with hearing loss. Beutelmann and Brand (2006) proposed a binaural extension of SII called the binaural speech intelligibility model (BSIM), which was later improved upon by Rennies *et al.* (2022a). STI was extended with a binaural front-end by van Wijngaarden and Drullman (2008). Developing upon many previously proposed binaural extensions of STOI, Andersen *et al.* (2018) proposed the modified binaural STOI (MBSTOI). Although there has been recent development (Lavandier *et al.*, 2023), HASPI has yet to see a widely accepted binaural extension.

### 1.8.1.1 Neurologically-Motivated Objective Predictors of Speech Intelligibility

The accuracy of SI predictors can be improved by introducing more detailed auditory modeling. Bruce *et al.* (2018) provided an auditory model that includes physiologically accurate modeling of ANF firing in response to acoustic stimuli. It builds upon the auditory periphery model provided by Zilany *et al.* (2014) and includes most of the nonlinearities in auditory nerve responses such as non-linear frequency tuning due to cochlear active amplification, dynamic range compression in the BM and hair cell responses, two-tone suppression effects, level-dependent phase responses, and shifts in the peak frequency of ANF tuning curves as a function of level. Configurable

sensorineural hearing loss is also provided, including impacts on hearing thresholds and degradations to encoding due to reductions in non-linearities and broadening of frequency tuning.

The model, shown in (figure), accepts the acoustic sound pressure at the ear drum as an input, and generates ANF spike patterns at each CF along the BM as output.

(figure from bruce 2018)

ANF spike patterns are often visualized via a neurogram which is a 2D representation of spike density as a function of CF and time. Similar to a spectrogram, a neurogram describes how energy is distributed in time and acoustic frequency from a neurological perspective. As such, it provides a visual representation of spectro-temporal modulation cues which are used by the brain to decode speech.

(figure ENV Neurogram and TFS Neurogram)

Hines and Harte (2010) presented two different types of neurograms: an average discharge neurogram (i.e., mean-rate or envelope neurogram, ENV) and a fine timing neurogram (i.e., spike timing or temporal fine structure neurogram, TFS). Both are smoothed in time by filtering the spike pattern with a 50% overlap hamming window. The mean-rate neurogram uses a longer window in the order of several milliseconds, while the spike timing neurogram uses a window in the order of several microseconds. In general, mean-rate neural cues have been shown to correlate more to envelop acoustic cues, and spike timing neural cues have been correlated more to temporal fine structure acoustic cues. Hines and Harte (2010) proposed an objective speech intelligibility predictor that used image processing of neurograms to compare the neural representation of a degraded signal to a clean reference signal. The degraded neurogram represents the result of a degraded acoustic signal and/or hearing

impairment, while the clean reference represents a clean acoustic signal and normal hearing. The comparison is done using the structural similarity index (SSIM) which measures image quality based on comparison three measured parameters: luminance (i.e., intensity), contrast (i.e., variance), and structure (i.e., cross-correlation). i.e.,

$$S(r, d) = l(r, d)^\alpha + c(r, d)^\beta + s(r, d)^\gamma$$

Where  $r$  is the reference image,  $d$  is the degraded image,  $l$  is luminance,  $c$  is contrast,  $s$  is structure, and  $\alpha$ ,  $\beta$  and  $\gamma$  are weights.

Hines and Harte (2012) developed the neurogram similarity index measure (NSIM) which improved upon the SSIM, providing optimal weighting values, and separately defining the mean-rate NSIM (MR NSIM) and fine timing NSIM (FT NSIM) for the respective neurogram types. The NSIM also dropped the contrast parameter for simplicity, since it was shown to have very little correlation to subjective speech intelligibility. **To do: How is NSIM mapped to an estimate of subjective SI?**

Zilany and Bruce (2007) extended the model to better represent how the central auditory system analyzes the effective spectrogram generated by the cochlear analysis and extracts the spectro-temporal modulation cues that are used to decode speech. This process is modeled as a bank of modulation-sensitive filters (i.e., a modulation filter bank), each having a corresponding impulse response called a spectro-temporal response field (STRF). Each STRF is centred around a certain time/frequency and is sensitive to a specific spectral modulation frequency (scale, i.e., density, in cycles/oct) and a specific temporal modulation frequency (rate, i.e., velocity, in Hz). The result is a 4D complex-valued analysis generated by convolving the auditory spectrogram with the bank of STRFs. This analysis is performed on the test signal and the clean

reference signal, and the two results are compared by a 4-dimensional distance metric, resulting in the so-called spectro-temporal modulation index (STMI).

$$STMI = \sqrt{1 - \frac{\|T - N\|^2}{\|T\|^2}}$$

Where  $T$  is the template stimulus (i.e., corresponds to the clean reference), and  $N$  is the test stimulus (i.e., corresponds to the degraded signal/representation).

(STMI and NSIM figure from Wirtzfeld et al)

Wirtzfeld *et al.* (2017) performed a comparison of the STMI, mean-rate NSIM and spike-timing NSIM for estimation of subjective speech intelligibility, and found that a synthesis of STMI and spike-timing NSIM provided the most consistent results.

While the auditory modeling described in this section is monaural, making it suboptimal for evaluating reverberation, an EC front-end could be added to provide a simplistic model of binaural perceptual adaptations.

### 1.8.2 Objective Predictors of Listening Effort

As previously discussed, SI is only impacted by reverberation in severe conditions which are not typically experienced in every day life, but LE is impacted even in mild reverb. In other words as reverberation time decreases, SI increases and LE decreases, but SI eventually plateaus at 100% (figure?), while LE continues to decrease (figure?).

Objective predictors of SI such as STI continue to increase after subjective SI ratings plateau. These ceiling effects are accounted for by applying a nonlinear mapping from objective predictor of SI to subjective SI rating. However, it has been suggested that the full range of these predictors can be used to predict LE due to the strong correlation between SI and LE (Schepker *et al.*, 2016).

### 1.8.3 Objective Predictors of Speech Quality

As reviewed by Torcoli *et al.* (2021), several objective predictors of SQ have been proposed which aim to estimate subjective ratings such as MOS. Generally, this is done by extracting and analyzing quality features such as loudness, coloration, noisiness and distortion. One of the earliest and most common predictors is the perceptual evaluation of speech quality (PESQ) (ITU P.862, 2001) and its successor the perceptual objective listening quality assessment (POLQA) (ITU P.863, 2011). Both of these predictors use a simplified perceptual model that emulates the time-frequency decomposition of the cochlea, and compare the extracted quality features of the degraded signal to a clean reference signal. More recently, Hines *et al.* (2015) proposed the virtual speech quality objective listener (VISQOL) which used an improved perceptual model. VISQOL was originally developed using the NSIM to compare the degraded and clean signals, but switched to using a spectrogram rather than a neurogram, which proved to be equally effective and much less complex. Compared to PESQ and POLQA, VISQOL has been shown to be less complex and equally effective at predicting subjective SQ (Hines *et al.*, 2013). Similar to HASPI for SI, Kates and Arehart (2022) proposed the hearing aid speech quality index (HASQI), which uses the same perceptual model as HASPI to predict SQ.

## 1.9 Summary and Motivation

**TODO if needed**

# **Chapter 2**

## **De-Reverberation Literature Review**

Intro: Overview of techniques to be discussed (breakdown of categories)

## 2.1 Reverberation Suppression

### 2.1.1 Beamforming

### 2.1.2 Linear Prediction Residual Enhancement

### 2.1.3 Statistical Methods

## 2.2 Reverberation Cancellation

### 2.2.1 Invertibility of Room Impulse Response

To perfectly cancel reverberation, an equalizer filter must be designed such that the result of cascading the RIR with the equalizer is an impulse. I.e., for a RIR  $g(n)$  and an equalizer  $h(n)$ , the ideal equalized impulse response (EIR)  $d(n)$  is

$$d(n) = g(n) * h(n) = \delta(n) \quad (2.1)$$

Which in the Z-transform domain is

$$D(z) = G(z)H(z) = 1 \quad (2.2)$$

$$H(z) = \frac{1}{G(z)} \quad (2.3)$$

Therefore, the ideal equalizer would be the inverse of the RTF. However Neely and Allen (1979) showed that RTFs are typically non-minimum phase, making the realization of a causal and stable inverse impossible. The non-minimum phase nature

of RTFs is related to the acoustics of the room and the positioning of the sound source and listener. In particular Neely and Allen (1979) showed that for synthetic room acoustics, there is a threshold of wall reflectivities over which the RTF becomes non-minimum phase. Similarly, it was shown that by increasing room size, increasing source/listener separation and placing the source and listener at more symmetrical positions, the RTF was more likely to be non-minimum phase. In typical conditions (e.g., an office room), these conditions for a minimum phase RTF are not met. From a time-domain perspective, to be minimum phase the first non-zero sample of the RIR (i.e., the direct sound or first arriving reflection when there is no direct sound) must be larger than the later reflections, and the RIR must decay rapidly. Even in rooms with relatively short reverberation times (e.g., approximately 200 ms), the decay is not short enough to produce a minimum phase RTF.

For typical RIRs, the theoretical inverse systems have very long impulse responses, often being infinite length (IIR) or even two-sided IIR. This can be explained largely by RTFs having strong notches which appear as zeros very close to or on the unit circle. The resulting inverse filter therefore has poles very close to the unit circle resulting in very long decay. For this reason, equalizer filter structure selection is an important factor in performance. While a FIR equalizer will always be an approximation of the true IIR inverse, even for a minimum phase system, reasonable performance can be achieved for a long enough FIR filter. On the other hand, an IIR filter can achieve perfect equalization for minimum phase systems and often requires lower complexity than its FIR counterpart.

Additionally, perfect equalization of strong spectral notches is undesirable in practice since the equalizer will include strong peaks which will substantially amplify noise.

In the extreme case, this narrowband noise resonance was reported by Neely and Allen (1979) as an audible chime-like artifact. Furthermore, if the RTF has zeros exactly on the unit circle, this results in complete loss of content at that frequency, making it unrecoverable even in absence of background noise.

For maximum phase RTFs with zeros strictly outside the unit circle, the inverse systems are one-sided IIR, and are either causal unstable (i.e., right-sided) or acausal stable (i.e., left-sided). For mixed-phase RTFs, the inverse system is always two-sided IIR regardless of stability. Since a practical filter must be stable, the ideal equalizer would have to be acausal or two-sided. Infinitely left-sided filters are not implementable in realtime since they would require prior knowledge of infinite future data. However, it is theoretically possible to implement an infinitely left-sided filter offline, by performing two filtering operations: one in forward-time (i.e., causal filtering) and one in reverse-time (i.e., acausal filtering) (Kormylo and Jain, 1974). However, Treitel and Robinson (1966) showed that by introducing a modeling delay  $D$  to the desired EIR (i.e., equalizing to a delayed impulse) enables partial implementation of the left side of the ideal system inverse. I.e.,

$$d(n) = g(n) * h(n) = \delta(n - D) \quad (2.4)$$

$$D(z) = G(z)H(z) = z^{-D} \quad (2.5)$$

$$H(z) = \frac{z^{-D}}{G(z)} \quad (2.6)$$

This has the effect of shifting some of the acausal portion of the stable inverse filter to causal side, and greatly improve equalizer performance. Increasing modeling

delay always improves equalizer performance, but equalization is still approximate since perfect equalization would in general require infinite delay. Additionally, introduction of significant delay can reduce user experience, and can result in audible artifacts due to equalizer error, i.e., pre-ringing and pre-echo, (Brannmark and Ahlén, 2009). The design of an effective equalizer must carefully manage the tradeoff between reverberation cancellation and these other adverse perceptual effects.

Another challenge in the design of a practical room response equalizer arises from the highly non-stationary nature of the RTF, both in space and time. Mourjopoulos (1985) showed that RIR varies significantly with respect to loudspeaker and microphone location and as a result an equalizer only applies exactly within a very small spatial region (i.e., the equalized zone). It was shown that the equalized zone is smaller than the interaural distance at high frequencies. Movement of the sound source, listener and objects in the room, as well as temperature variations result in variation of the RIR over time (Omura *et al.*, 1999). For similar reasons, it has been shown that small errors in the equalizer (e.g., due to errors in the model of the RIR and due to computational error) result in significant worsening of equalizer performance, often resulting in making the effect of reverberation worse. To make equalizers more robust to variation, several design approaches have been proposed which attempt to equalize the room response at multiple locations simultaneously (Elliott and Nelson, 1989; Haneda *et al.*, 1997). This reduces equalizer performance at each individual location, but results in a more stable solution.

### **Ill-Conditioning: Add to next section (More on the context of solving for the inverse)**

In the context of dereverberation for speech perception, it is also important to

consider the perceptual benefit of early reflections which provide an effective SNR boost as previously described. Several authors have proposed modifications to existing equalizer design methods which maintain early reflections (Karjalainen and Paatero, 2006; Maamar *et al.*, 2006; Mei *et al.*, 2009). These approaches are referred to as room response reshaping, channel shortening or partial equalization.

It is also important to make a distinction between the problem of equalizing the RTF at a certain location by preprocessing the signal sent to a spatially separated loudspeaker, and equalizing the RTF locally at the microphone (e.g., on a hearing aid). **In the context of loudspeaker room equalization...**

## 2.2.2 Single Channel Room Response Equalization

### 2.2.2.1 Homomorphic Approaches to Room Response Equalization

The first approach to equalization of a non-minimum phase RTF, proposed by Neely and Allen (1979), decomposed the RTF,  $G(z)$ , into its minimum phase and allpass mixed phase components,

$$G(z) = G_{\min}(z)G_{\text{allpass}}(z) \quad (2.7)$$

and designed an equalizer,  $H(z)$ , by inverting only the minimum-phase component.

$$H(z) = \frac{1}{G_{\min}(z)} \quad (2.8)$$

The resulting EIR,  $D(z)$ , is

$$D(z) = G(z)H(z) = G_{\text{allpass}}(z) \quad (2.9)$$

The authors modeled the RTF with a FIR RIR, and estimated the minimum phase component by computing the cepstrum (i.e., the real cepstrum) of the RIR, and flipping/adding the negative quefrency cepstral coefficients with the positive quefrency coefficients. The processed cepstrum is returned to the time domain by an inverse complex cepstrum transformation. Since the real cepstrum represents a magnitude response (i.e., zero phase) and a right-sided complex cepstrum represents a minimum phase sequence, the resulting time-domain sequence represents the equivalent minimum phase representation of the original RIR. This process uses the inverse DFT to compute the equalizer, therefore the DFT size must be large enough to minimize distortions due to time domain aliasing.

This approach perfectly equalizes the magnitude response of the channel, but the excess phase response of the allpass component,  $G_{\text{allpass}}(z)$ , and as such is referred to as magnitude equalization or excess phase equalization. The residual phase is visible in the group delay, which is flat except for significant deviations near the maximum phase zeros. However it has been shown that the excess phase in the allpass component contain most of the reverberant energy and as such is not perceptually negligible (Johansen and Rubak, 1996). In other words, the allpass component is responsible for the temporal smearing of reverberation. The significant perceptual impact of this can be explained by the fact that the short term frequency spectral analysis performed by the human auditory system is sensitive to excess phase.

Perfect equalization to a delay is theoretically possible by convolving the output of the magnitude equalizer through a time-reversed version of the all-pass component (i.e., matched filter). However, for an IIR filter this will impose infinite delay, and is equivalent to the modeling delay discussed in the previous section.

The shortcomings of the excess phase equalizer proposed by Neely and Allen (1979) motivates the need for an alternative form of partial equalization which emphasizes the importance of phase equalization, i.e., makes trade off between magnitude and phase equalization. Radlovic and Kennedy (2000) and subsequently Maamar *et al.* (2006), proposed iteratively flattening the magnitude response while monitoring the excess phase response as a means to trade off the two.

### 2.2.2.2 Linear Prediction Approaches to Room Response Equalization

An alternative method for coming up with an estimate of the minimum phase component discussed in the previous section is accomplished via linear prediction. This idea has been explored by several authors, such as Mourjopoulos and Paraskevas (1991) and Haneda *et al.* (1997). In this approach, the RTF is modeled as an all-pole filter, and a FIR equalizer is designed by minimization of the error  $e(n)$  between the actual channel RIR  $g(n)$  and a predicted autoregressive model of the RIR  $\hat{g}(n)$ . I.e.,

$$e(n) = g(n) - \hat{g}(n) \quad (2.10)$$

$$= g(n) - \sum_{k=1}^p \alpha_k g(n-k) \quad (2.11)$$

$$\boldsymbol{\alpha} = \begin{bmatrix} \alpha_1 & \alpha_2 & \dots & \alpha_p \end{bmatrix} = \arg \min_{\boldsymbol{\alpha}} e(n) \quad (2.12)$$

By using the autocorrelation method for linear prediction, the minimum phase component of the RTF is estimated and is equalized by the prediction error filter. Since poles ring longer than zeros, the method also generally produces a lower order

model of the RTF peaks, and therefore also produces lower order equalizer. Compared to the FIR model in the previous section all-pole modeling of the RTF is more perceptually relevant since it does a better job of modeling high energy spectral peaks (Toole and Olive, 1988). Additionally, by focusing less on modeling the RTF notches, the all-pole model is less sensitive to their high spatial/time variance (Mourjopoulos, 1985), which is especially impactful on avoiding over amplification of noise at the frequencies of deep spectral notches (i.e., the tonal artifacts reported by Neely and Allen (1979)). The linear prediction approach also enables usage of the computationally efficient Levinson Durbin algorithm, and is a more numerically stable technique due shorter equalizer filter lengths and avoidance of temporal aliasing due to the DFT used in cepstral analysis. However, unlike the homomorphic method which separately predicts the minimum phase and all-pass components, linear prediction only predicts the minimum phase component. Therefore to equalize the excess phase (e.g., via a matched filter), the excess all-pass phase response must be estimated by other means.

### **what about covariance approach to LPC?**

#### **2.2.2.3 Frequency Domain Approaches to Room Response Equalization**

Perhaps the most obvious approach to RTF inversion is to take the DFT of the RIR, compute its inverse, and then thake the inverse DFT to compute the FIR equalizer coefficients. Authors such as Kulp (1988) have explored this topic, and the challenges and design considerations associated with it. Most importantly, DFT size must be carefully selected to minimize distortions due to temporal aliasing. Since the inverse of RTFs is generally infinite in length, aliasing cannot be completely avoided, but the amount of aliased energy can be reduced. Many authors have suggested RIR

pre-processing techniques to further mitigate this issue, such as applying a window function to emphasize key parts of the RIR (Kulp, 1988) and using regularization to reduce depth of spectral notches with the goal of reducing noise amplification (Bean and Craven, 1989; Kirkeby *et al.*, 1996). As in previous methods, delay can be introduced to partially shift the acausal portion of the RTF inverse to the causal side. Unlike the minimum phase equalization method discussed already, the frequency domain inversion directly computes the inverse to the full RTF and in absense of RIR pre-processing is not constrained. As such, it has been shown that with sufficient delay and a large enough DFT size, perfect equalization of a non-minimum phase system can be effectively achieved. Computing the inverse filter in the frequency domain additionally makes it possible to perform the deconvolution filtering process in the frequency domain, i.e., using an FFT to perform fast convolution. However, this approach is still always approximate, and is still susceptible to the issues of RTF variation in space and time, and artifacts such as noise amplification, pre-ringing and pre-echo.

#### **2.2.2.4 Least Squares Optimization Approaches to Room Response Equalization**

To better account for the importance of the all-pass component in terms of reverberant energy, several authors (e.g., Clarkson *et al.* (1985)) have proposed the usage of least squares optimization to minimize the error energy between the desired EIR  $\tilde{y}(n)$  and the achieved EIR  $y(n) = h(n) * g(n)$ . The desired EIR is set to a delayed impulse, i.e.,  $\tilde{y}(n) = \delta(n - d)$  to enable partial cancelation of the acausal portion of the ideal RTF inverse. The modeling error is thus

$$e(n) = \tilde{y}(n) - y(n) = \delta(n - d) - h(n) * g(n) \quad (2.13)$$

and the equalizer is designed to minimize the modeling error energy, i.e.,

$$I = \sum_{n=0}^N e^2(n) \quad (2.14)$$

$$h(n) = \arg \min_{h(n)} I \quad (2.15)$$

which is solved via the well known normal equations already discussed.

As previously mentioned, the selection of the delay is represents a trade off between equalizer performance, and undesirable perceptual effects such as delay and pre-ringing/pre-echo. Several authors have proposed methods for determining the optimal delay in this regard (Clarkson *et al.*, 1985; Ford, 1978).

Where the previously discussed approaches come up with a specific deterministic minimum-phase approximation of the non-minimum phase inverse, this approach uses least squares to directly minimize the modeling error, without constraining the implications on the magnitude and phase responses. The least squares approach has been shown to outperform the minimum-phase qualization in terms of excess reverberant energy (Mourjopoulos *et al.*, 1982).

**add proof that EQ of FIR channel with FIR filter is numerically impossible (matrix inversion dimensions dont work – see note on paper)**

### 2.2.3 Multiple Input-Output Inverse Theorem (MINT)

In their seminal paper Miyoshi and Kaneda (1986) proposed the multiple-input/output inverse theorem (MINT), which performed RTF equalization by exploiting multiple acoustic channels, i.e., multiple spatially separated loudspeakers and/or microphones. Two separate forms for MINT equalizers were presented, and their applications were described as sound reproduction and dereverberation (figure).

(figure sound reproduction vs dereverberation)

Sound reproduction describes a multiple-input single-output (MISO) system, where each loudspeaker signal is pre-processed with a unique FIR equalizer so as to equalize the RTF at a certain location in the room. Dereverberation describes a single-input multiple-output (SIMO) system where the microphone signals are filtered and summed, with the intention obtaining a clean signal that can be played back elsewhere (e.g., a hearing aid loudspeaker inside the ear canal).

In the SIMO dereverberation case, which is relevant to this thesis, the solution can be derived as follows. Let  $g_i(n)$  be the length- $n$  FIR RIR corresponding to acoustic RTF between the source loudspeaker and microphone  $i$ . Let  $h_i(n)$  be the length- $m$  FIR equalizer applied to microphone  $i$  before summation with the other channels.

$$G_i(z) = Z\{g_i(n)\} = \sum_{k=0}^{n-1} g_i(k)z^{-k} \quad (2.16)$$

$$H_i(z) = Z\{h_i(n)\} = \sum_{k=0}^{m-1} h_i(k)z^{-k} \quad (2.17)$$

(2.18)

The inverse filtering problem can be stated in matrix form as

$$G\mathbf{h} = \mathbf{d} \quad (2.19)$$

$$G\mathbf{h} = \begin{bmatrix} G_1 & G_2 & \dots & G_N \end{bmatrix} \begin{bmatrix} \mathbf{h}_1 \\ \mathbf{h}_2 \\ \vdots \\ \mathbf{h}_N \end{bmatrix} = \begin{bmatrix} d(0) \\ d(1) \\ \vdots \\ d(m+n-2) \end{bmatrix} = \mathbf{d} \quad (2.20)$$

Where  $\mathbf{h}_i$  is the vector form of the FIR equalizer applied to microphone  $i$ , i.e.,

$$\mathbf{h}_i = \begin{bmatrix} h_i(0) & h_i(1) & \dots & h_i(m-1) \end{bmatrix}^T \quad (2.21)$$

and  $G_i$  is the filter matrix (i.e., the Sylvester matrix) corresponding to the convolution of  $g_i(n)$  with  $h_i(n)$ , i.e.,

$$G_i = \begin{bmatrix} g_i(0) & 0 & 0 & \dots & 0 \\ g_i(1) & g_i(0) & 0 & \dots & 0 \\ g_i(2) & g_i(1) & g_i(0) & \dots & 0 \\ \vdots & \vdots & \vdots & \ddots & \vdots \\ g_i(n-1) & g_i(n-2) & g_i(n-3) & \dots & 0 \\ 0 & g_i(n-1) & g_i(n-2) & \dots & 0 \\ 0 & 0 & g_i(n-1111) & \dots & 0 \\ \vdots & \vdots & \vdots & \ddots & \vdots \\ 0 & 0 & 0 & \dots & g_i(n-1) \end{bmatrix} \in \mathbb{R}^{(m+n-1) \times m} \quad (2.22)$$

To achieve perfect zero-delay equalization, the desired EIR should be  $d(n) = \delta(n)$ , and therefore

$$\mathbf{d} = \begin{bmatrix} 1 & 0 & \dots & 0 \end{bmatrix}^T \quad (2.23)$$

Since  $G \in \mathbb{R}^{(m+n-1) \times Nm}$ , equation 2.19 represents a problem with  $m + n - 1$  equations and  $Nm$  variables. A perfect solution exists provided  $G$  is invertible, which requires that it is square and full rank. For  $G$  to be square, that the equalizer filter length,  $m$ , must be

$$m = \frac{n-1}{N-1} \quad (2.24)$$

Provided  $G$  is full rank, the MINT can be computed as

$$\mathbf{h} = G^{-1}\mathbf{d} \quad (2.25)$$

For  $m < \frac{n-1}{N-1}$ , the problem is overdetermined and no perfect solution exists, i.e., it can only be solved by least squares. However, for  $m > \frac{n-1}{N-1}$ , the problem is underdetermined and therefore has infinite perfect solutions provided its rank is greater than or equal to the number of columns/unknowns. In this case the pseudo-inverse can be used to select the minimum norm solution. I.e.,

$$\mathbf{h} = G^+ \mathbf{d} = G^T (G G^T)^{-1} \mathbf{d} \quad (2.26)$$

**Confirm that this form of the psuedo inverse is required for solving an underdetermined system, and is different from the other form which is used for solving an overdetermined system (i.e., least squares)**

Therefore, for the SIMO dereverberation case, the equalizer filter length,  $m$  is required to be

$$m \geq \frac{n-1}{N-1} \quad (2.27)$$

where  $m$  is the length of the individual FIR equalizers,  $n$  is the length of the individual FIR channels, and  $N$  is the number of microphones. Note that although the individual FIR channels are not necessarily the same length, they can be zero padded to the longest length.

Equivalently, for the MISO sound reproduction case, the equalizer filter length requirement was shown to be

$$m >= \frac{n-1}{M-1} \quad (2.28)$$

where  $M$  is the number of loudspeakers.

Miyoshi and Kaneda (1986) proved that in order to be invertible (i.e., in order for  $G$  to be full rank), there could not be any zeros that were common to all RTFs. It was therefore shown that a MINT equalizer can achieve perfect zero-delay equalization, even when the individual RTFs are non-minimum phase, provided the equalizer filter lengths are sufficiently long and the individual RTFs do not have common zeros anywhere in the z-plane. This result is different from single channel methods which only approach perfect equalization of non-minimum phase channels as the modeling delay approaches infinity.

It is interesting to note that FIR channels would inheritly have inverse filters that are all-pole and therefore IIR. Single channel FIR equalization of a FIR channel will thus always be approximate, even if the channel is minimum phase. This makes sense intuitively, but Miyoshi and Kaneda (1986) also proved this numerically by demonstrating that the matrix formulation of the single channel equalization problem is always overdetermined regardless of equalizer filter length. Remarkably, the MINT can acheive perfect equalization of a FIR channel with individual FIR equalizer filters that are shorter in length than the FIR channels. It is important to remember that real RTFs are not generally speaking FIR, so the MINT is still approximate. However, for a sufficiently long FIR measurement of the true RIR, the residual reflections may be considered negligible. The MINT was proven to greatly outperform the single channel least squares equalization method, acheiving more than 40 dB additional reverberation attenuation accross all frequencies.

In an extended discussion of the MINT, Miyoshi and Kaneda (1988) explored the MIMO case for sound reproduction as shown in (figure)  
 (figure MIMO MINT)

They proved that it is possible to perform sound reproduction at  $N$  listening positions using  $M$  loudspeakers provided the channels had no common zeros,

$$M > N \quad (2.29)$$

and

$$m >= \frac{N(n-1)}{M-N} \quad (2.30)$$

In an extension of the MINT, Nakajima *et al.* (1997) proposed the indefinite MINT filter (IMF) which exploits the additional degrees of freedom gained when the FIR equalizer length  $m$  is strictly greater than its minimum required length. In this underdetermined case, there are infinite solutions. While the classical MINT recommended using the pseudo inverse to compute the minimum norm solution, IMF makes use of the additional degrees to equalize nearby points. This has the effect of expanding the equalized zone and improving robustness to spatial variation of the RTF.

### 2.2.4 Blind Deconvolution Problem

The RTF equalization approaches discussed in the previous section were reliant on having prior knowledge of the RIR (e.g., by measurement). However, typically in the context of dereverberation, the RIR is not known and must be estimated by other

means. The approaches to estimation of an unknown linear system can be divided into supervised methods (i.e., trained/supervised deconvolution) and unsupervised methods (i.e., blind/unsupervised deconvolution).

#### 2.2.4.1 The Wiener Filter (Supervised Optimal Filtering)

Traditional supervised optimal filtering is formulated as the selection of a filter  $H(z)$  which, for a known input sequence  $x(n)$ , produces a output  $y(n)$  that is optimally close (in a mean-squared error sense) to a desired/reference signal  $d(n)$ . I.e., the goal is to design  $H(z)$  such that the energy in the error signal  $e(n) = d(n) - y(n)$  is minimized.

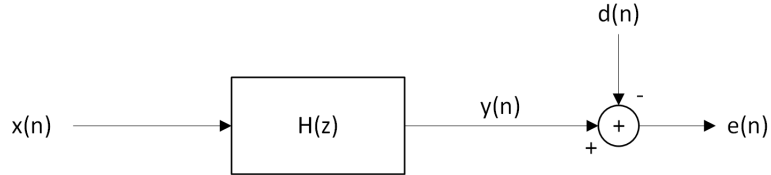


Figure 2.1: Block diagram for supervised optimal filtering, which attempts to produce a desired output,  $d(n)$ , from a known input,  $x(n)$

When applied to system equalization (e.g., RTF equalization), as depicted in Figure 2.2, the desired/reference signal is the input to the unknown system, i.e.,  $d(n) = s(n)$ , and input to the equalizer filter,  $H(z)$ , is the output of the unknown system, i.e.,  $x(n) = m(n)$ .

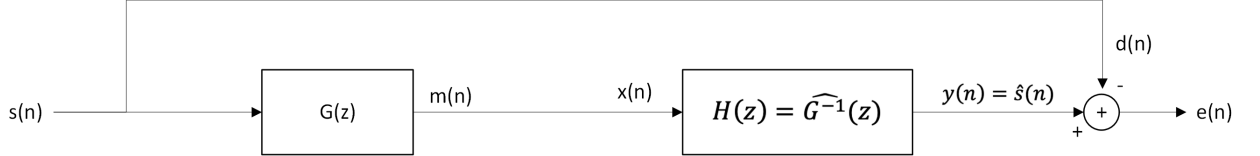


Figure 2.2: Block diagram for supervised inverse filtering / equalization, which attempts to produce reproduce the known input,  $s(n)$ , to an unknown system  $G(z)$ , from the measured system output,  $m(n)$ , using a filter,  $H(z)$

The derivation for this optimal solution, originally proposed by Wiener (1949), is performed in a stochastic framework using expectations for computing mean-squared error. The resulting solution is referred to as the Wiener filter. Considering a length- $N$  FIR filter,  $H(z) = \sum_{k=0}^{N-1} h_k z^{-k}$ , this is mathematically formulated as

$$\mathbf{x}(n) = \begin{bmatrix} x(n) & x(n-1) & \dots & x(n-N+1) \end{bmatrix}^T \quad (2.31)$$

$$\mathbf{h} = \begin{bmatrix} h_0^* & h_1^* & \dots & h_{N-1}^* \end{bmatrix}^T \quad (2.32)$$

$$e(n) = d(n) - y(n) = d(n) - \mathbf{h}^H \mathbf{x}(n) \quad (2.33)$$

$$J(\mathbf{h}) = E [|e(n)|^2] = E [e(n)e^H(n)] \quad (2.34)$$

$$J(\mathbf{h}) = E \left[ (d(n) - \mathbf{h}^H \mathbf{x}(n)) (d(n) - \mathbf{h}^H \mathbf{x}(n))^H \right] \quad (2.35)$$

$$J(\mathbf{h}) = \sigma_d^2 - \mathbf{h}^H \mathbf{p} - \mathbf{h}^T \mathbf{p}^* + \mathbf{h}^H R \mathbf{h} \quad (2.36)$$

Where  $\mathbf{p} = E [\mathbf{x}(n)d^*(n)]$  is the cross-correlation vector between the input process and the desired/reference process, and  $R = E [\mathbf{x}(n)\mathbf{x}^H(n)]$  is the autocorrelation matrix of the input process.

Since the highest-order factor in Equation 2.36, i.e.,  $\mathbf{h}^H R \mathbf{h}$  is a quadratic form and the autocorrelation matrix  $R$  is Hermitian positive semidefinite (assuming the input

process is stationary),  $J(\mathbf{h})$  represents a quadratic bowl in  $N + 1$  dimensions with exactly one global minimum. This minimum can be found by taking the derivative of the cost function and setting it equal to zero. I.e.,

$$\frac{\partial J(\mathbf{h})}{\partial \mathbf{h}^*} = 0 \quad (2.37)$$

$$R\mathbf{h} = \mathbf{p} \quad (2.38)$$

Equation 2.38 is referred to as the Wiener-Hopf equation and can be solved by any number of methods for solving systems of linear equations. This equation can also be viewed as a stochastic extension of the LS normal equations, and equivalently the Yule-Walker equations in linear prediction. I.e., the Wiener filter is optimal for known stationary processes, whereas the LS normal equations produce a filter that is optimal for a known set of data.

In practice the statistical correlation functions that make up  $\mathbf{p}$  and  $R$  in the Wiener-Hopf equations must be estimated from a finite set of data, and given certain short-term estimation techniques, the Wiener-Hopf equations become identical to the LS normal equations.

The conditioning of the Wiener-Hopf equation is dictated by the eigenvalue spread of the autocorrelation matrix,  $R$ , which has been shown to be correlated to the dynamic range of the input spectrum (i.e., the “peakiness”). When the input process is white, the eigenvalue spread is equal to 1, and the autocorrelation matrix is the identity matrix. When the input sequence is coloured, the non-zero off-diagonal auto-correlation values result in a larger eigenvalue spread (i.e., higher condition number), which can lead to a less numerically stable solution.

In practice there is always additional sensor noise present which interferes with the measured input,  $x(n)$ , and/or error signal,  $e(n)$ . This interference leads to additional misadjustments of the final solution due to distortions in the autocorrelation matrix.

The Wiener filter has also been extended to the optimal derivation of an IIR filter (i.e., the unconstrained Wiener filter), which results in the following frequency domain solution.

$$\mathbf{h}(e^{j\omega}) = \frac{\Phi_{dx}(e^{j\omega})}{\Phi_{xx}(e^{j\omega})} \quad (2.39)$$

Where  $\Phi_{dx}(e^{j\omega})$  is the cross-PSD of  $d(n)$  and  $x(n)$ , and  $\Phi_{xx}(e^{j\omega})$  is the PSD of  $x(n)$ .

The Wiener filter and all resulting adaptive extensions can be applied to both transversal filters (as described above) and linear combiners (e.g., beamforming).

#### 2.2.4.2 Supervised Adaptive Filtering

To allow tracking of time-varying systems, adaptive algorithms have been proposed which aim to converge on the Wiener filter. Adaptive filtering theory leverages the fact that the MSE cost function forms a quadratic error surface, and generally performs some form of gradient descent to make iterative steps towards the optimal solution. A detailed discussion of the details of adaptive filtering theory can be found in Farhang-Boroujeny (2013), but an overview of the most common algorithms will be provided below.

The steepest descent algorithm (SD) estimates the gradient,

$$\nabla J(\mathbf{h}) = \frac{\partial J(\mathbf{h})}{\partial \mathbf{h}^*} = \frac{\partial E [e(n)e^H(n)]}{\partial \mathbf{h}^*} \quad (2.40)$$

of the MSE error surface and steps in the direction opposite to it. The shape of

the error surface is dictated by the eigenvalue spread of the autocorrelation matrix for the input sequence, and therefore also the peakiness of the input spectrum. For a white input spectrum, the equal-MSE contours for the error surface are circular, and the negative gradient points directly towards the optimal solution. For more coloured/peaky spectra, the equal-MSE contours of the error surface become elongated, resulting in a negative gradient which does not point directly towards the optimal solution. The Newton descent (ND) algorithm modified SD by deriving the optimal vector-valued step such that the direction of iteration always points directly to the optimal solution regardless of eigenvalue spread

Both SD and ND require estimation of the autocorrelation matrix,  $R$ , and the cross-correlation vector,  $p$ . This is computationally expensive, and also it is common for the desired/reference process to be unknown (i.e., only the error sequence is known), making the cross-correlation vector,  $p$ , impossible to estimate. This motivated the usage of the stochastic gradient which is computed solely based on the measured error sequence. The stochastic gradient, defined as

$$\frac{\partial (e(n)e^H(n))}{\partial \mathbf{h}^*} = -\mathbf{x}(n)e^*(n) \quad (2.41)$$

,

represents an instantaneous stochastic estimate of the true gradient,  $\frac{\partial E[e(n)e^H(n)]}{\partial \mathbf{h}^*}$ .

The commonly used least-mean-squares (LMS) algorithm, steps in the direction of the negative stochastic gradient, using the filter update equation

$$\mathbf{h}(n+1) = \mathbf{h}(n) - \mu \frac{\partial (e(n)e^H(n))}{\partial \mathbf{h}^*(n)} = \mathbf{h}(n) + \mu \mathbf{x}(n)e^*(n) \quad (2.42)$$

Where  $\mu$  is the step size used to control the rate of adaptation.

The LMS algorithm is very low complexity, does not require prior knowledge/estimation of the statistics of the input process or desired/reference process, and its adaptation trajectory has been shown to match (in the ensemble average) that of the steepest descent algorithm. However, the step size must be carefully selected based on an estimate of the eigenvalue spread of the input process to ensure stable convergence.

The Normalized LMS (NLMS) algorithm added a step size that was normalized based on input signal energy so that a standard step size of  $\mu = 1$  could always be considered optimal (in practice  $\mu < 1$  is often required due to numerical error). The NLMS update equation is

$$\boldsymbol{h}(n+1) = \boldsymbol{h}(n) + \mu(n)\boldsymbol{x}(n)e^*(n) = \boldsymbol{h}(n) + \frac{\mu}{\boldsymbol{x}^H(n)\boldsymbol{x}(n) + \varphi}\boldsymbol{x}(n)e^*(n) \quad (2.43)$$

Where  $\varphi$  is a small regularization offset used to avoid filter divergence during periods of very low input energy (i.e., to avoid effective division by zero).

Separate from gradient-based algorithms described above, the recursive least squares (RLS) algorithm forms an adaptive extension of least squares optimization. This data-centric approach minimizes deterministic total-squared-error for the specific data observed. RLS performs LS optimization over all data observed since the start of time, with an added forgetting factor to allow tracking of time-varying systems.

As was the case with Wiener filtering, in practice there is additional sensor noise present in the measured input signal,  $x(n)$ , and/or error signal,  $e(n)$ , which interferes with the adaptation and leads to misadjustments. This can be particularly problematic when the interfering noise is correlated with itself.

All adaptive algorithms are derived in the complex domain to allow implementation in the frequency domain and subband domain. Adaptation in the frequency/-subband domain is often desirable for computational efficiency and to allow control of the adaptation on a frequency-selective basis. Additionally, convergence tends to be faster in the frequency/subband since narrowband signals tend to have flatter spectra than wideband signals. However, the DFT/Inverse DFT or subband filterbank adds computational complexity and memory of its own, and increases system latency which may not be desirable.

#### 2.2.4.3 Blind Deconvolution

Blind deconvolution (i.e., unsupervised inverse filtering) refers to the problem of equalization (Figure 2.2) when the input,  $s(n)$ , to the unknown system,  $G(z)$ , is unknown. According to the previous discussion, this implies that the desired output of the equalizer being designed is unknown, and equivalently the error signal is also unknown. For completeness, measurement noise,  $v(n)$ , is included.

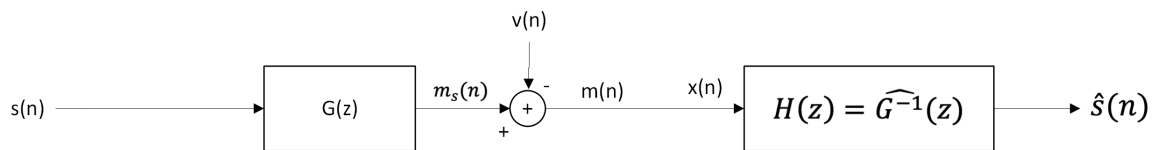


Figure 2.3: Block diagram for supervised blind deconvolution, which attempts to produce reproduce the unknown input,  $s(n)$ , to an unknown system  $G(z)$ , from the measured system output,  $m(n)$ , including additive noise  $v(n)$ , using a filter,  $H(z)$

Speech dereverberation is generally a blind problem since the source is a human talker, and the corresponding speech signal is only measured at the listening point (i.e., only the RTF system output is available). This creates a challenging problem

since the system input,  $s(n)$ , and system itself,  $G(z)$ , are both unknown and must be derived from the measured signal at the output,  $m(n)$  (i.e., microphone signal). Therefore, there is an ambiguity as to whether the poles and zeros of the measured output signal correspond to the input signal or the system.

In the context of blind wireless channel equalization, the unknown source often falls into a discrete set of known symbols that are stationary within a symbol period. This can be exploited to make assumptions about the source when estimating the system. Conversely, in speech dereverberation, the speech signal is virtually arbitrary and highly non-stationary, making the problem even more challenging.

Additionally, as discussed in Section 2.2.1, reverberant channels vary significantly with respect to spatial location and slight misadjustments to the equalizer can result in making the effects of reverberation worse. This spatial variance results in a highly time-varying channel, which must be tracked adaptively. Also, as discussed, RTFs tend to be non-minimum-phase thus not having a causal stable single-channel inverse, and may have strong or perfect zeros which can result in severe narrowband noise amplification.

As with traditional supervised system equalization, interfering noise can result in miconvergence of the inverse filter, and must be handled accordingly.

Lastly, since reverberation times can be in the order of several seconds, resulting in sampled RIRs spanning thousands or even tens of thousands of taps, computations in reverberation cancellation also tend to be very complex and sensitive to numerical error.

#### 2.2.4.4 Practical Blind Deconvolution in Wireless Systems

The topic of blind deconvolution originated in geophysics and wireless communication, and has been studied extensively in these fields. A full discussion of the topic of blind wireless channel inversion can be found in Ding and Li (2018), but some of the most common practical approaches will be summarized here. As will be shown, these approaches generally rely on assumptions about the source signal which do not hold in the context of speech dereverberation.

In wireless systems, where the input signal is controlled by a radio base station and the output is detected by a mobile phone, often a periodic training sequence (i.e., a reference symbol) is used as a reference for performing periodic supervised adaptive channel estimation. However to provide continuous tracking of the time-varying channel without using too much channel bandwidth for reference symbols, additional unsupervised adaption is often employed.

The first unsupervised approach, proposed by Lucky (1965), was the so-called decision-directed approach, in which the system which toggled between supervised and unsupervised adaptation periodically. A non-linear decision device at the output of the equalizer was used to select the most likely symbol (e.g., closest symbol in the magnitude-phase symbol constellation), and during periods of unsupervised adaptation this estimated symbol was used as the desired equalizer output to make adaptations. This concept was highly reliant on the theory of Bussgang statistics which allows important assumptions about the statistics of a stochastic process before and after a memoryless non-linear operation. This approach has been shown to work well provided the channel is slowly time-varying and there is minimal misconvergence during supervised training so that deviations during unsupervised training

are minimal. Building on this concept the Sato method (Sato, 1975) and the Constant Modulus algorithm (Godard, 1980) were proposed which improved robustness to larger deviations by adapting using an error metric between measured signal and the set of possible symbols, instead of a hard symbol decision.

These algorithms laid the groundwork for the approaches used in practice, most of which rely on the fact that the transmitted symbols may only fall into a set of known symbols. This assumption of course does not hold for speech dereverberation where the source signal is highly non-stationary speech. Truly blind adaptation without exploiting knowledge of a symbol dictionary, which has applications in speech dereverberation, will be explored in the subsequent sections.

### **2.2.5 HOS Methods for Blind Deconvolution**

### **2.2.6 SOS Methods for Blind Deconvolution**

#### **2.2.6.1 Subspace Methods**

#### **2.2.6.2 MC-LPC-based approaches**

#### **2.2.6.3 STFT Spectrum Estimation (Furuya 2007)**

#### **2.2.6.4 Estimation Theory Approaches (BSI using estimation theory)—**

### **2.2.7 Adaptive Implementations**

### **2.2.8 Subband Implementations**

# Chapter 3

## Delay and Predict Dereverberation Parameters

### 3.1 Multi-channel Linear Prediction Order

MINT Results

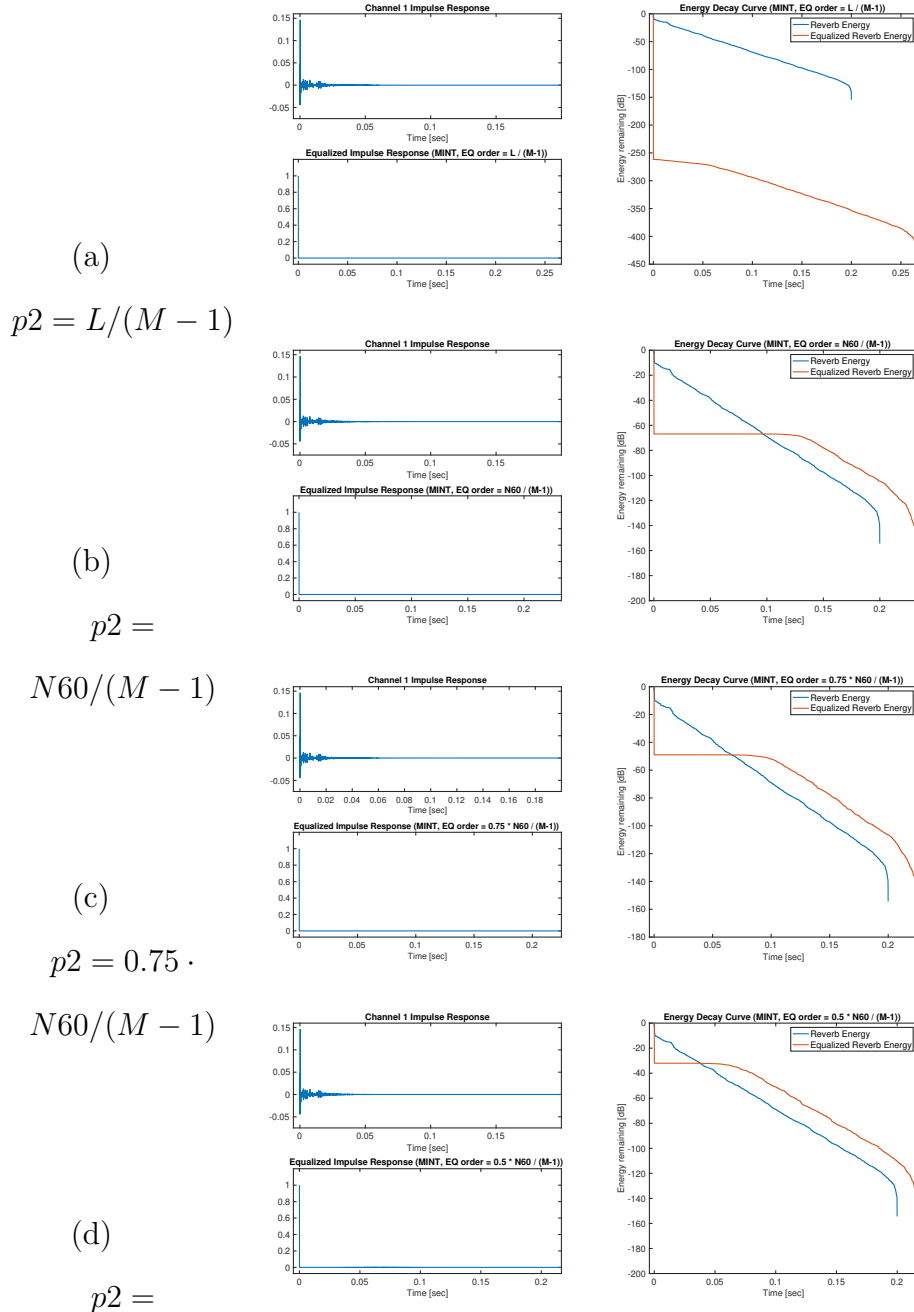


Figure 3.1: MINT equalizer performance for various equalizer orders relative to the actual length of the FIR channel ( $L$ ) and the number of samples corresponding to the T60 of the channel ( $N60 = T60 * \text{sample rate}$ )

Test Conditions for all: - Source Signal = SA1.WAV - Source length = 348366 - RIR = MYRiAD SAL Measured RIR ( $T_{60} = 2100$  msec, Truncated Exponentially to  $T_{60} = 100$  msec) - RIR length = 3200 -  $T_{60} = 100$  msec ( $N_{60} = 1600$  samples) - SNR = 300 dB - Noise Signal = office ventilation - SIR = Inf dB - Interference Signal = None

Delay-and-Predict config: - Number of Microphones ( $M$ ) = 4 - Source whitening order ( $p_1$ ) = 4000 - Multichannel Linear Prediction order ( $p_2$ ) = varied - Source whitening Enabled? = 1 - Source whitening on clean speech? = 1

### **Source Whitening stage, the same in all tests ( $p_1 = 4000$ )**

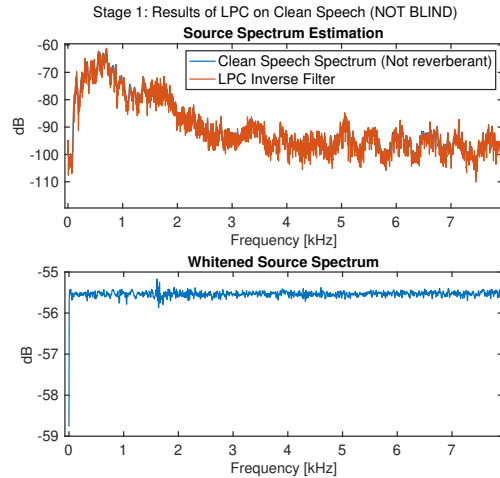


Figure 3.2: Source whitening results using a  $p_1 = 4000$  order linear predictor. The prediction error filter coefficients were computed based on clean speech and the same filter was used in all tests in this section to assess the multichannel prediction stage of the delay-and-predict algorithm in isolation.

### **$p_2 = L / (M-1)$ (MINT Condition)**

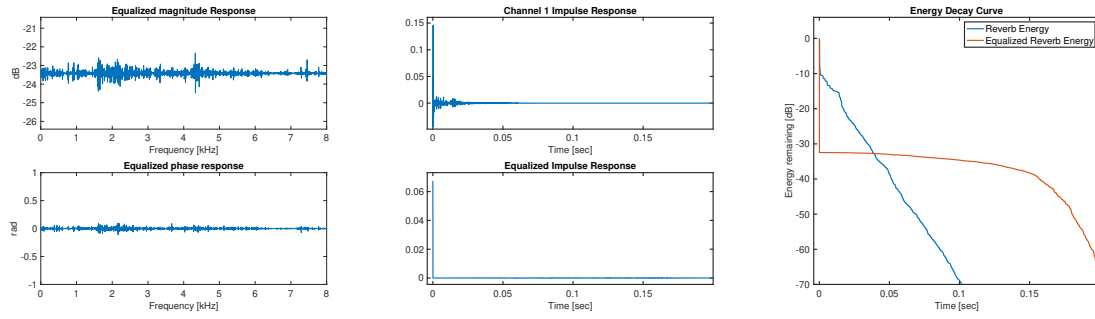


Figure 3.3: Delay-and-Predict dereverberation performance with multichannel linear prediction order  $p2 = L / (M-1)$ , where  $L$  is the FIR RIR length and  $M$  is the number of channels. Figure 3.2 shows the common source whitening filter used.

**Comparison:**  $p2 = [L \ N60 \ 0.75*N60 \ 0.5*N60] / (M-1)$

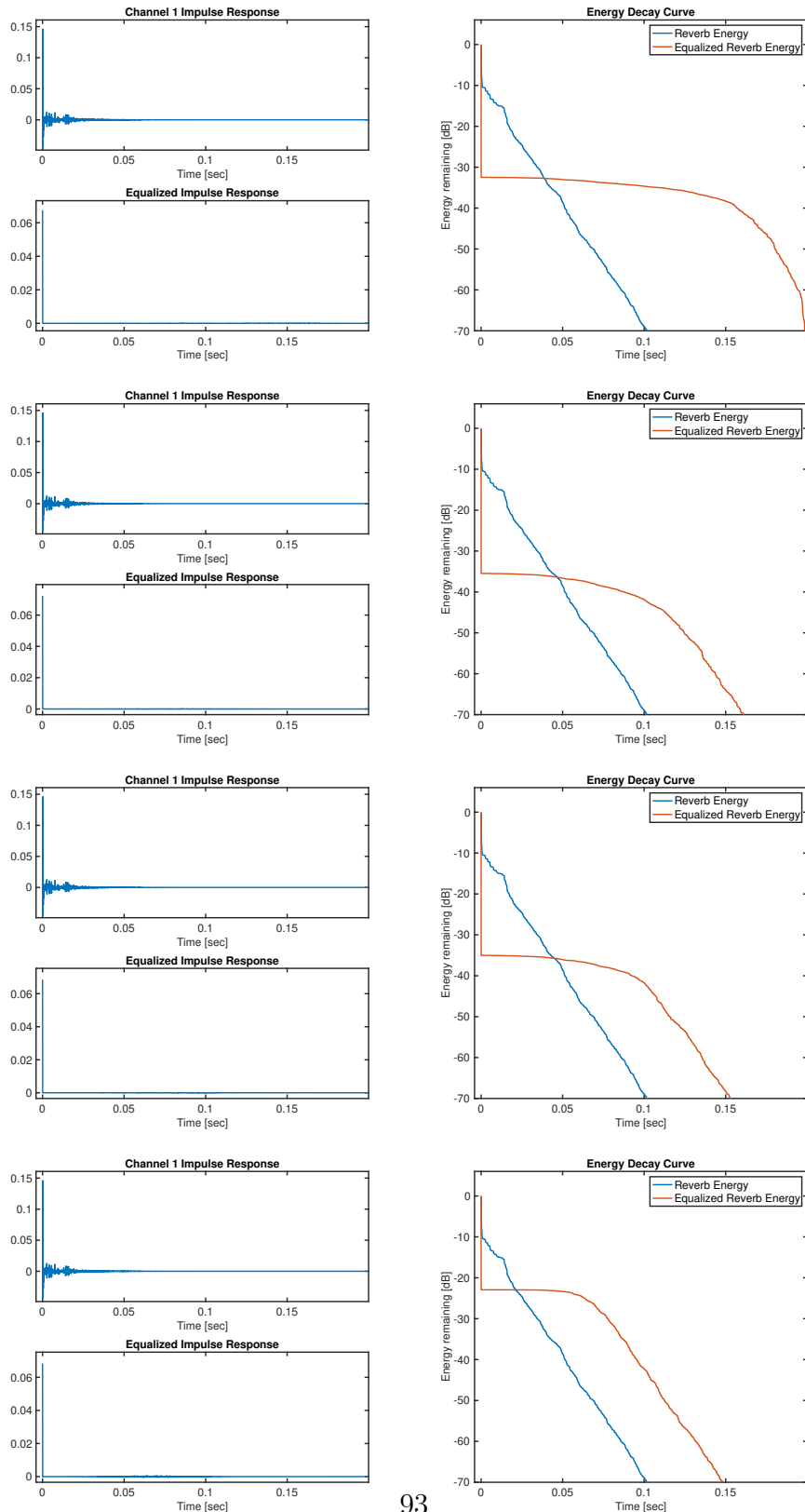


Figure 3.4: Delay-and-Predict dereverberation performance with various multichannel linear prediction orders ( $p_2$ ) relative to the actual length of the FIR channel ( $L$ ) and the number of samples corresponding to the T60 of the channel ( $N_{60}$ ). Figure 3.2

### 3.2 Source Whitening Linear Prediction Order

Test Conditions: - Source Signal = SA1.WAV - Source length = 348366 - RIR = MYRiAD SAL Measured RIR ( $T_{60} = 2100$  msec, Truncated Exponentially to  $T_{60} = 100$  msec) - RIR length = 3200 -  $T_{60} = 100$  msec ( $N_{60} = 1600$  samples) - SNR = 300 dB - Noise Signal = office ventilation - SIR = Inf dB - Interference Signal = None

Delay-and-Predict config: - Number of Microphones (M) = 4 - Source whitening order (p1) = varied - Multichannel Linear Prediction order (p2) = 533 ( $N_{60} / (M-1)$ ) - Source whitening Enabled? = 1 - Source whitening on clean speech? = 1

**p1 = 200 (Original Paper)**

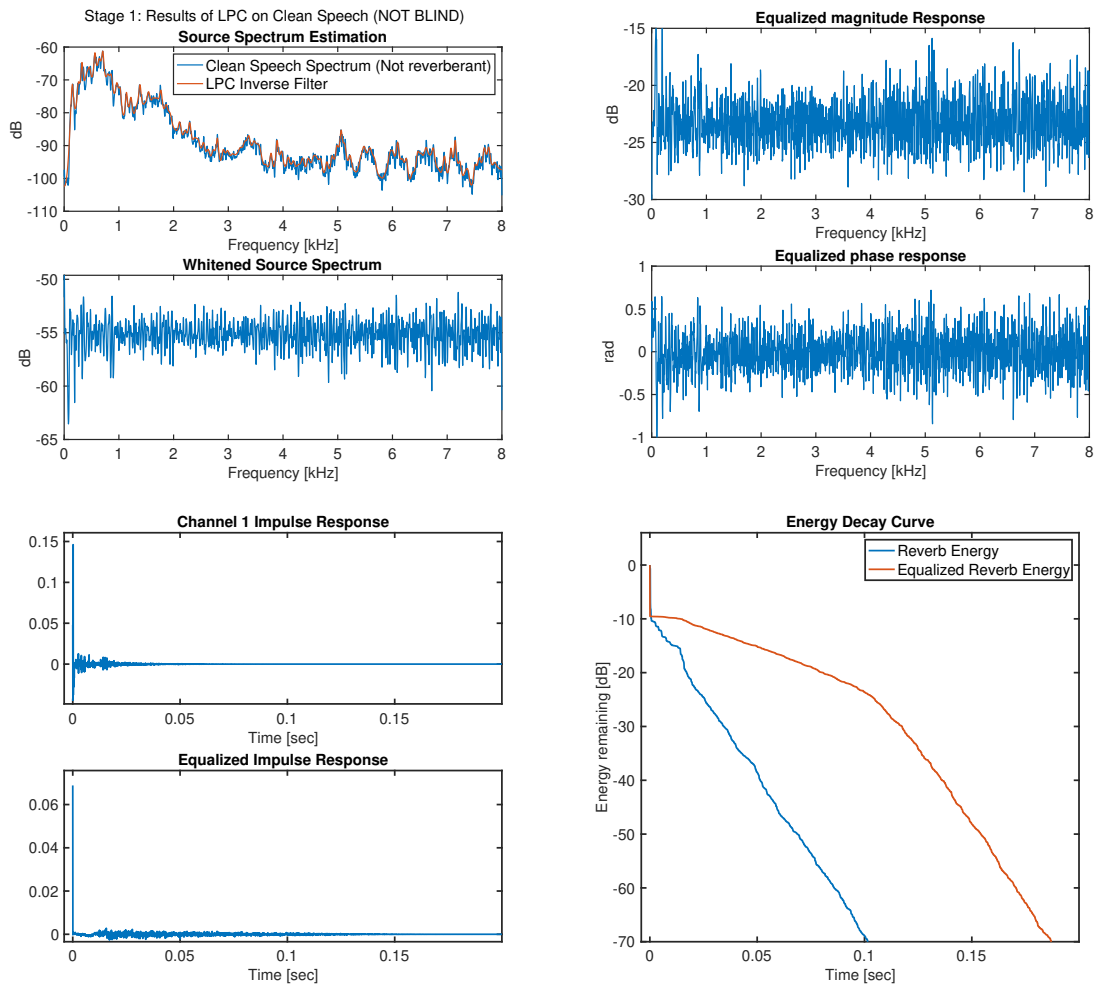


Figure 3.5: Delay-and-Predict dereverberation performance with source whitening prediction order  $p_1 = 200$  and multichannel linear prediction order  $p_2 = N60 / (M-1)$ .

**Comparison:**  $p_1 = [200 \ 1000 \ p_2 * (M-1) \ 2 * p_2 * (M-1)]$

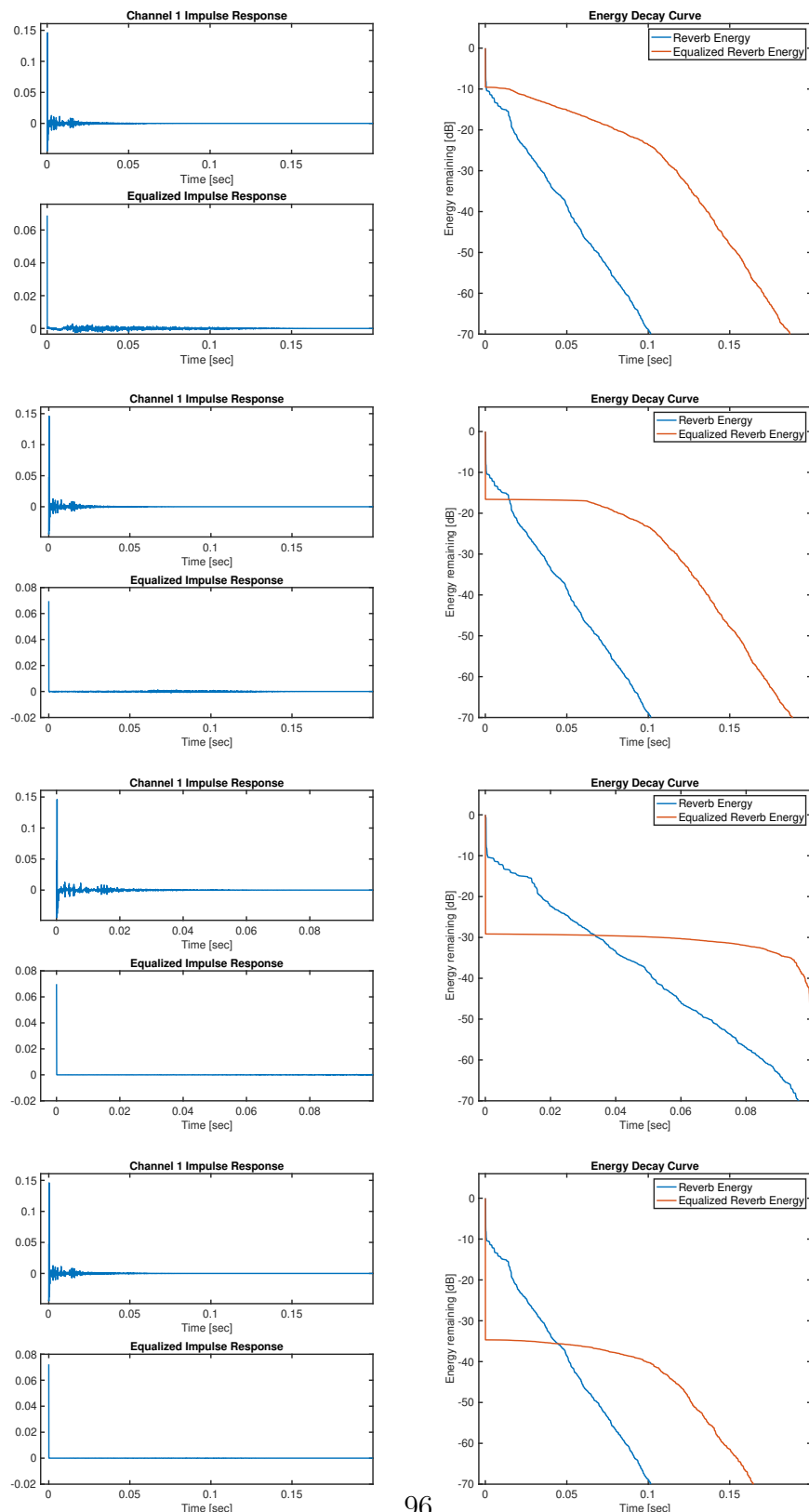


Figure 3.6: Delay-and-Predict dereverberation performance with various source whitening prediction orders ( $p_1$ ) relative to the multichannel linear prediction order  $p_2 = N60 / (M-1)$

... beyond about  $p_1 = 1.25 * p_2 * (M-1)$  EDC performance saturates at approximately -35 dB reverb attenuation.

### 3.3 Blind Deconvolution Performance

Compare Spectrogram/EDC of Blind DAP, Supervised DAP and MINT

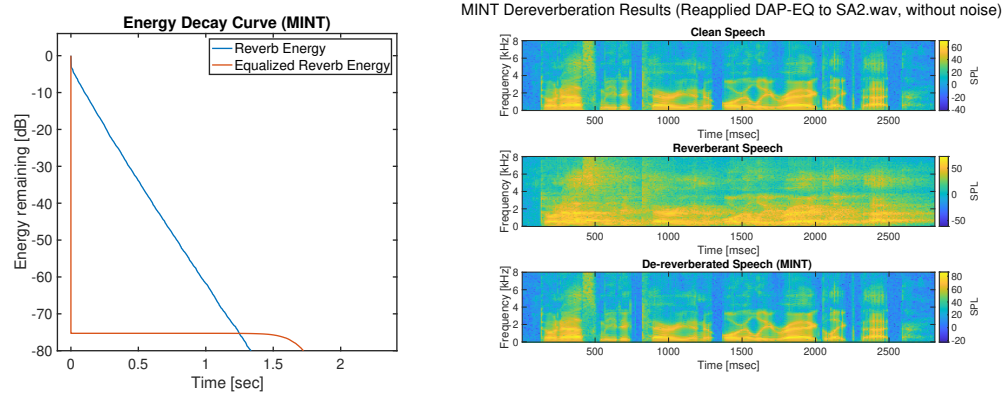


Figure 3.7: MINT Equalizer performance (EDC and Spectrogram)

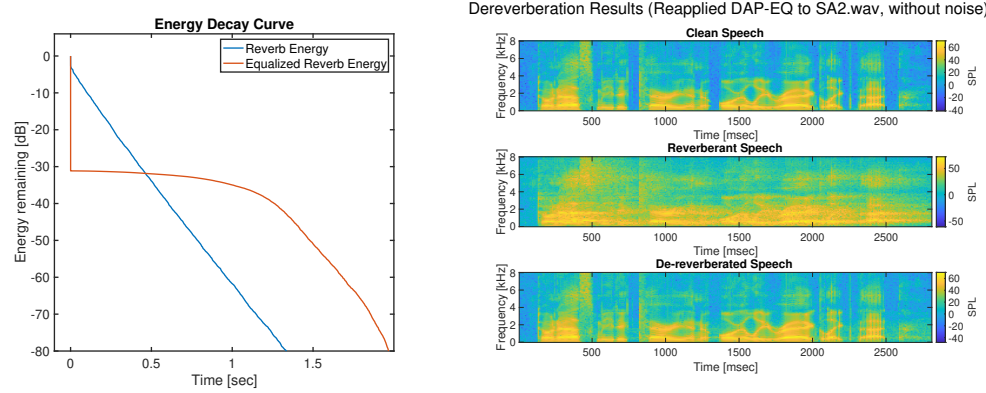


Figure 3.8: Delay-and-Predict Equalizer performance (EDC and Spectrogram) with the source-whitening filter computed using clean speech (i.e., not blind)

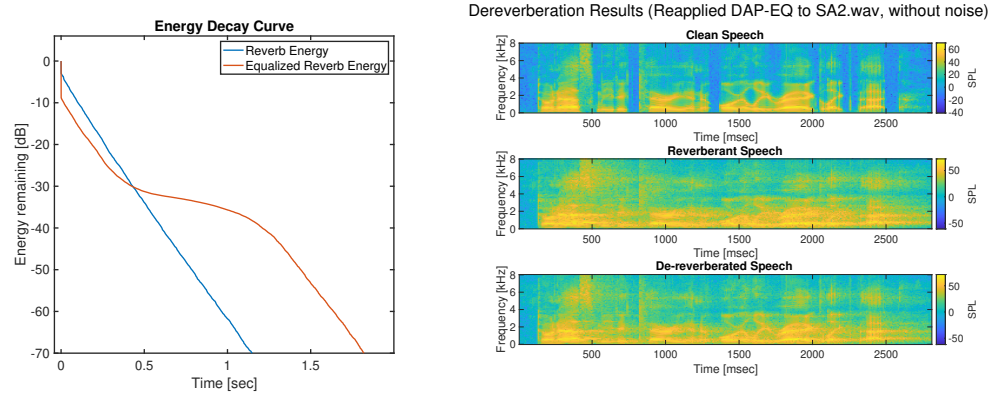


Figure 3.9: Delay-and-Predict Equalizer performance (EDC and Spectrogram) with the source-whitening filter computed using reverberant speech (i.e., blind)

## 3.4 Source Properties

### 3.4.1 Source Data Length

Test: Same spectrum different length • Run 2x with source whitening done on clean (supervised) and reverberant signals (blind) • Speech is SA1.wav looped X times • RIR = SAL truncated to 100 msec = 1600 samples, M = 4 mics • P1 =  $2 * p2 * (M-1)$  • P2 =  $N60 / (M-1)$  • Reran exact same test for longer source sequences generated by looping SA1 – Exact same spectrum just more data (excludes spectrum dependency)

**Source Data Length Compare, Length = [58061 116122 174183 232244], Blind**

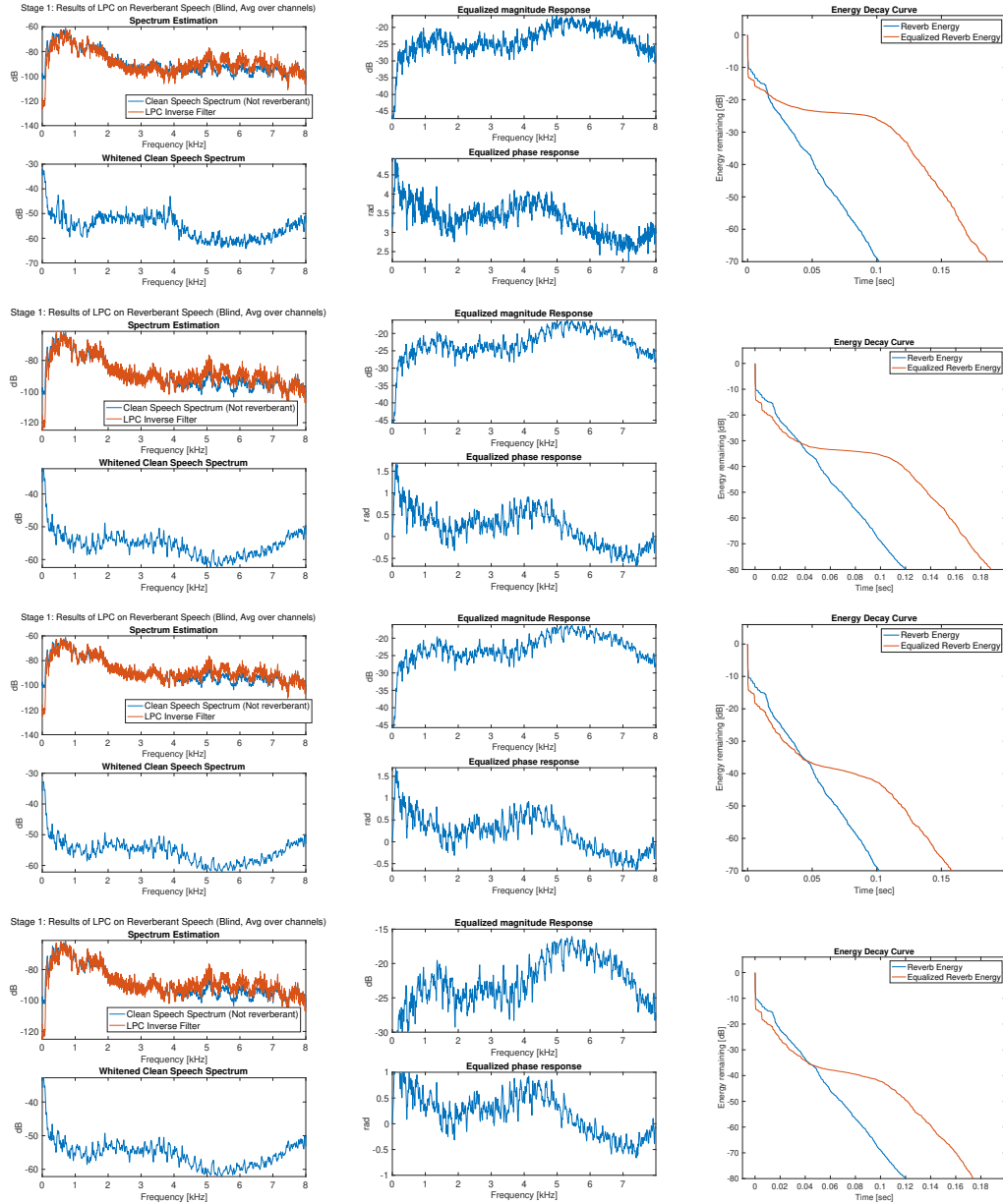


Figure 3.10: Delay-and-Predict dereverberation performance with the same speech sample (SA1.WAV, 58061 samples) looped to various data lengths to preserve the same spectrum. Source whitening prediction order was  $p_1 = 2 * p_2 * (M-1)$  and multichannel linear prediction order was  $p_2 = N60 / (M-1)$ . Source Whitening stage was performed on reverberant speech (i.e., blind).

**TODO:** Generate missing figures above, also add detailed ones to appendix, I think we can remove all the non blind ones from appendix

...EDC Performance saturates around -35 dB beyond 3 loops.

This shows the dependency of LP performance on data length (reduces correlation variance).

Conclusion: • Performance depends on data length regardless of spectrum • Note: In LPC work I've done in the past, I got good performance for very short sequences (single phonemes), but this is for a very low-order LPC (order of 8-16 poles) – a couple thoughts / explanations about this: a. Higher order LPC requires a lot of data is needed to analyze the fine time frequency characteristics (in low order, coarse resolution is sufficient to observe the location of a couple poles)? b. Higher order LPC requires a lot of data to estimate autocorrelation function out to very long lags? c. White noise filtered by a single pole (very low spectrum complexity) performs slightly better at low frequencies suggesting (a) may be partially true d. As a final test, pre-computed and saved the whitened speech signal using very long sequence, but then extracted one 1:58061 iteration, and reran on just that. No improvement in performance compared to running on Signal Length = 58061 of non-whitened speech (SA1.wav). Reinforces that the source whitening dependency on data length exists regardless of speech spectrum. \*Note: Surprising that the whitened spectrum is identical for the two cases

### 3.4.2 Source Spectrum

Test: Same length different spectrum • Source whitening done on clean speech (no blind estimation) • Test: Speech is different length white noise sequences looped

to length = 60 sec = 960000 (as original sequence length goes down, peakiness of spectrum goes up but final length doesn't change) • RIR = SAL truncated to 100 msec = 1600 samples, M = 4 mics • P1 = 2 \* p2 \* (M-1) • P2 = N60 / (M-1)

### Source Spectrum Compare, Initial White noise sequence length = [0.1 sec 1 sec 10 sec], Blind

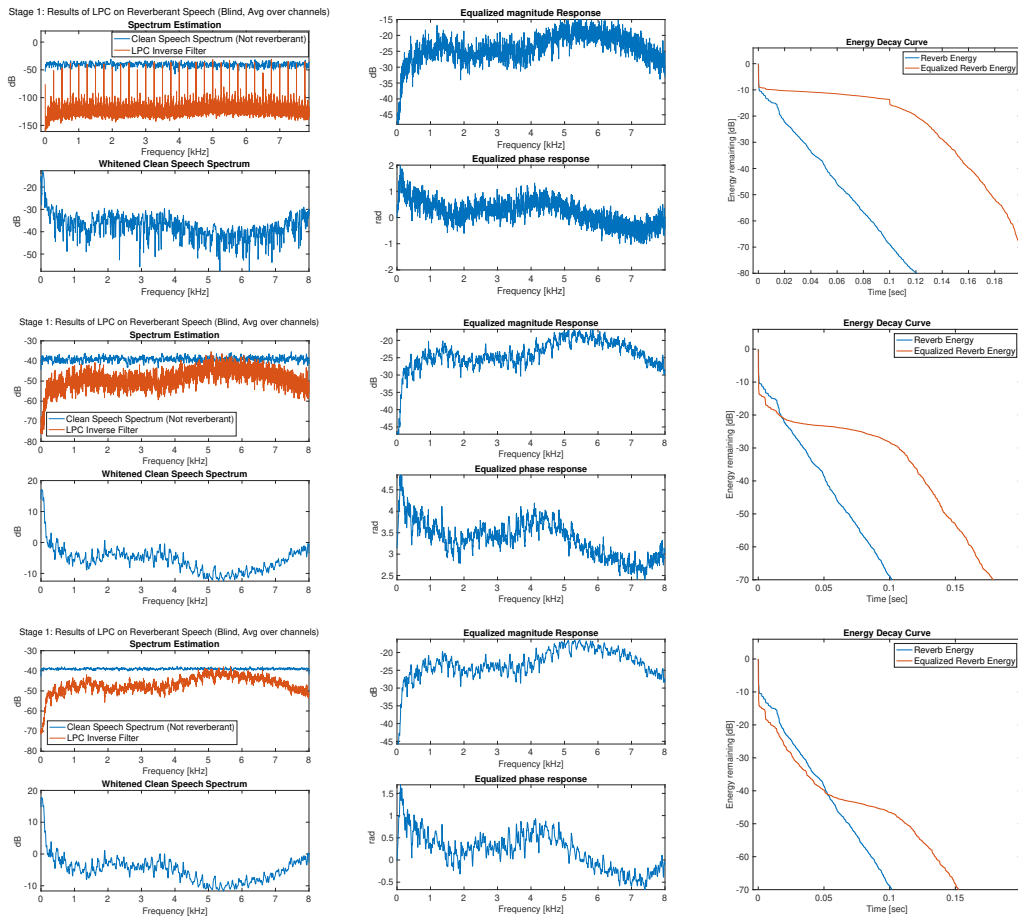


Figure 3.11: Delay-and-Predict dereverberation performance with the source signal generated by looping various length white noise sequences looped the same data length (i.e., same data length, different spectra). Source whitening prediction order was  $p_1 = 2 * p_2 * (M-1)$  and multichannel linear prediction order was  $p_2 = N60 / (M-1)$ . Source Whitening stage was performed on reverberant speech (i.e., blind).

**Source Spectrum Compare, Initial SHAPED White noise sequence  
length = [0.1 sec 1 sec 10 sec], Blind**

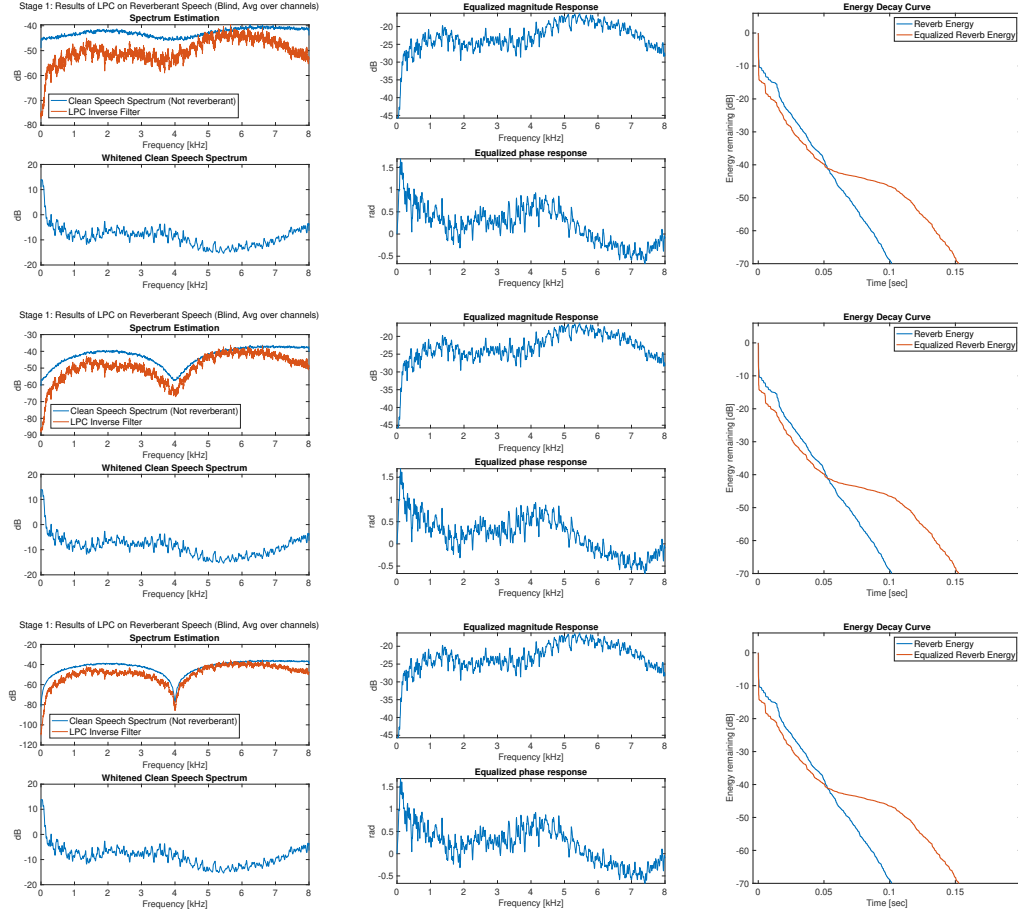


Figure 3.12: Delay-and-Predict dereverberation performance with the source signal generated by filtering 60 msec of speech with filters of various peakiness. Source whitening prediction order was  $p1 = 2 * p2 * (M-1)$  and multichannel linear prediction order was  $p2 = N60 / (M-1)$ . Source Whitening stage was performed on reverberant speech (i.e., blind).

Conclusion: • Spectrum has a huge impact on performance, independent of signal length • It seems more related to complexity of spectrum than to peakiness a. Peakiness and complexity increase – major impact

### 3.5 Time Alignment of RIRs and Linear Combiner

Test:

- Synthetic RIRs, delayed manually (incremental delay added per channel),  $T60=100\text{msec}$
- L channel =  $N60 * 2 = 3200$  samples ( 120 dB attenuation)
- Source = SA1.wav looped for 20 sec
- S1 on clean speech
- Figures saved (.fig)

#### Incremental delay of 2 sample

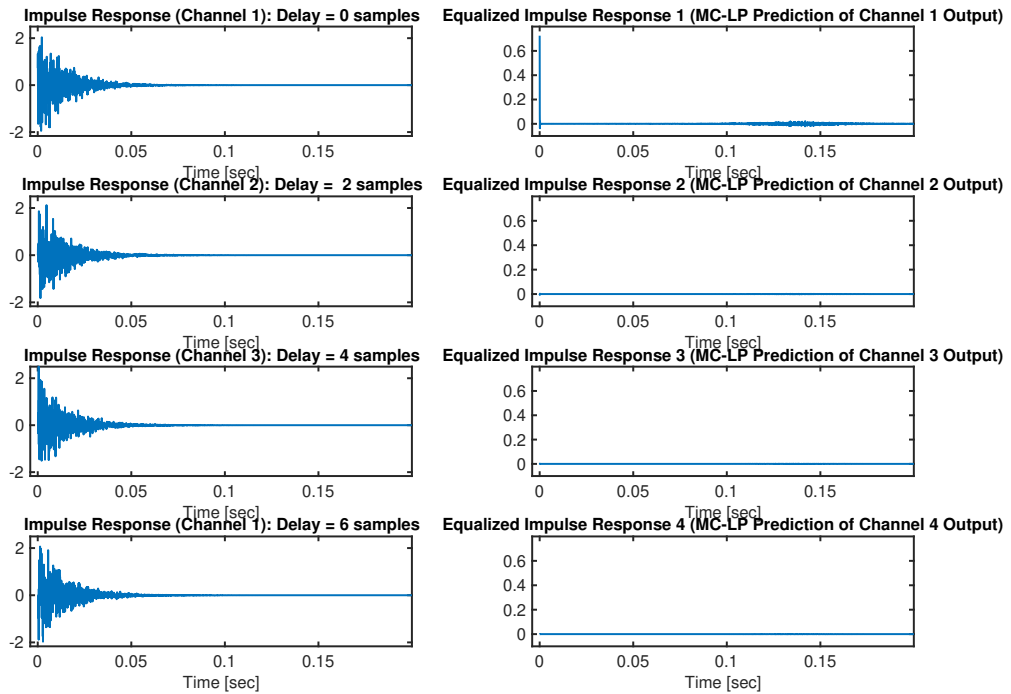


Figure 3.13: Showing the impact of RIR time alignment on multichannel linear prediction performance. The RIRs (left column) were synthetically generated exponentially decaying gaussians and an incremental delay of 2 samples was added to each channel. The right column shows the result of each individual prediction error filter (i.e., the top-most one is the result of predicting the current sample of microphone 1 from the past samples of microphones 1-4)

See discussion in notes.

Add discussion about linear combiner and why the weighting vector suggested by slock makes sense (all based on time alignment)

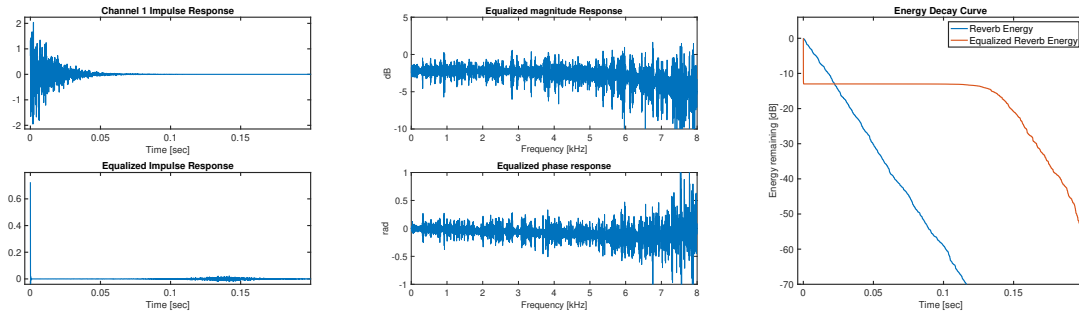


Figure 3.14: Delay-and-Predict dereverberation performance an incremental 2 sample delay added to each channel.

### No Delay

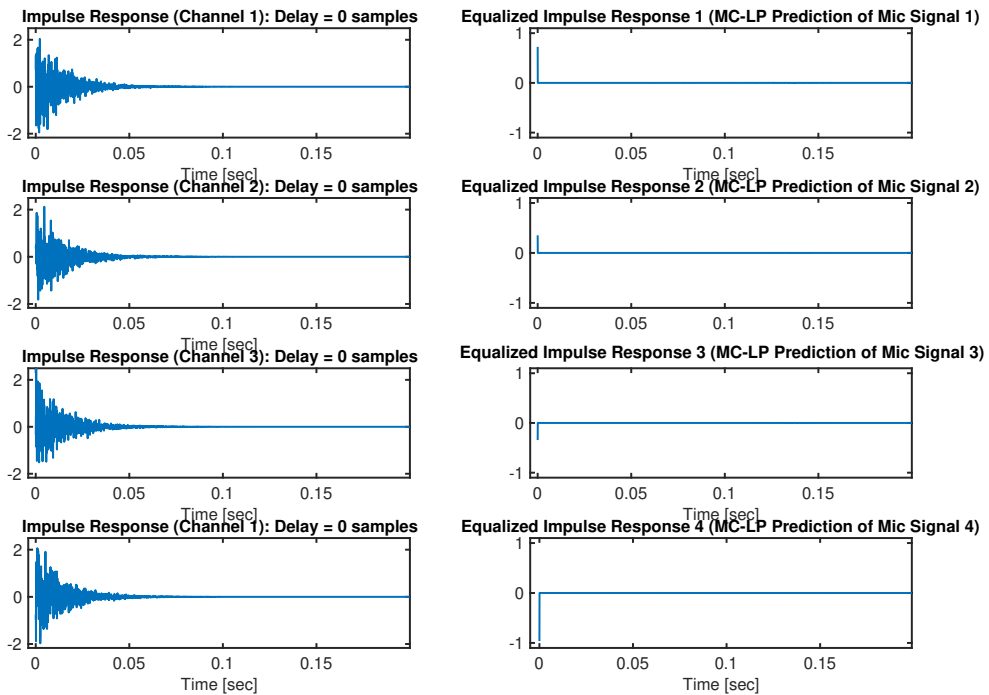


Figure 3.15: Repeating with no time delay

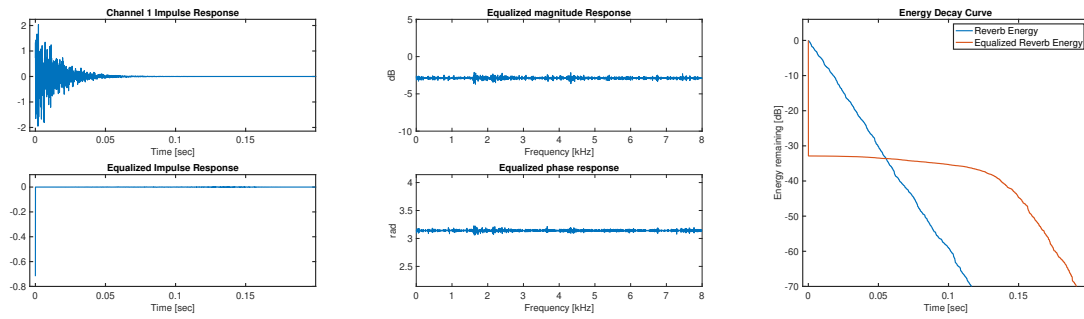


Figure 3.16: Delay-and-Predict dereverberation performance for perfectly time-aligned RIRs

### 3.6 Algorithmic Complexity Analysis

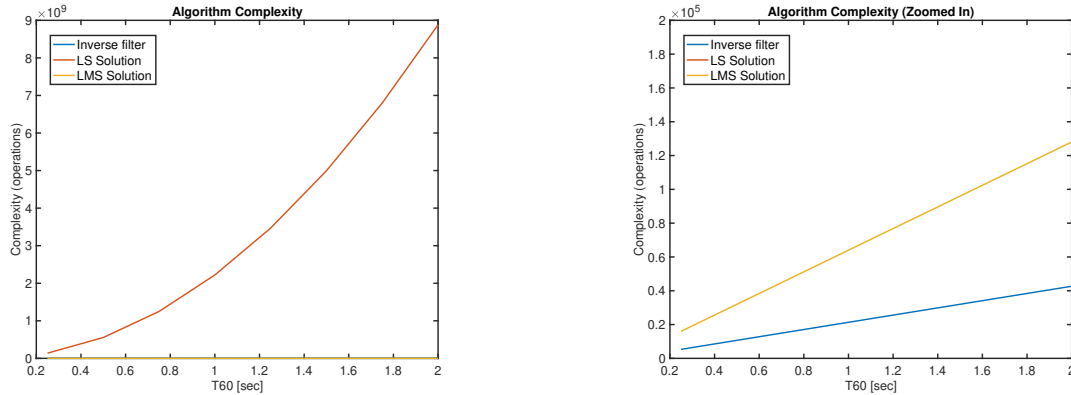


Figure 3.17: Analysis of the computational complexities of Least Squares solution and Inverse filter implementations as a function of T60, For M=4 microphones,  $p_2 = N60/(M-1)$  and  $p_1 = 1.25 \cdot p_2^2 \cdot (M-1)$ . Complexity of LMS Solution also shown for comparison.

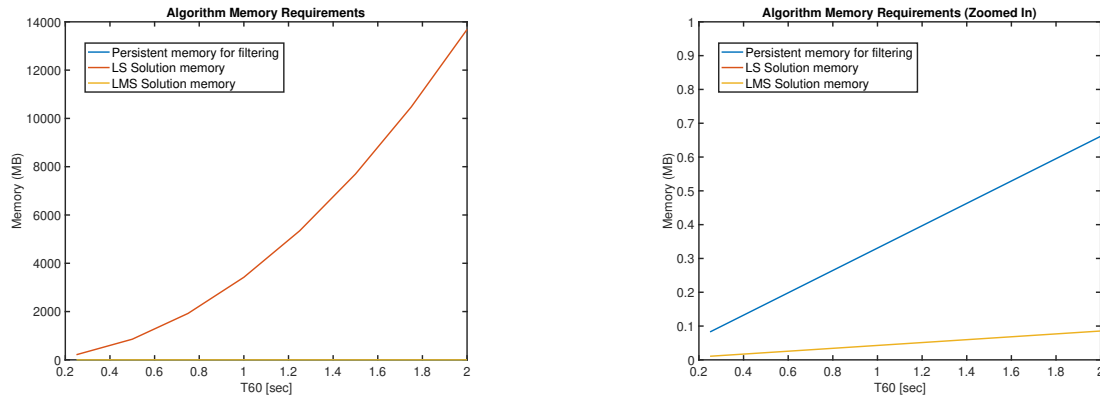


Figure 3.18: Analysis of the algorithmic memory requirements of Least Squares solution (could be temporary memory) and Inverse filter implementations (persistent memory) as a function of T60, For M=4 microphones,  $p_2 = N_{60}/(M-1)$  and  $p_1 = 1.25 * p_2 * (M-1)$ . Memory requirements of LMS Solution also shown for comparison.

## 3.7 Conclusions

Summarize the role and requirements for each parameter

## 3.8 Appendices

### 3.8.1 MC-LP Order

$$p_2 = N_{60} / (M-1) \text{ (MINT based on T60)}$$

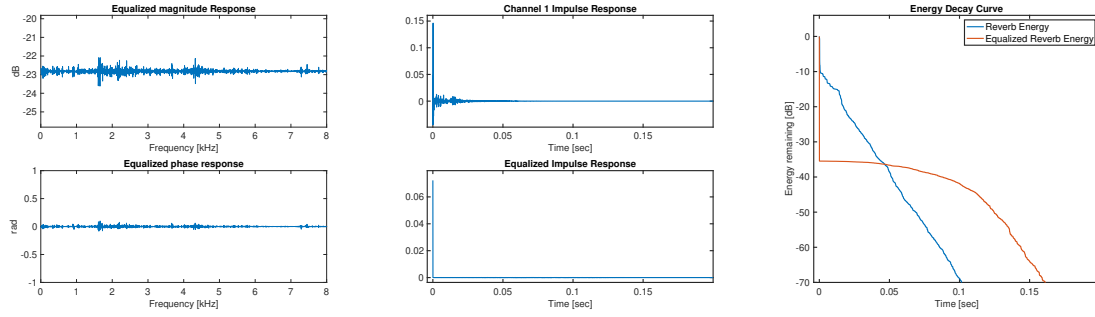


Figure 3.19: Delay-and-Predict dereverberation performance with multichannel linear prediction order  $p2 = N60 / (M-1)$ , where  $N60$  is the number of samples corresponding to the  $T60$  and  $M$  is the number of channels (i.e., the MINT condition based on  $T60$  rather than the FIR RIR length). Figure 3.2 shows the common source whitening filter used.

$$p2 = 0.75 * N60 / (M-1) \text{ (Suboptimal)}$$

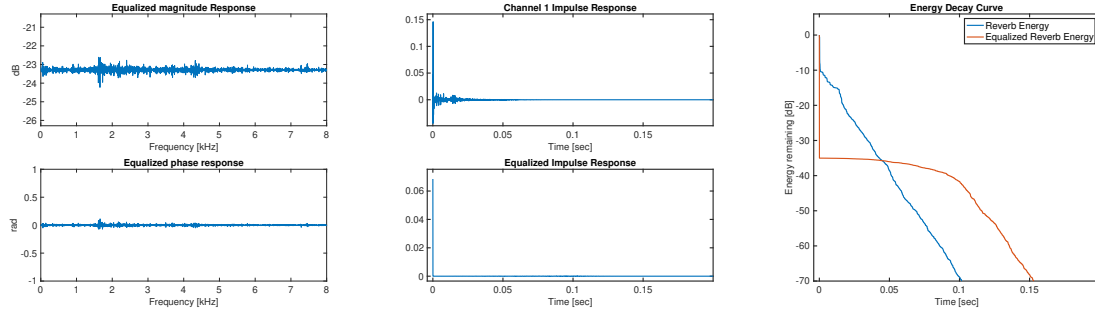


Figure 3.20: Delay-and-Predict dereverberation performance with multichannel linear prediction order  $p2 = 0.75 * N60 / (M-1)$ , where  $N60$  is the number of samples corresponding to the  $T60$  and  $M$  is the number of channels (i.e., suboptimal with respect to the MINT condition based on  $T60$  rather than the FIR RIR length). Figure 3.2 shows the common source whitening filter used.

$$p2 = 0.5 * N60 / (M-1) \text{ (More suboptimal)}$$

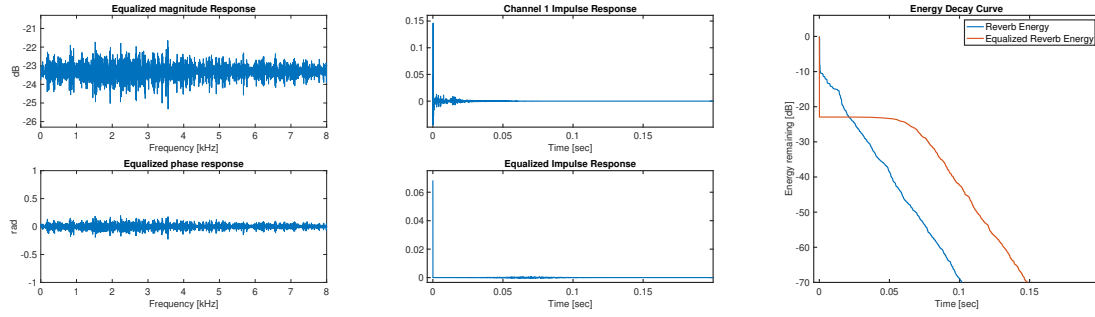


Figure 3.21: Delay-and-Predict dereverberation performance with multichannel linear prediction order  $p_2 = 0.5 * N_{60} / (M-1)$ , where  $N_{60}$  is the number of samples corresponding to the T60 and M is the number of channels (i.e., More suboptimal with respect to the MINT condition based on T60 rather than the FIR RIR length). Figure 3.2 shows the common source whitening filter used.

### 3.8.2 Source Whitening Order

**p1 = 1000**

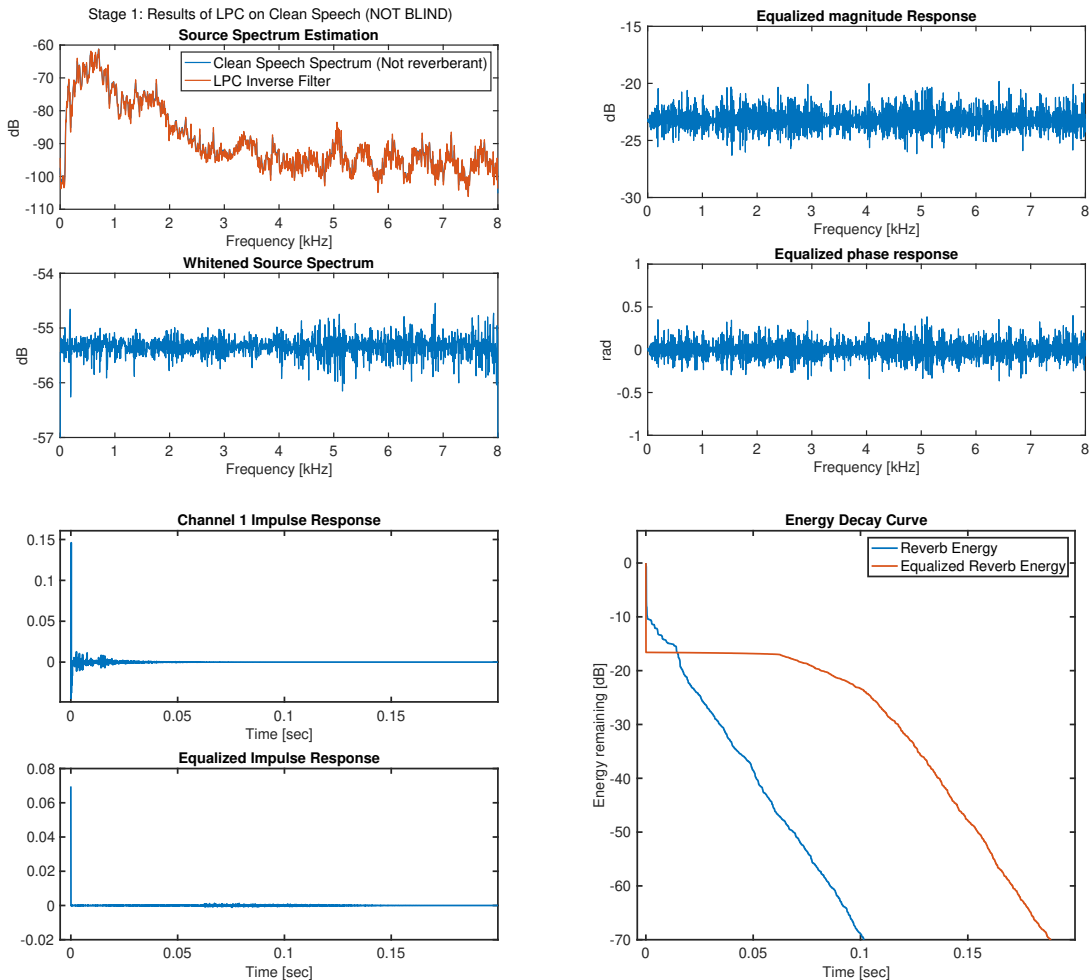


Figure 3.22: Delay-and-Predict dereverberation performance with source whitening prediction order  $p1 = 1000$  and multichannel linear prediction order  $p2 = N60 / (M-1)$ .

**$p1 = p2 * (M-1)$  (whitened on the same spectral resolution as the MC-LP equalizer)**

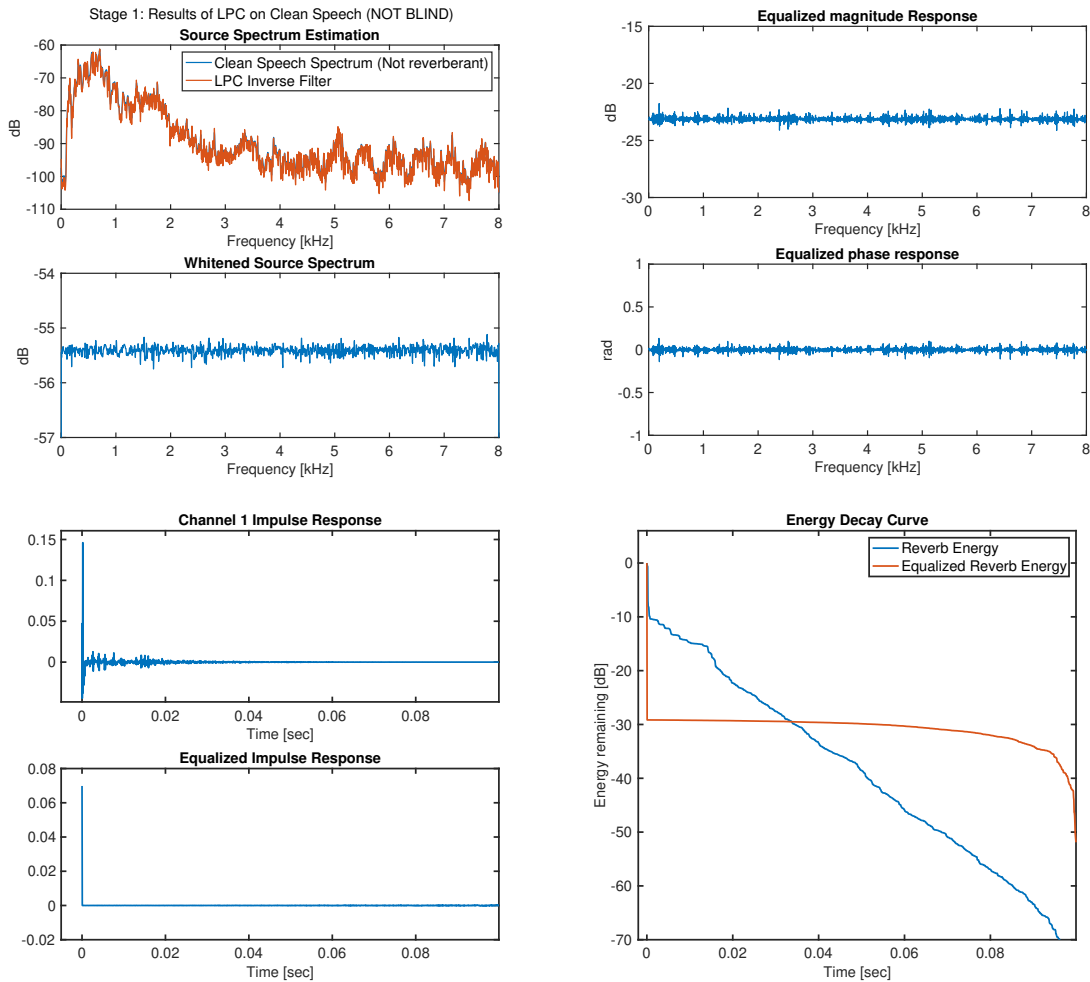


Figure 3.23: Delay-and-Predict dereverberation performance with source whitening prediction order  $p1 = p2 * (M-1)$  and multichannel linear prediction order  $p2 = N60 / (M-1)$ . I.e., The source whitening filter order is the same as the effective MINT filter order.

$$p1 = 2 * p2 * (M-1) \text{ (Extra headroom)}$$

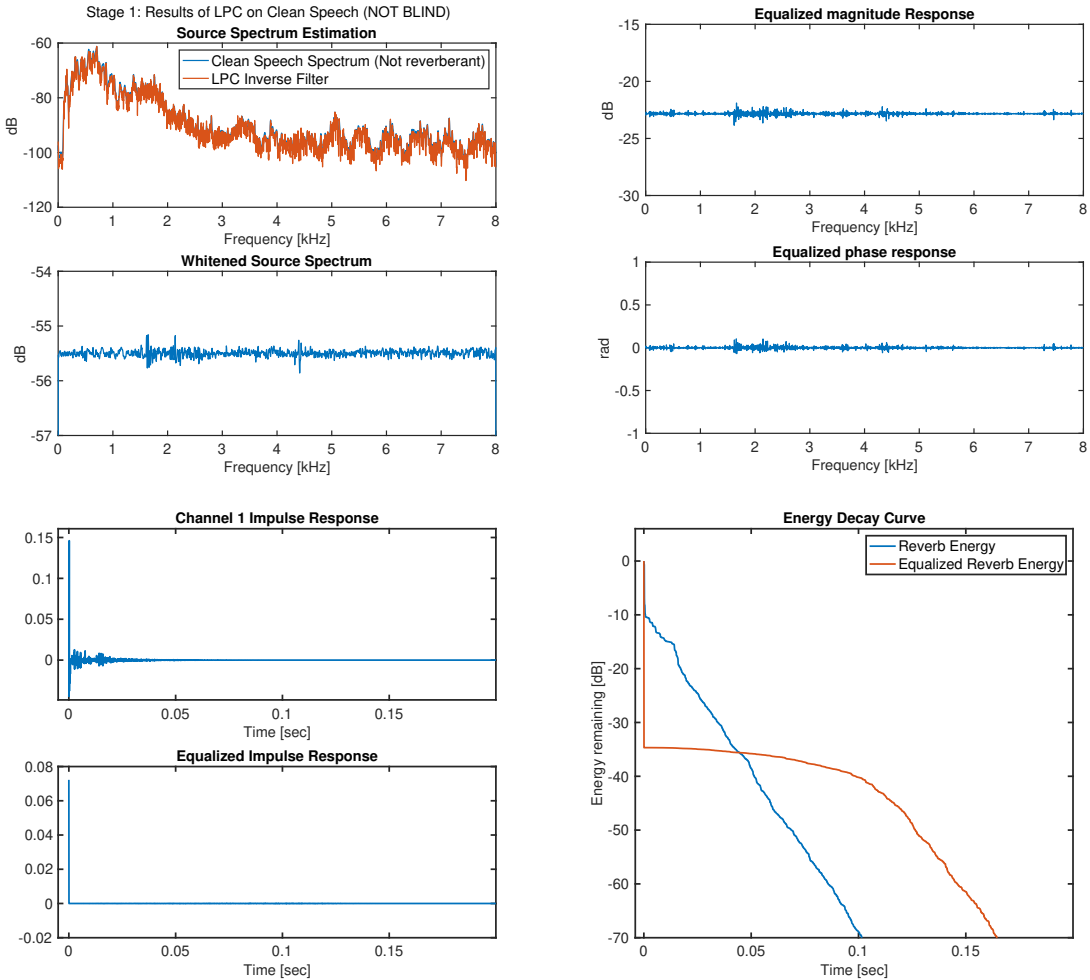


Figure 3.24: Delay-and-Predict dereverberation performance with source whitening prediction order  $p_1 = 2 * p_2 * (M-1)$  and multichannel linear prediction order  $p_2 = N60 / (M-1)$ . I.e., The source whitening filter order is twice the effective MINT filter order.

... beyond about  $p_1 = 1.25 * p_2 * (M-1)$  EDC performance saturates at approximately -35 dB reverb attenuation.

### 3.8.3 Source Properties: Data Length

**Signal Length = 58061 (num loops = 1)**

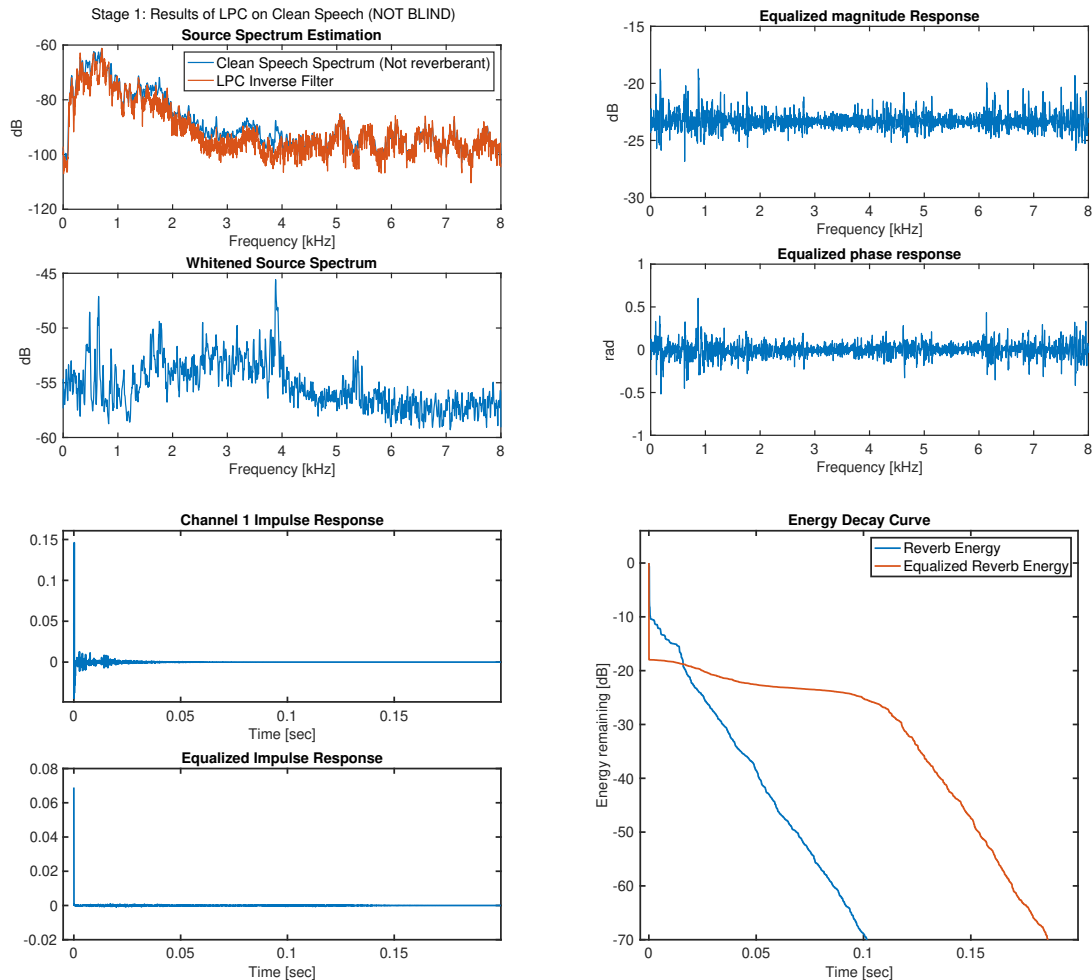


Figure 3.25: Delay-and-Predict dereverberation performance for a 3.6 second speech source (58061 samples). Source whitening prediction order was  $p_1 = 2 * p_2 * (M-1)$  and multichannel linear prediction order was  $p_2 = N60 / (M-1)$ . Source whitening filter was estimated using clean speech.

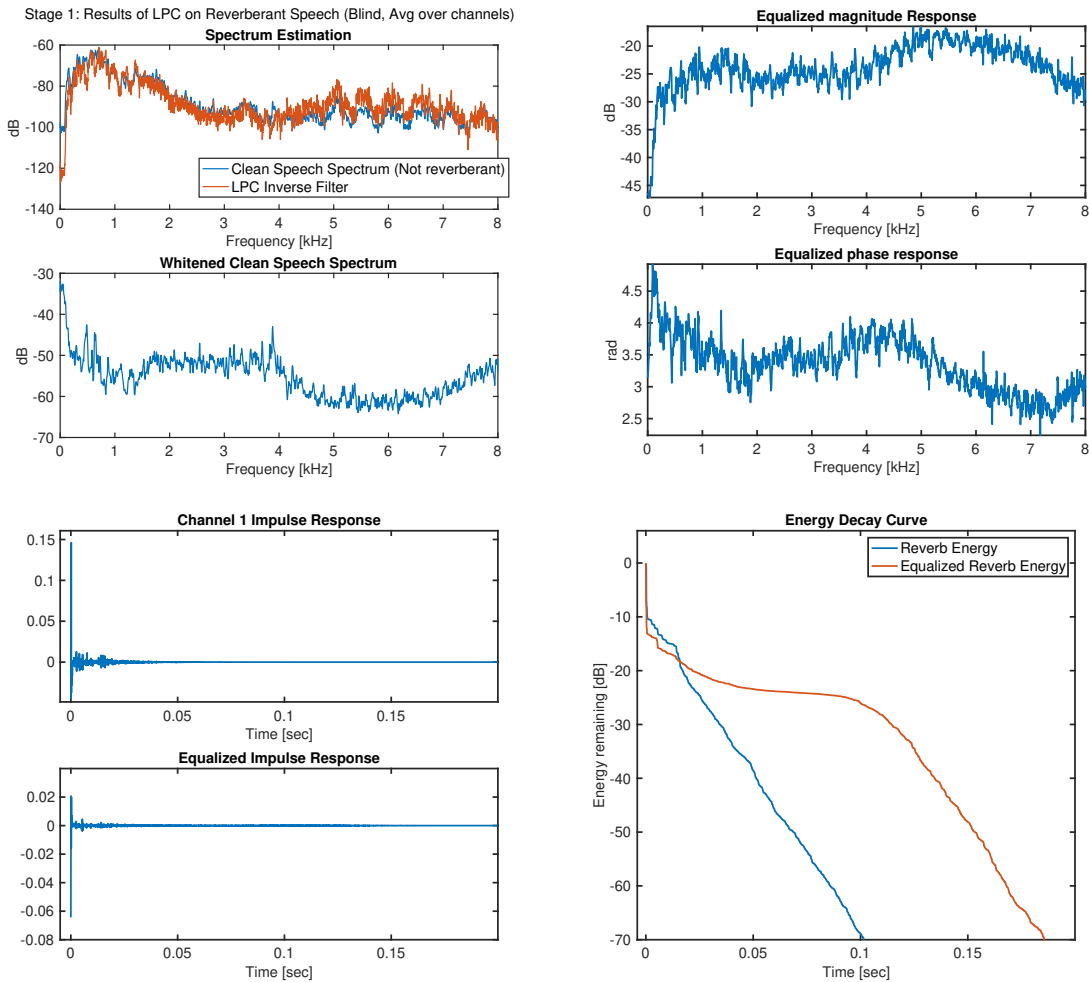


Figure 3.26: Delay-and-Predict dereverberation performance for a 3.6 second speech source (58061 samples). Source whitening prediction order was  $p_1 = 2 * p_2 * (M-1)$  and multichannel linear prediction order was  $p_2 = N60 / (M-1)$ . Source whitening filter was estimated using reverberant speech (blind estimation).

**Signal Length = 174183 (num loops = 3)**

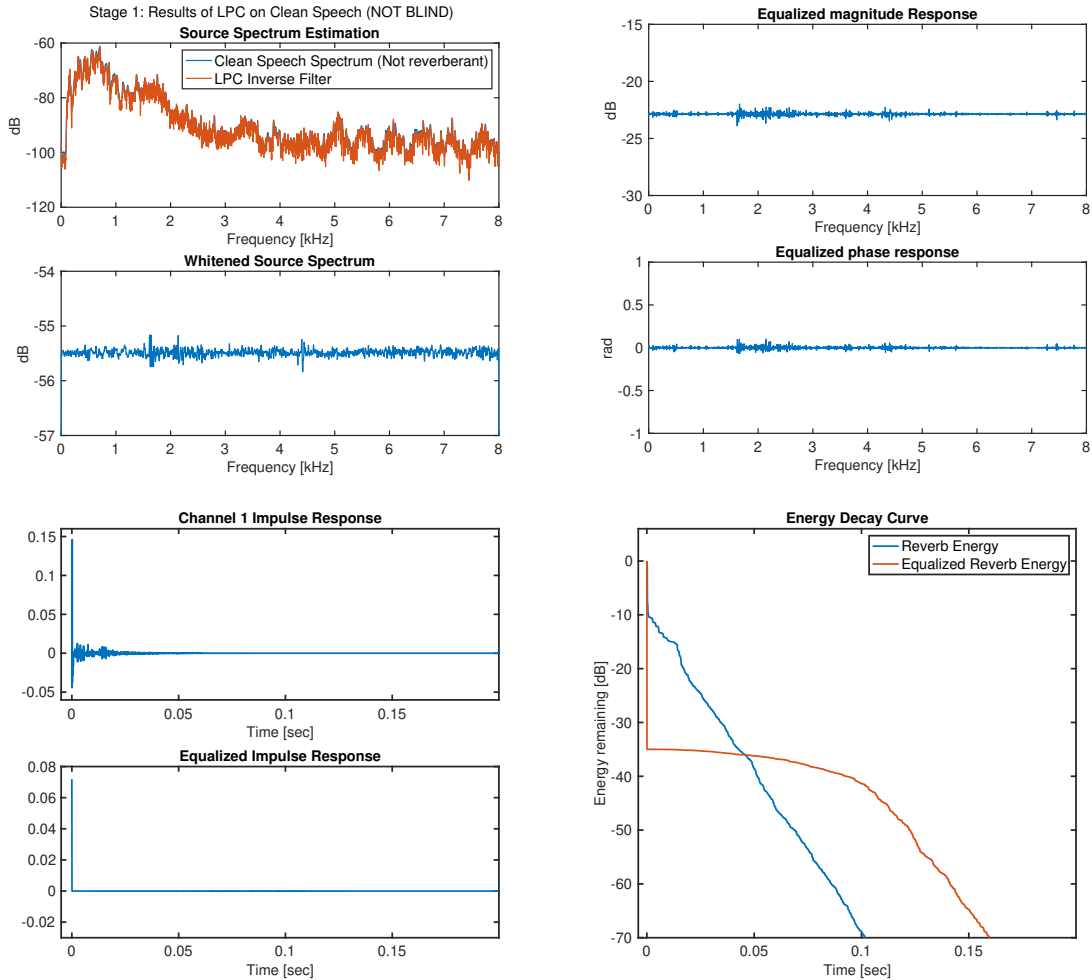


Figure 3.27: Delay-and-Predict dereverberation performance for a 10.9 second speech source (174183 samples). The source was generated by looping the same 3.6 secound source 3 times to maintain the same spectrum. Source whitening prediction order was  $p_1 = 2 * p_2 * (M-1)$  and multichannel linear prediction order was  $p_2 = N60 / (M-1)$ . Source whitening filter was estimated using clean speech.

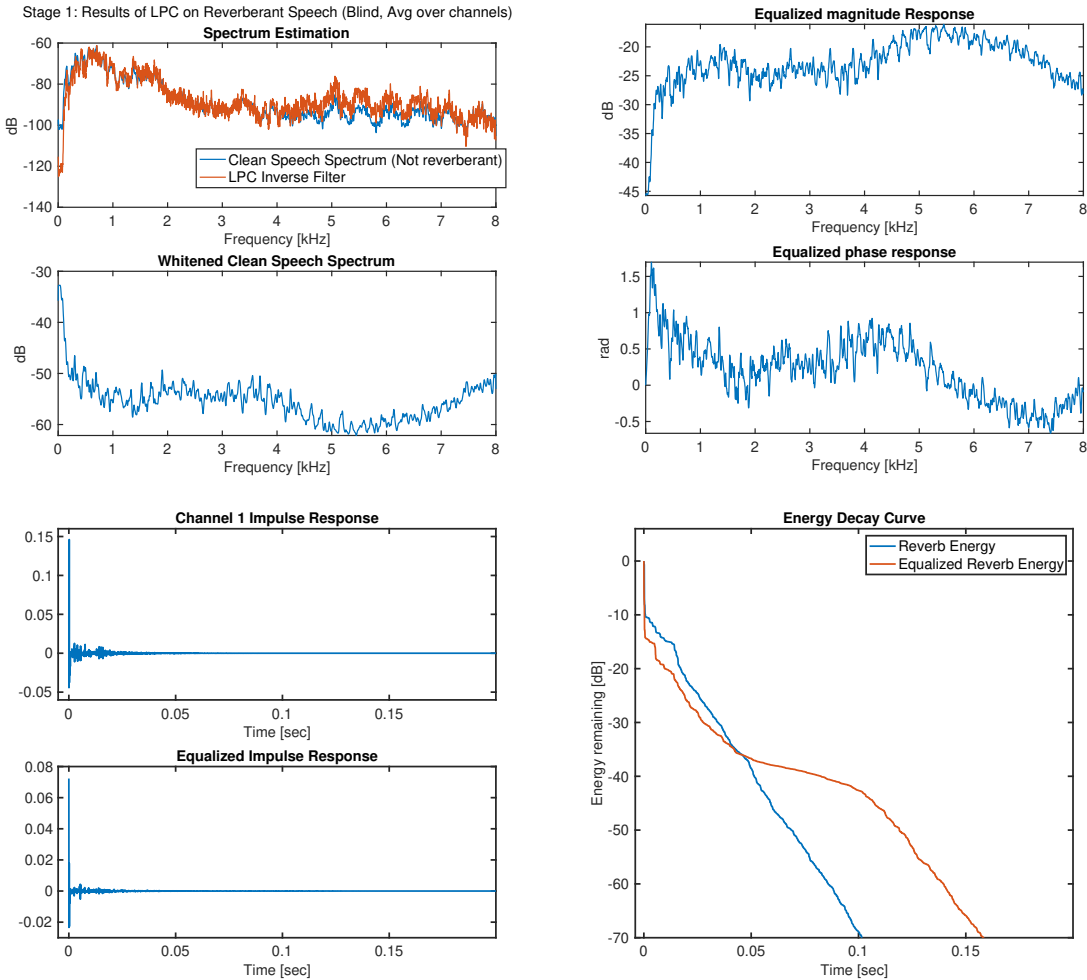


Figure 3.28: Delay-and-Predict dereverberation performance for a 10.9 second speech source (174183 samples). The source was generated by looping the same 3.6 secound source 3 times to maintain the same spectrum. Source whitening prediction order was  $p1 = 2 * p2 * (M-1)$  and multichannel linear prediction order was  $p2 = N60 / (M-1)$ . Source whitening filter was estimated using revererant speech (blind estimation).

### 3.8.4 Source Properties: Spectrum

Original length = 1 sec white noise, loop count = 60

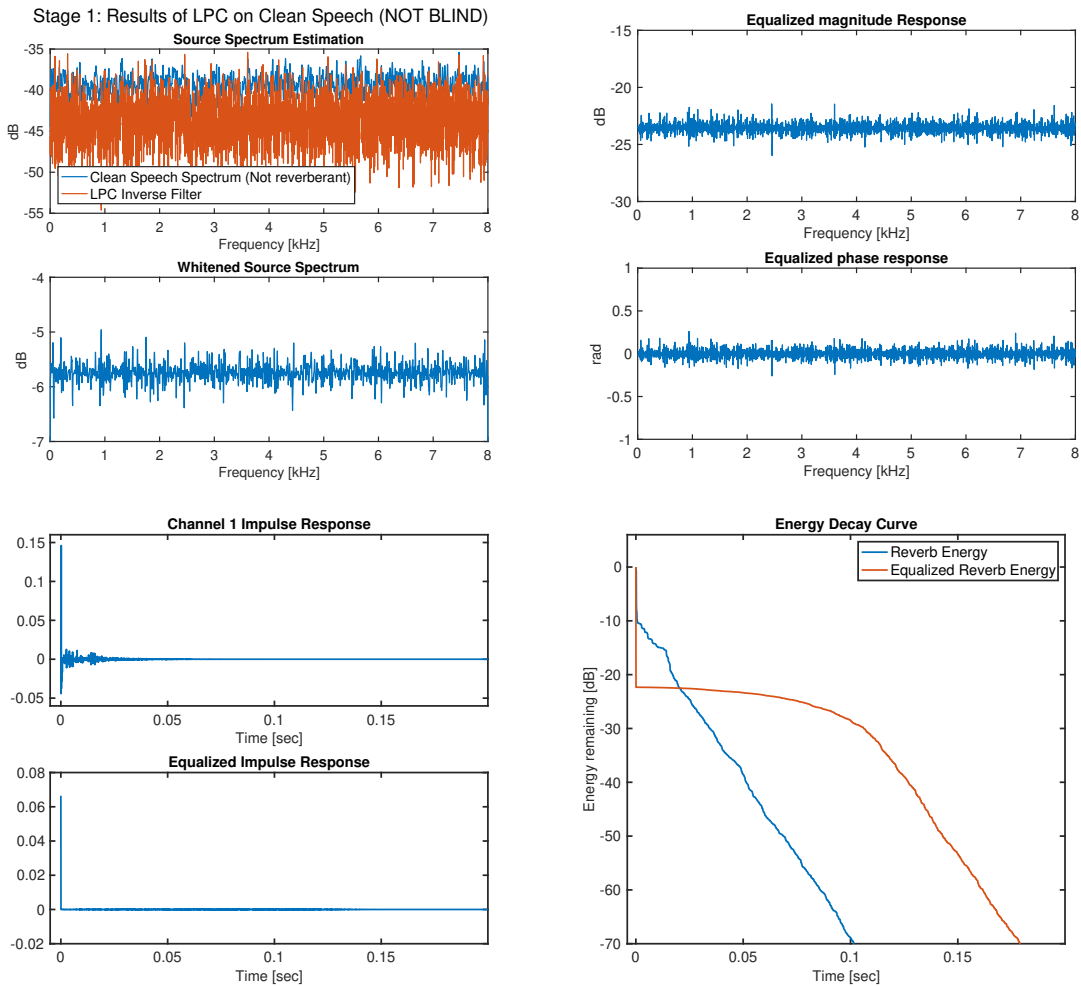


Figure 3.29: Delay-and-Predict dereverberation performance with source being 1 second of white noise looped to 60 sec. Source whitening prediction order was  $p_1 = 2 * p_2 * (M-1)$  and multichannel linear prediction order was  $p_2 = N_{60} / (M-1)$ . Source whitening filter was estimated using clean speech.

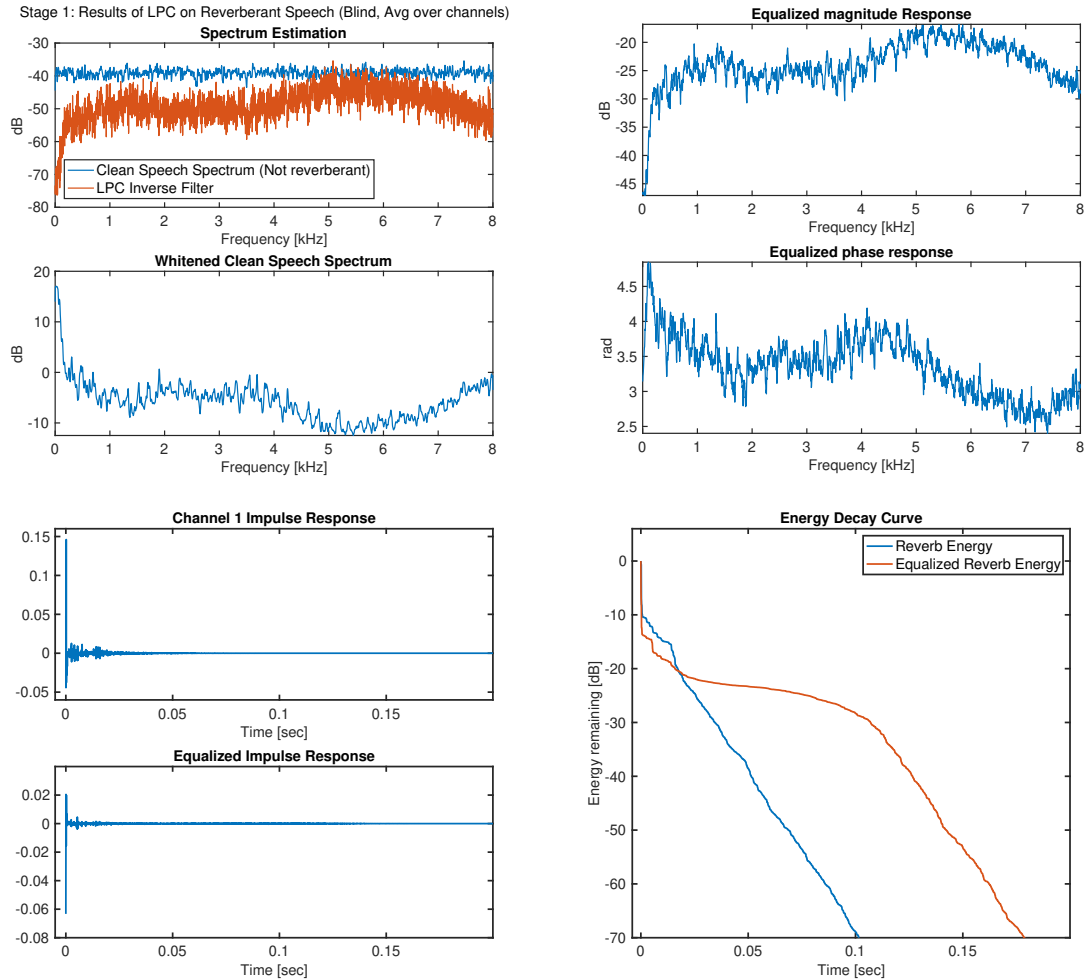


Figure 3.30: Delay-and-Predict dereverberation performance with source being 1 second of white noise looped to 60 sec. Source whitening prediction order was  $p_1 = 2 * p_2 * (M-1)$  and multichannel linear prediction order was  $p_2 = N_{60} / (M-1)$ . Source whitening filter was estimated using reverberant speech (blind estimation).

**Original length = 10 sec white noise, loop count = 6**

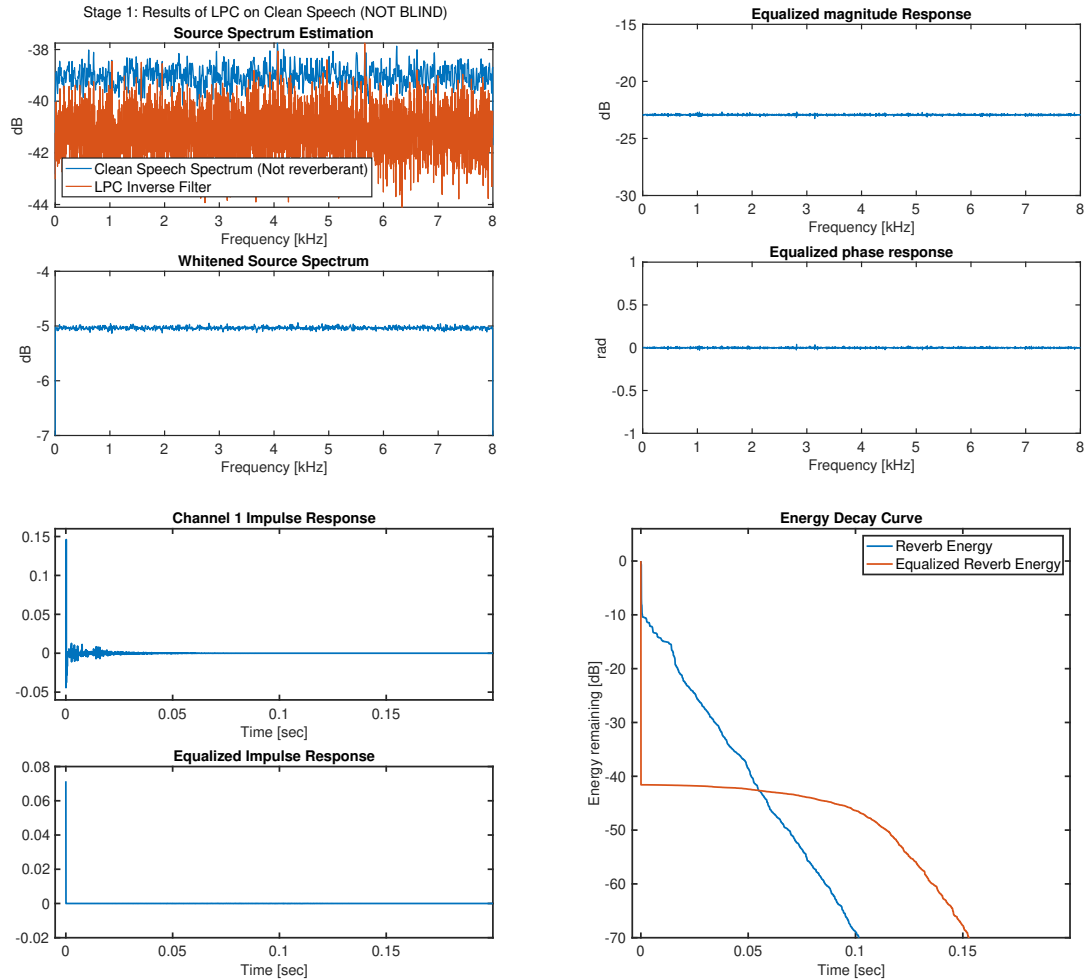


Figure 3.31: Delay-and-Predict dereverberation performance with source being 10 second of white noise looped to 60 sec (i.e., source is less peaky than the previous case). Source whitening prediction order was  $p_1 = 2 * p_2 * (M-1)$  and multichannel linear prediction order was  $p_2 = N60 / (M-1)$ . Source whitening filter was estimated using clean speech.

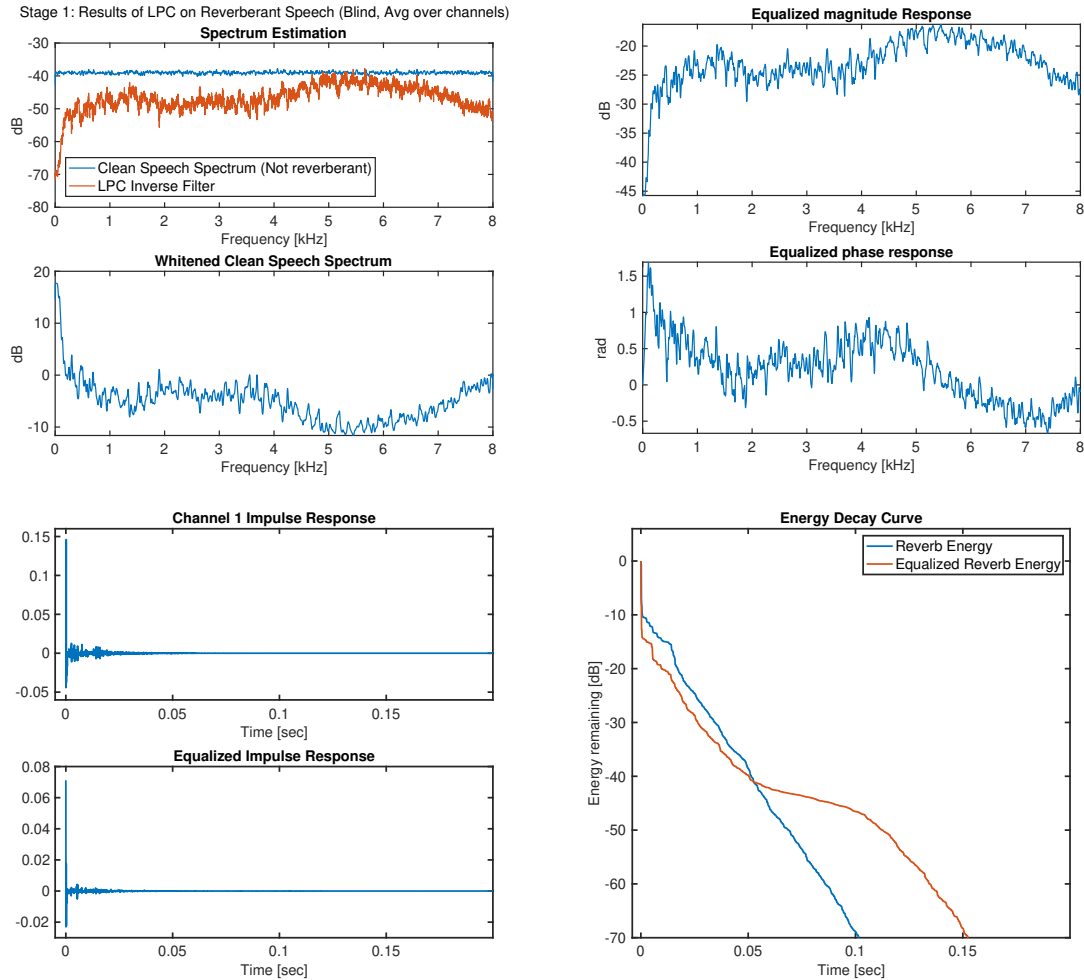


Figure 3.32: Delay-and-Predict dereverberation performance with source being 10 second of white noise looped to 60 sec (i.e., source is less peaky than the previous case). Source whitening prediction order was  $p_1 = 2 * p_2 * (M-1)$  and multichannel linear prediction order was  $p_2 = N60 / (M-1)$ . Source whitening filter was estimated using reverberant speech (blind estimation).

# **Chapter 4**

## **Methods and Results**

### **4.1 Evaluation of Proposed Speech Intelligibility Prediction Method for Reverberation**

#### **4.1.1 Proposed Method**

The goal outlined in this thesis was to analyze the perceptual impacts of reverberation for hearing aid users, and evaluate the perceptual benefit of applying delay-and-predict dereverberation (i.e., DAP dereverberation, Section 2.2.6.2) to remove reverberant effect. It was intended to perform an evaluation of realistic and practical conditions, and use performance metrics that reflect realistic perceptual impacts with and without hearing loss.

As described in Section 1.6.1, perception is commonly characterized by speech intelligibility (SI), listening effort (LE) and speech quality (SQ). To accurately evaluate the perceptual impacts of reverberation, a perceptually accurate predictor of SI

is needed, which will also correlate implicitly to LE. Among the objective predictors of SI described in Section 1.8.1, the MR NSIM, FT NSIM and STMI were selected since they provide the most physiologically accurate model of the auditory system and the impacts of hearing loss. Although HASPI incorporates a more simplisitic model the auditory system and hearing loss, it is standard in the hearing aid industry and therefore was included to provide a data that could be easily understood by researchers in the field. Lastly STOI, which includes no explicit modeling of the auditory system or hearing loss, was included as because of its standardization accross the entire speech processing industry. Since these are all monaural predictors, an equalization-cancellation (EC) front-end was included to provide some modeling of binaural perceptual benefits (i.e., spatial release from masking, 1.6.5.2). Recall, however, that the EC algorithm is simplistic and provides no modeling of degradations due to hearing loss.

**this is the PROPOSED method, modified after analysis of components below.**

For each SI predictor, the impacts of reverberation and benefit of DAP dereverberation were analyzed as follows:

...

### 4.1.2 Analysis of RIR Databases

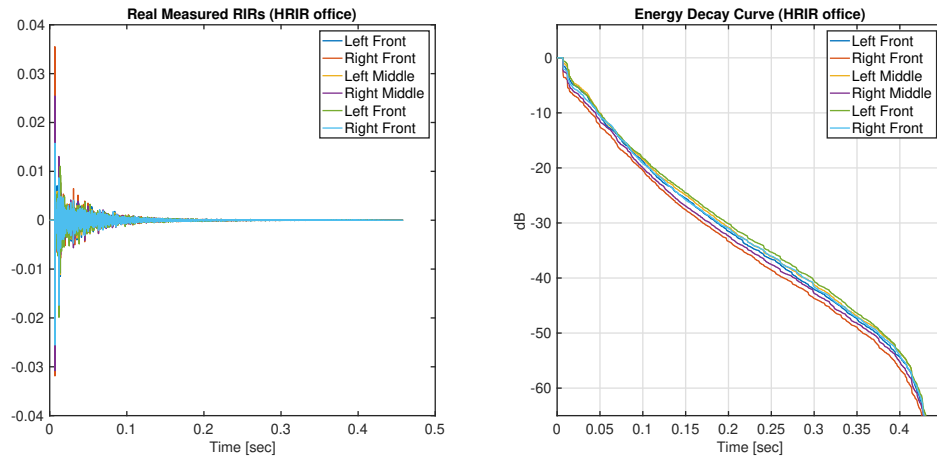


Figure 4.1: HRIR database office II room

- Listed as 300 msec in paper
  - Measured as approx
    - o  $T_{60} = 420 - 7 = 413$  msec
    - o  $T_{30} = 2^*(225-25) = 400$  msec

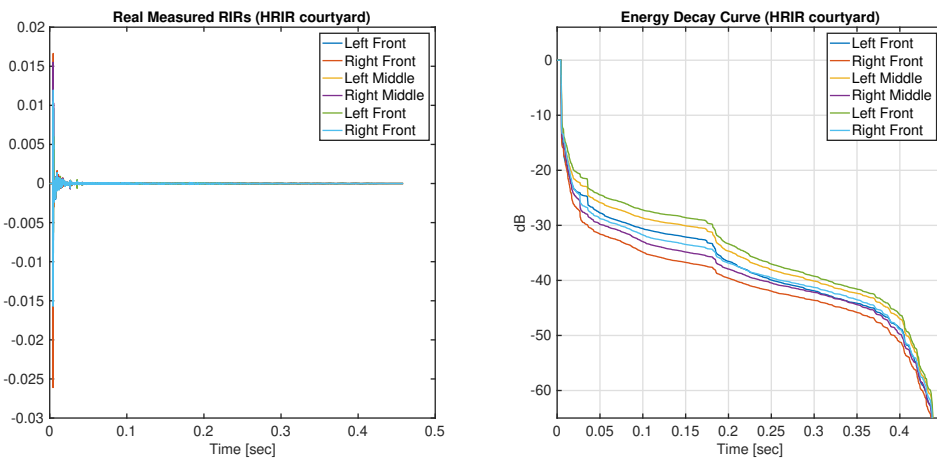


Figure 4.2: HRIR database courtyard room

- Listed as 900 msec in paper
- Measured as approx.
  - o  $T_{60} = 430 - 4 = 426$  msec
  - o  $T_{30} = 2^*(200-5) = 390$  msec

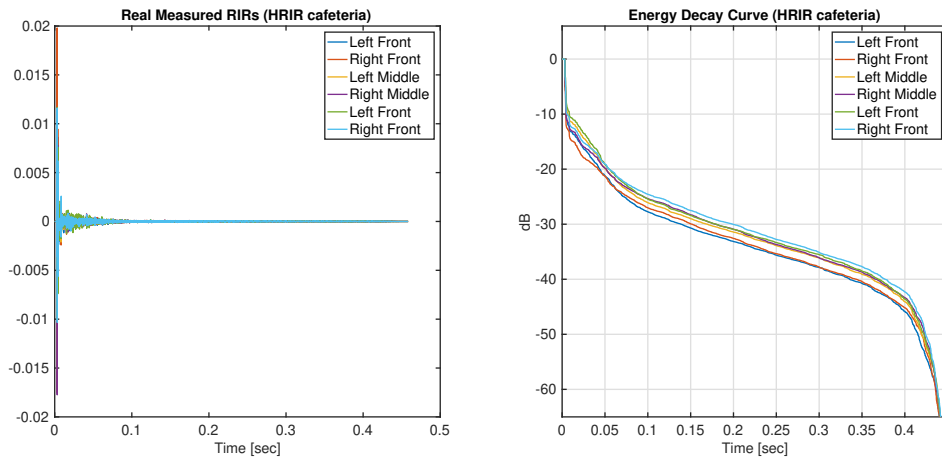


Figure 4.3: HRIR database cafeteria room

- Listed as 1.25 sec in paper
- Measured as approx.
  - o  $T_{60} = 440 - 3 = 437$  msec
  - o  $T_{30} = 2^*(275 - 4) = 542$  msec

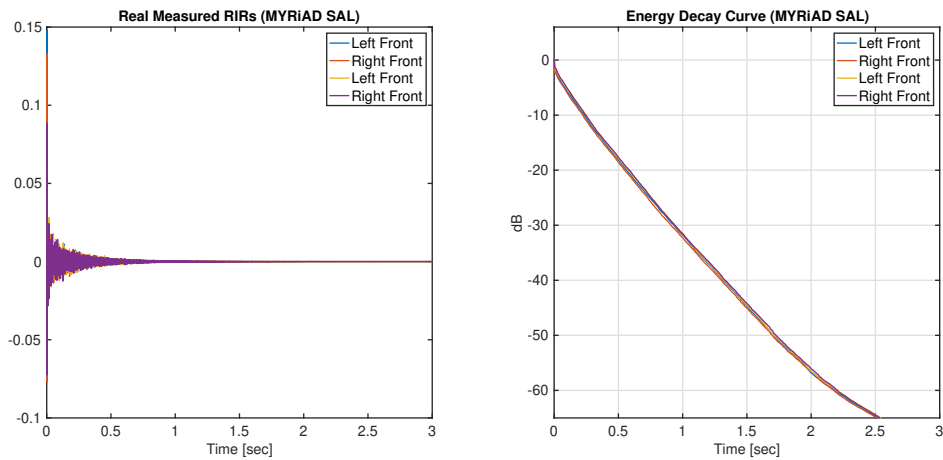


Figure 4.4: MYRiAD database SAL room

- Listed as 2.1 sec (2100 msec) in paper
- Measured as approx..
  - o  $T_{60} = 2200$  msec
  - o  $T_{30} = 2 * (1159 - 100) = 2118$  msec

Discuss:

- Add early decay time (EDT) to chapter 1
- How  $T_{60}$ s were calculated in the papers compared to true  $T_{60}$ s I'm citing
- EDT of each
- Noise data available also in HRIR (and MYRiAD?)

#### 4.1.3 Evaluation of Equalization-Cancellation Front-End

##### SRM

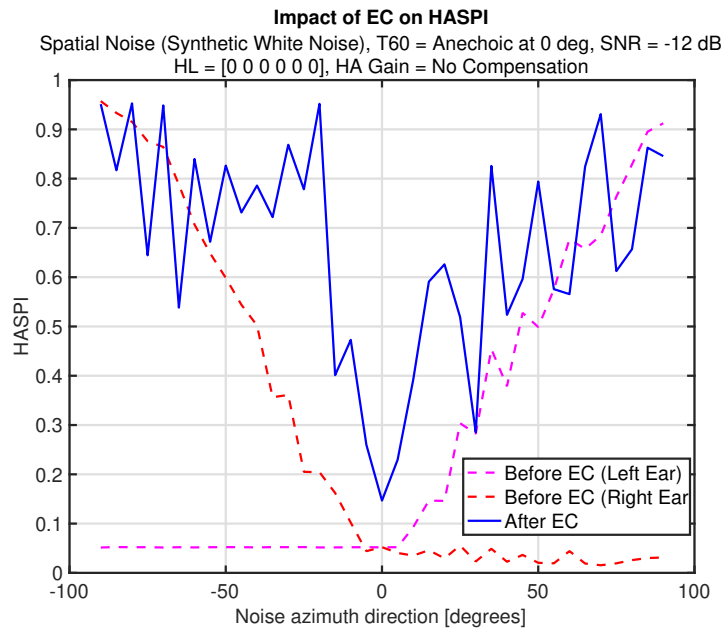


Figure 4.5: Impact of EC algorithm on speech intelligibility (using HASPI) as a function of noise direction, anechoic directional speech and noise

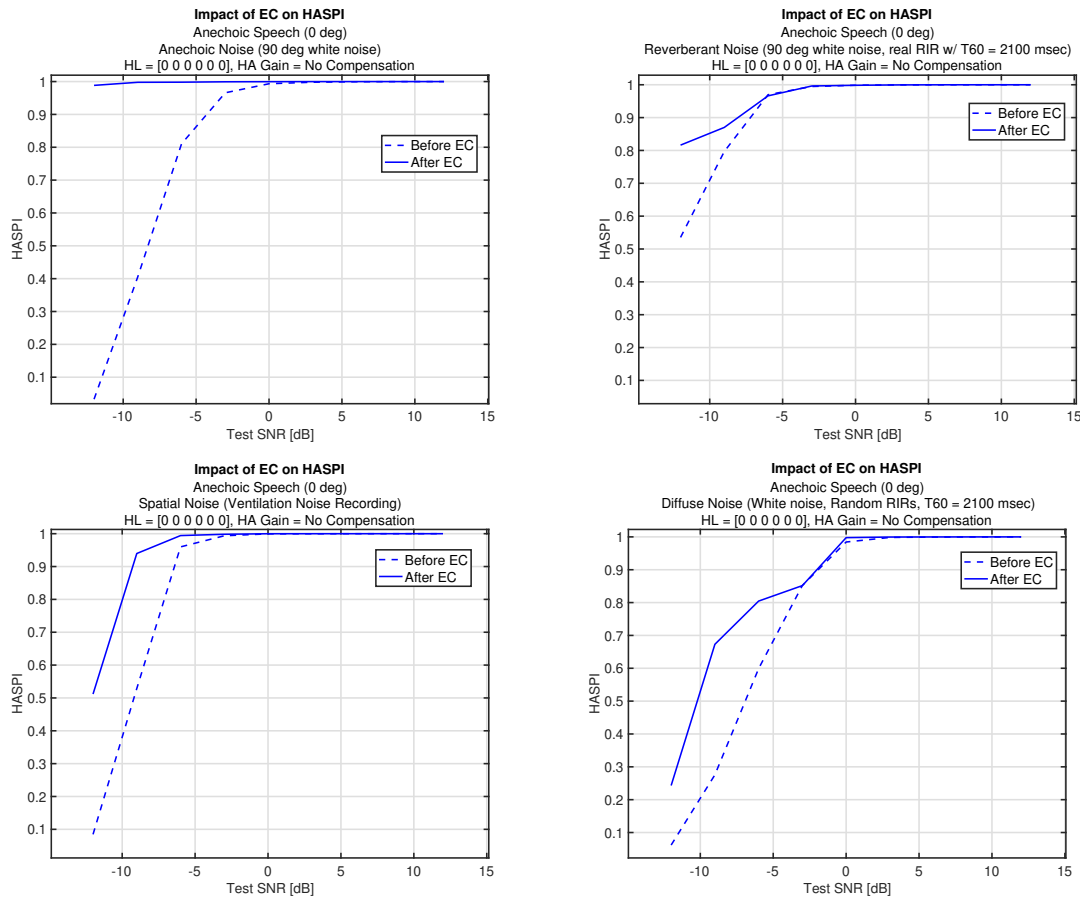


Figure 4.6: Impact of EC algorithm on speech intelligibility (using HASPI) as a function of SNR, for anechoic directional speech and various noise types (anechoic directional, reverberant, spatial recording, diffuse)

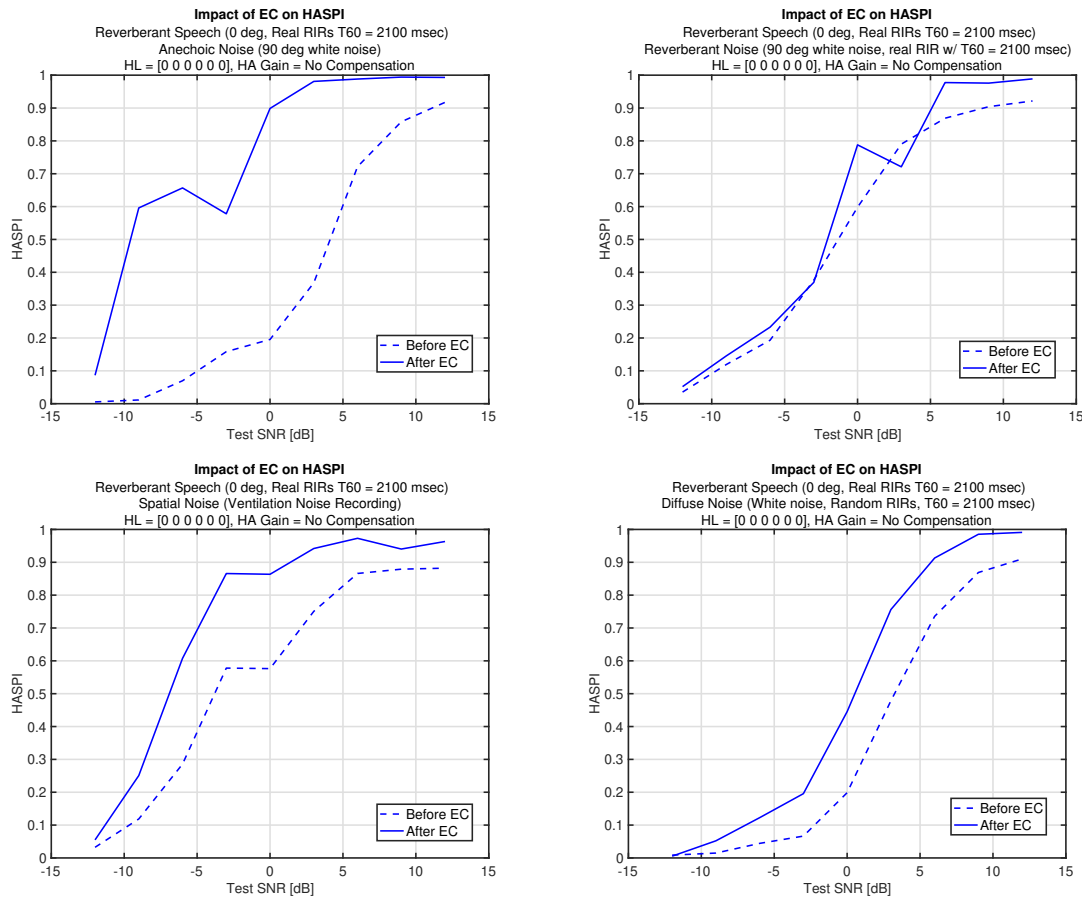


Figure 4.7: Impact of EC algorithm on speech intelligibility (using HASPI) as a function of SNR, for reverberant speech and various noise types (anechoic directional, reverberant, spatial recording, diffuse)

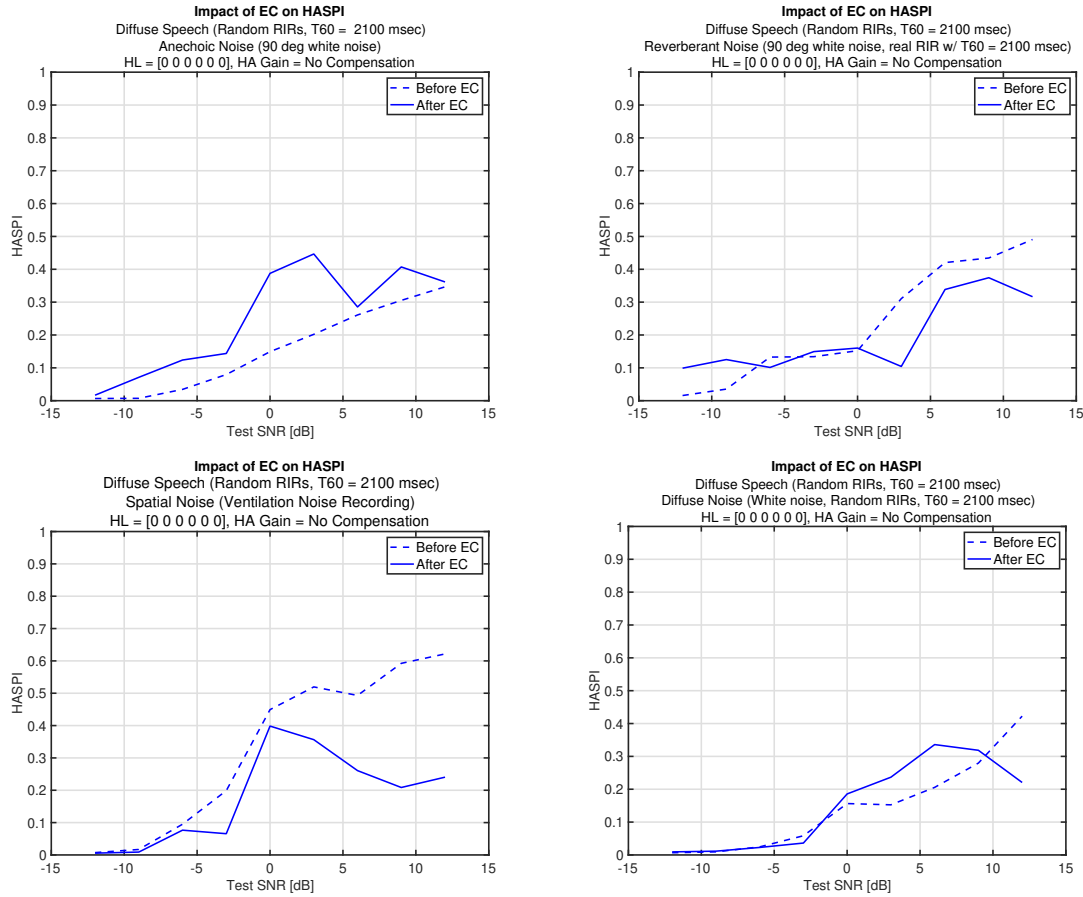


Figure 4.8: Impact of EC algorithm on speech intelligibility (using HASPI) as a function of SNR, for diffuse speech and various noise types (anechoic directional, reverberant, spatial recording, diffuse)

### Impact of reverb on binaural benefit modeled by EC

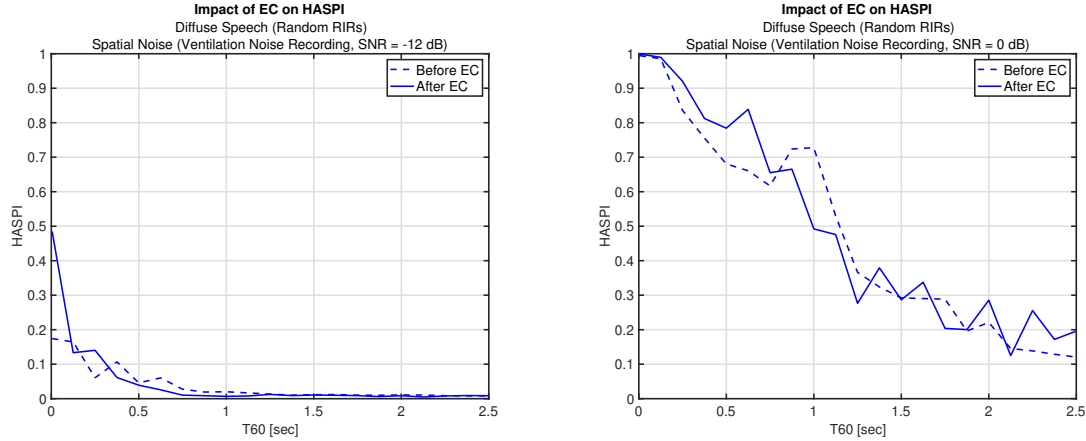


Figure 4.9: Impact of EC algorithm on speech intelligibility (using HASPI) as a function of varying amounts of synthetic reverb, for spatial noise recording with SNR = -12 dB and SNR = 0 dB

- Diffuse reverb destroys binaural cues and reduces the binaural benefit modeled by the EC (this provides modeling of the reduction in SRM due to reverb). However at low T60s the RIR is less diffuse and therefore can randomly have more emphasized directions thus sometimes providing some binaural benefit - Note distinction between SRM for noise and reverb (EC models reduction in SRM due to reverb, but doesn't model reduction in reverb itself)
- SNR = 0 dB: SI is already saturated, so only evaluating impact of reverb (essentially SNR = infinity)

**Does EC capture any of the benefits of early reflections?**

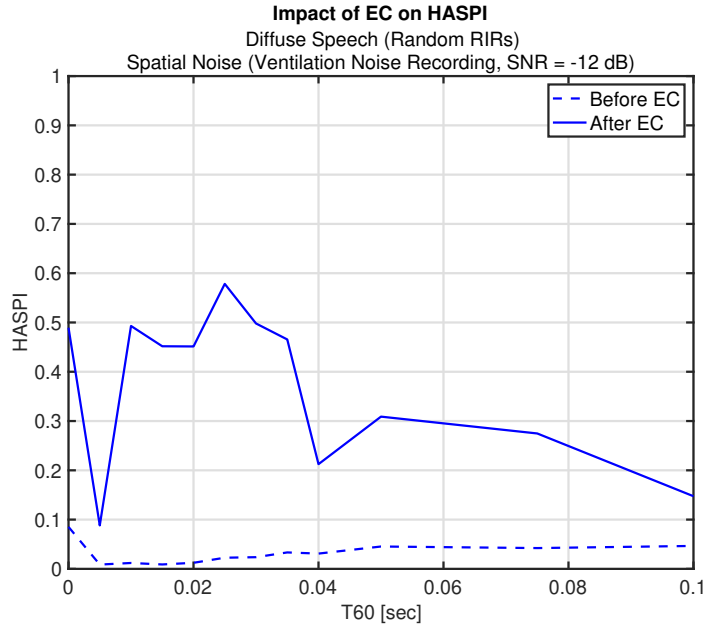


Figure 4.10: Impact of EC algorithm on speech intelligibility (using HASPI) as a function of varying amounts of synthetic reverb, for spatial noise recording with SNR = -12 dB

- Diffuse reverb (white noise) used to focus on temporal integration rather than spatial separation – Most significant binaural benefit for  $T60 = 0$  (no benefit of early reflections) – However repeating the experiment several times reveals occasional benefit depending on the randomly generated RIR – assumed this is just due to sometimes the very short number of simulated reflections effectively coming from similar directions thus providing SRM
- I would expect that using real RIRs would result in some SRM from early reflections (since they tend not to be diffuse)
- Essentially all this shows that EC may provide some modeling of BINAURAL benefit of reverb in low SNR environments (SRM), but no modeling of MONAURAL benefit of reverb (PE temporal integration)

### EC on reverb only

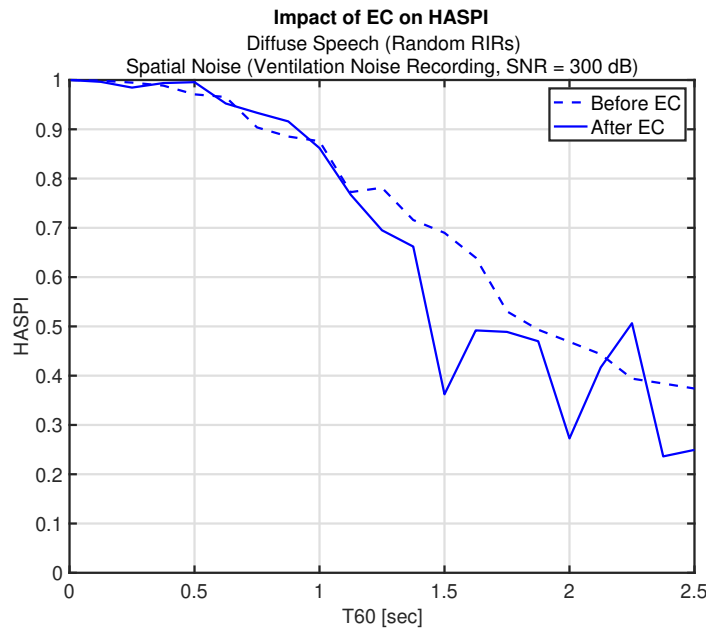


Figure 4.11: Impact of EC algorithm on speech intelligibility (using HASPI) as a function of varying amounts of synthetic reverb, noise-free

- EC does not provide binaural benefit in reverb
- EC focuses on canceling interfering noise from certain directions, which doesn't apply to reducing reverb since (for high T60s) reverb tends towards diffuse, and the interfering reflections are correlated to the clean speech

#### 4.1.4 Hearing Aid Gain Comparison

Ian:

- Loudness recruitment and its influence on WDRC design (Threshold of hearing increasing doesn't increase in upper limit where loudness becomes too much – reduced dynamic range)

- Question: Do nonlinearities in auditory system still apply at same higher SPL with hearing loss? If so then this is another reason for not doing mirror audiogram compensation (not just comfort, but going to these high levels will distort cues making SI worse – Shouldnt this be picked up by the metrics?)
- Look at Hearing Aid textbook from Harvey Dillon
- NAL-R ideal at conversational speech, quieter you want closer to mirror audiogram, and louder sounds you want less than NAL-R
  - Generally speaking in terms of restoring the representation (maybe also in STMI/NSIM – pretty sure Ian knows but im missing something) mirror audiogram will be optimal for SI, NAL-R is more about comfort – We cant do mirror audiogram because users wont like it, NAL-R is better in terms of trade off of SI and comfort

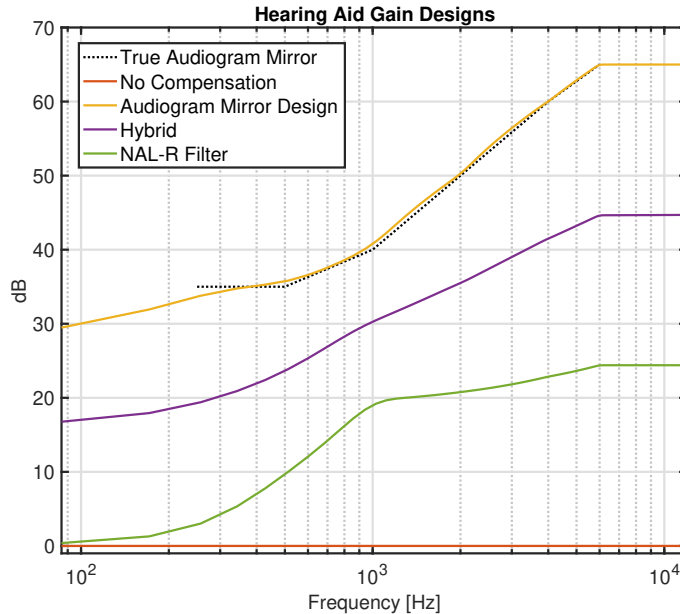


Figure 4.12: Hearing aid gains to be used in evaluation

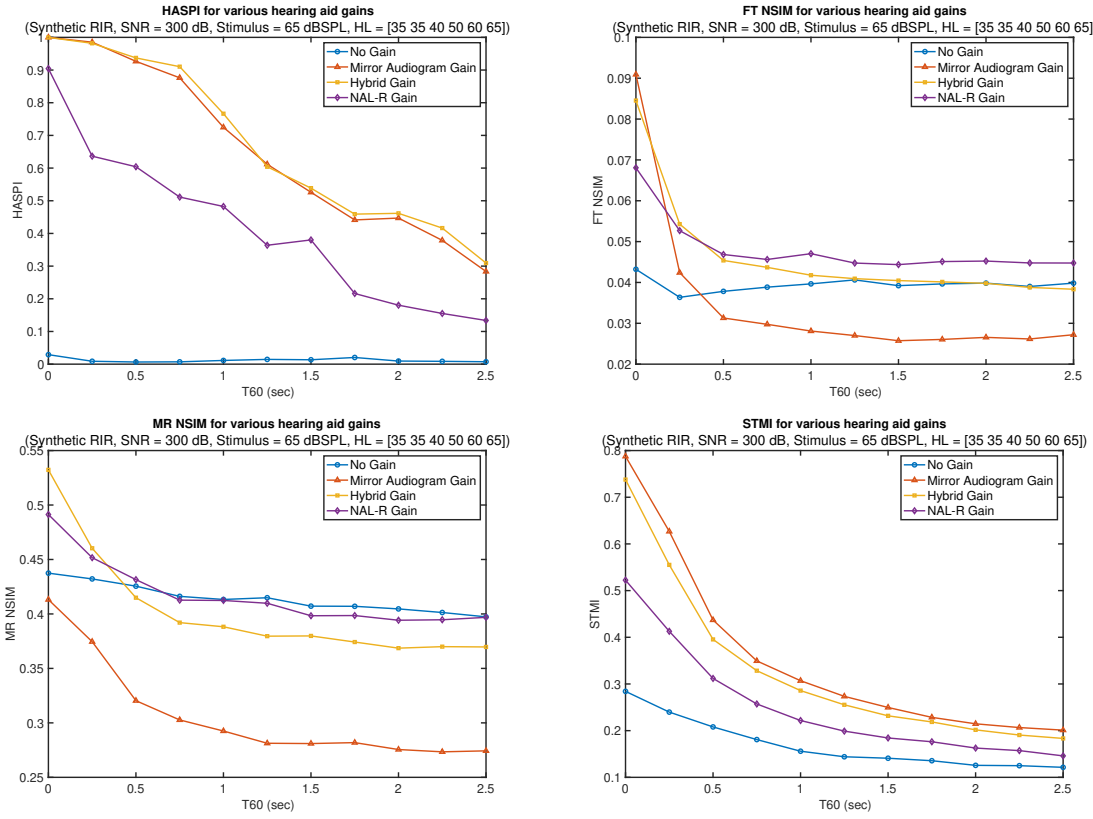


Figure 4.13: Comparison of perceptual benefit of four different linear hearing aid gains in the presence of reverberation. Moderate high frequency hearing loss used in the perceptual models (IEC 60118-15 Moderate HL, Moderately Sloping Group), and RIRs were generated synthetically

### 4.1.5 Evaluation of Monaural Speech Intelligibility Metrics In Context of Reverberation

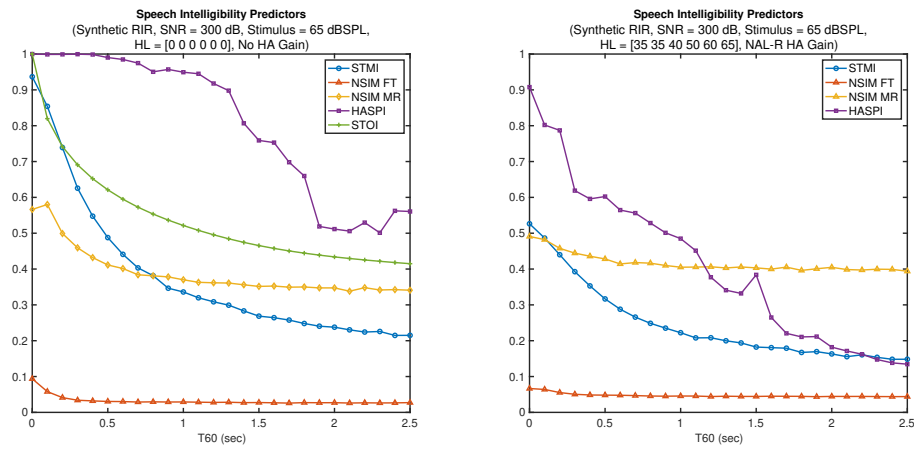


Figure 4.14: Impact of synthetic reverberation (exponentially decaying gaussian RIRs) on SI predictors with and without hearing loss. NAL-R linear hearing aid amplification included in hearing loss case for metrics that including modeling of hearing loss

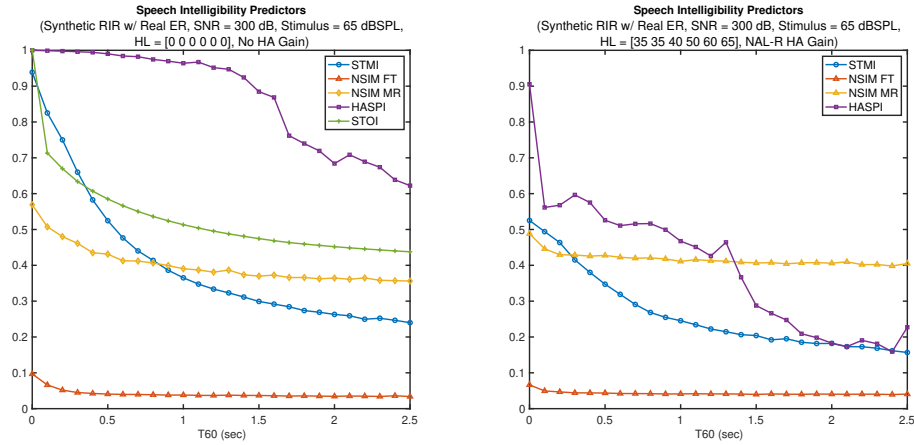


Figure 4.15: Impact of synthetic reverberation (exponentially decaying gaussian RIRs) with added real early reflections generated by truncating a real RIR (Office II RIR from the HRIR database) on SI predictors with and without hearing loss. NAL-R linear hearing aid amplification included in hearing loss case for metrics that including modeling of hearing loss

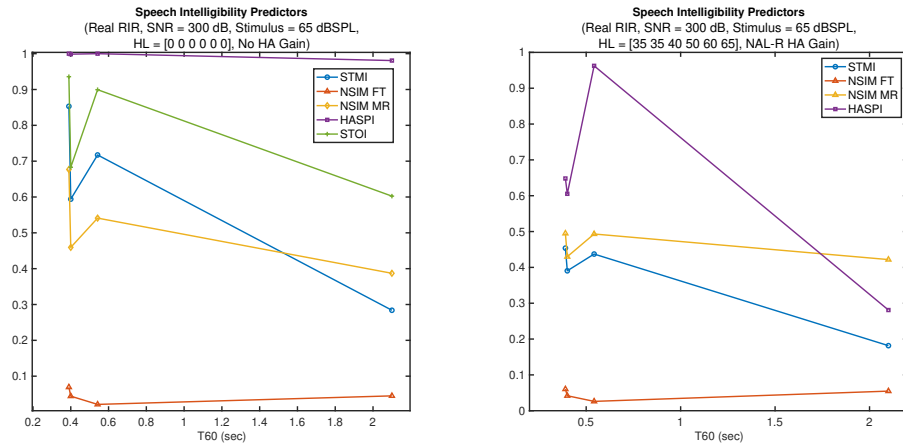


Figure 4.16: Impact of practical reverberation (several real measured RIRs) on SI predictors with and without hearing loss. NAL-R linear hearing aid amplification included in hearing loss case for metrics that including modeling of hearing loss

- Discussion of how SAL was truncated synthetically to control T60

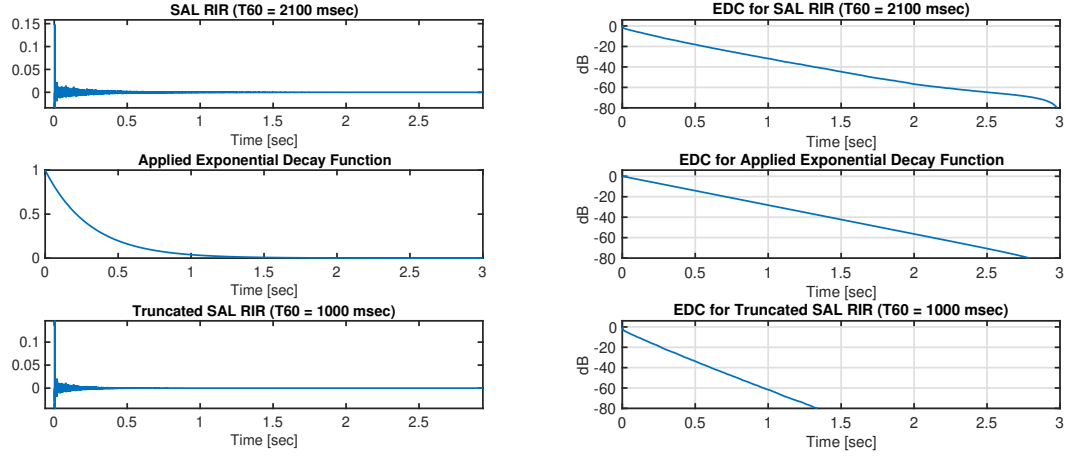


Figure 4.17: TODO: REPLOT THIS WITH SAME X-AXIS USED IN ALL PLOTS FOR EDC. Example of how SAL was truncated by applying additional exponential decay as a window to manipulate T60 synthetically

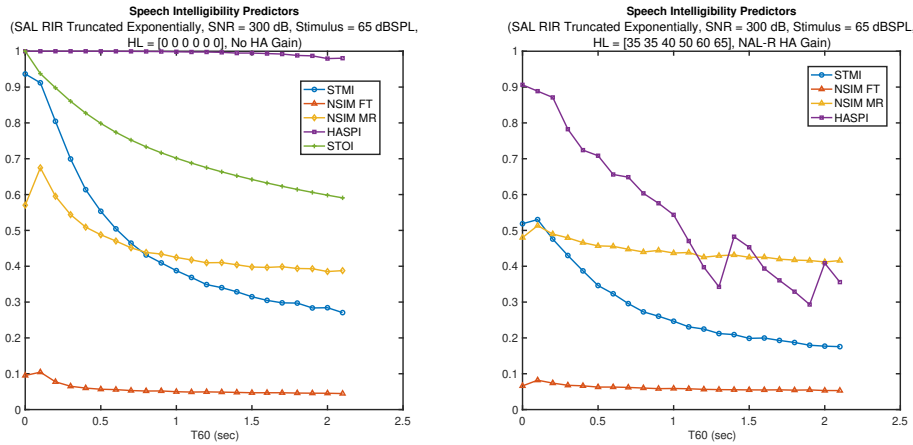


Figure 4.18: Impact of practical reverberation (SAL room from MYRiAD database exponentially truncated to control T60) on SI predictors with and without hearing loss. NAL-R linear hearing aid amplification included in hearing loss case for metrics that include modeling of hearing loss

- Discussion of how ER of SAL were reduced to make reverberation effect stronger

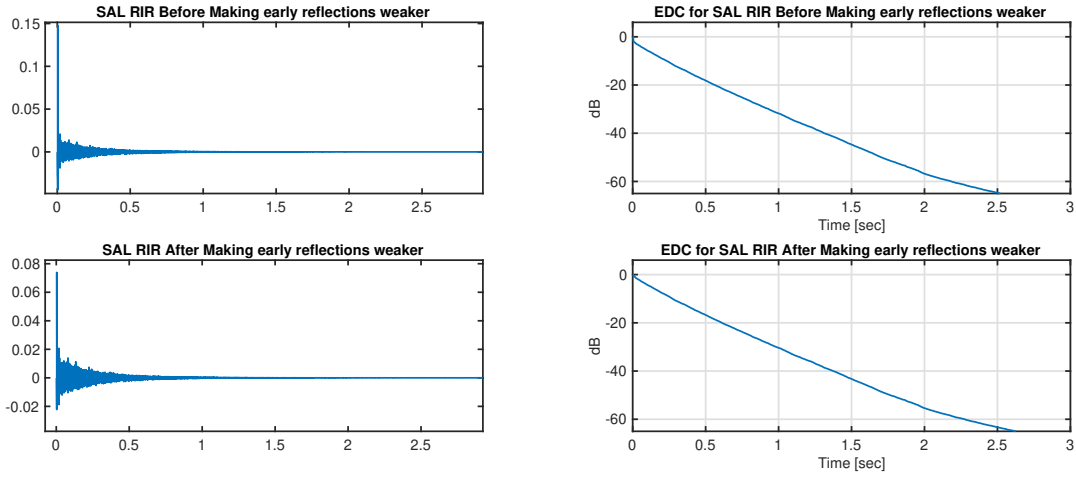


Figure 4.19: Example of how early reflections of SAL RIR were reduced in magnitude (by 6 dB) to make reverberation effect stronger

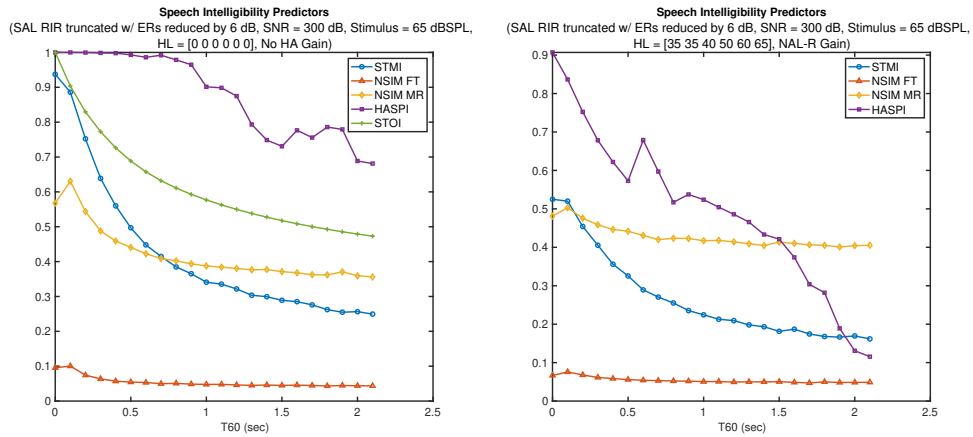


Figure 4.20: Impact of reducing early reflections of SAL RIR (i.e., Figure 4.19). SI shown before RIR processing (left) and after RIR processing (right) for comparison

- Discussion of how T60 is not a complete picture of the effects of reverb, EDT and SI together provide a more complete description. Generally speaking these are both encapsulated collectively in DRR
- Discussion of how NSIM and STMI continue to increase where HASPI plateaus

suggesting that they can be used to reflect listening effort (NSIM and STMI still have some saturation, but not as much as subjective speech intelligibility). NSIM, STMI have no explicit application of a nonlinear P/I function to map to SI, see notes about on how P/I function varies greatly depending on many factors so cant really be universal. The exact value of NSIM and STMI is not as meaningful, its moreso the how it changes with respect to control variables

- HASPI is mapped to SI, but I dont think it has an explicity P/I function – not clear need to investigate. It clearly does strongly saturate in a way the resembles subjective SI more accurately
- Discussion of how NSIM and STMI were scaled (with a constant scaling factor accross all plots) to better view the trends accross all metrics on the same plot.

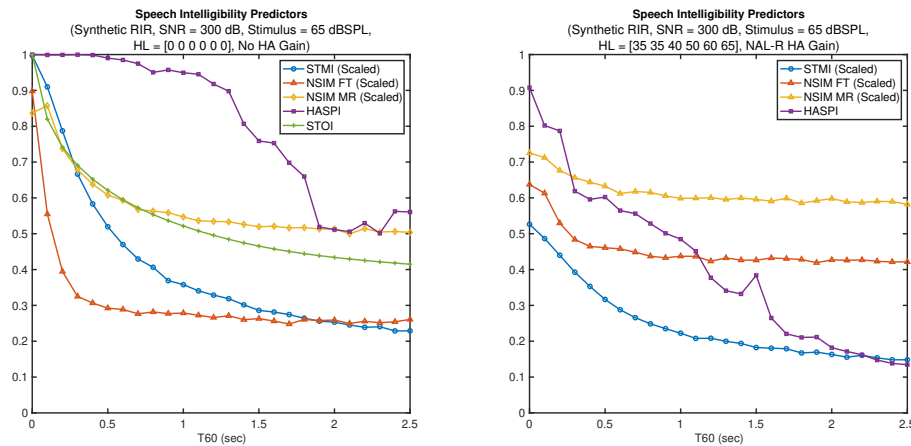


Figure 4.21: Impact of synthetic reverberation (exponentially decaying gaussian RIRs) on SI predictors with and without hearing loss. NAL-R linear hearing aid amplification included in hearing loss case for metrics that including modeling of hearing loss. Scaling applied to NSIM and STMI values to better view all metrics on the same plot.

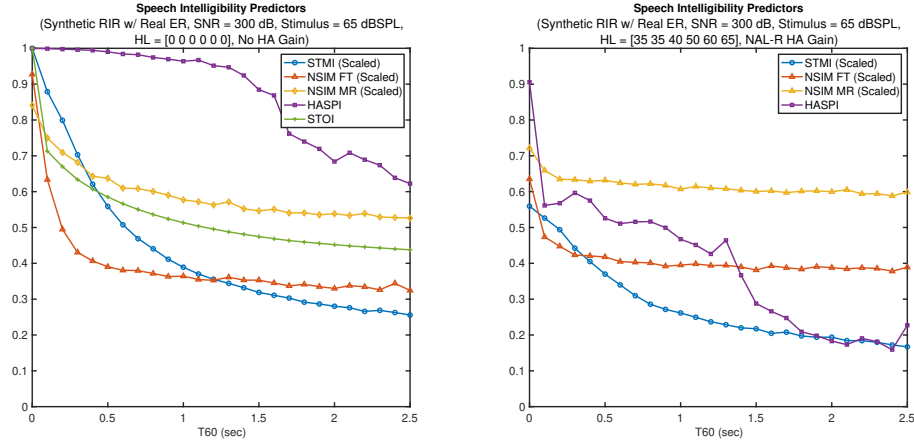


Figure 4.22: Impact of synthetic reverberation (exponentially decaying gaussian RIRs) with added real early reflections generated by truncating a real RIR (Office II RIR from the HRIR database) on SI predictors with and without hearing loss. NAL-R linear hearing aid amplification included in hearing loss case for metrics that including modeling of hearing loss. Scaling applied to NSIM and STMI values to better view all metrics on the same plot.

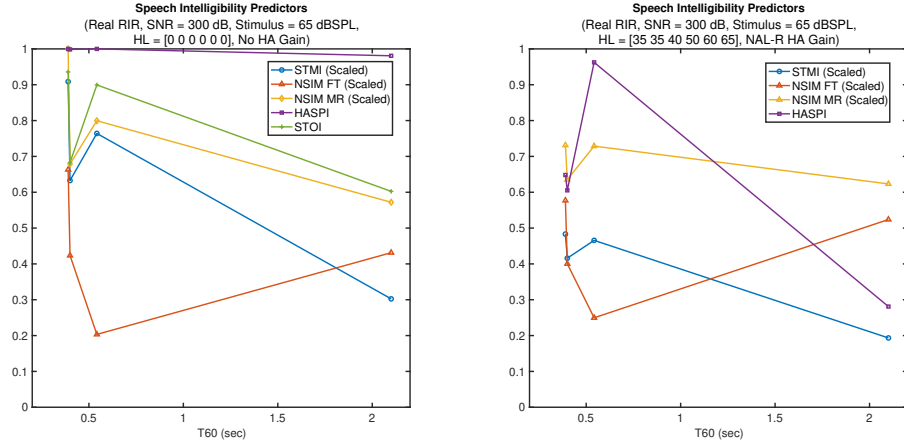


Figure 4.23: Impact of practical reverberation (several real measured RIRs) on SI predictors with and without hearing loss. NAL-R linear hearing aid amplification included in hearing loss case for metrics that including modeling of hearing loss. Scaling applied to NSIM and STMI values to better view all metrics on the same plot.

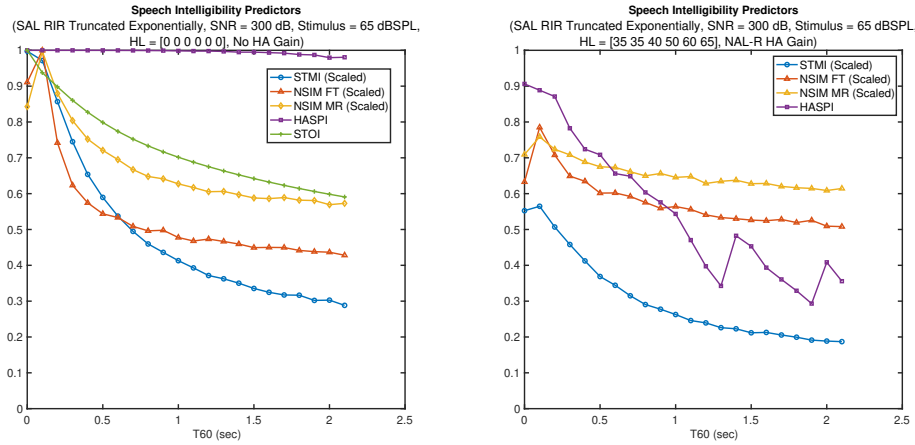


Figure 4.24: Impact of practical reverberation (SAL room from MYRiAD database exponentially truncated to control T60) on SI predictors with and without hearing loss. NAL-R linear hearing aid amplification included in hearing loss case for metrics that including modeling of hearing loss. Scaling applied to NSIM and STMI values to better view all metrics on the same plot.

## 4.2 Final Method Used

## 4.3 Delay-and-Predict Dereverberation Evaluation with Synthetic Reverberation

SI/SQ/Clarity v T60 w/ no noise

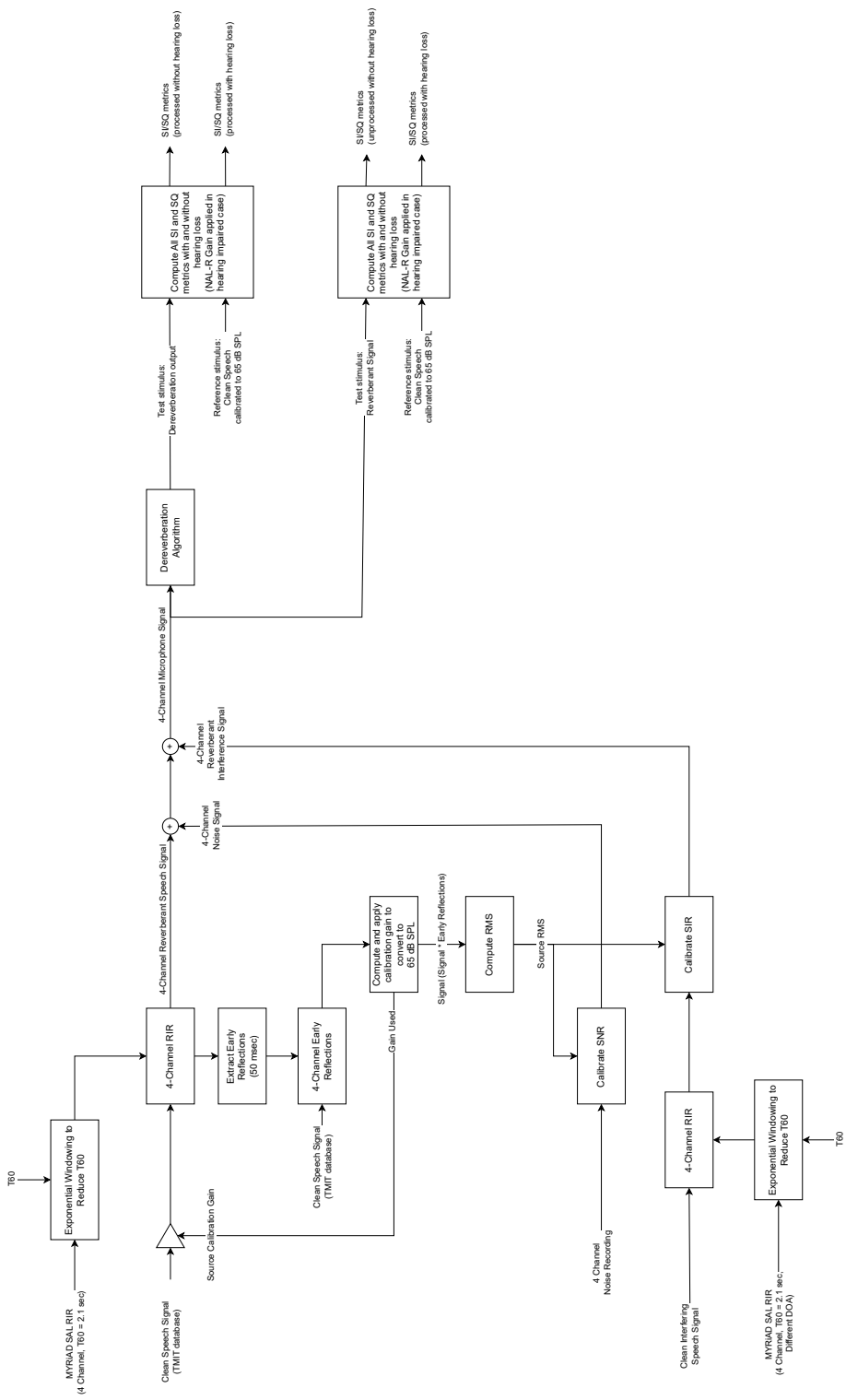


Figure 4.25: Block diagram for method used in evaluating dereverberation algorithm performance. Microphone signals include reverberant speech (MYRIAD SAL RIR windowed exponentially to control T60) with added noise signal (real multichannel noise recordings) and added reverberant interference signal. All SI and SQ predictors were computed for the unprocessed microphone signals and the dereverberation output both with and without hearing loss included in all models of speech perception.

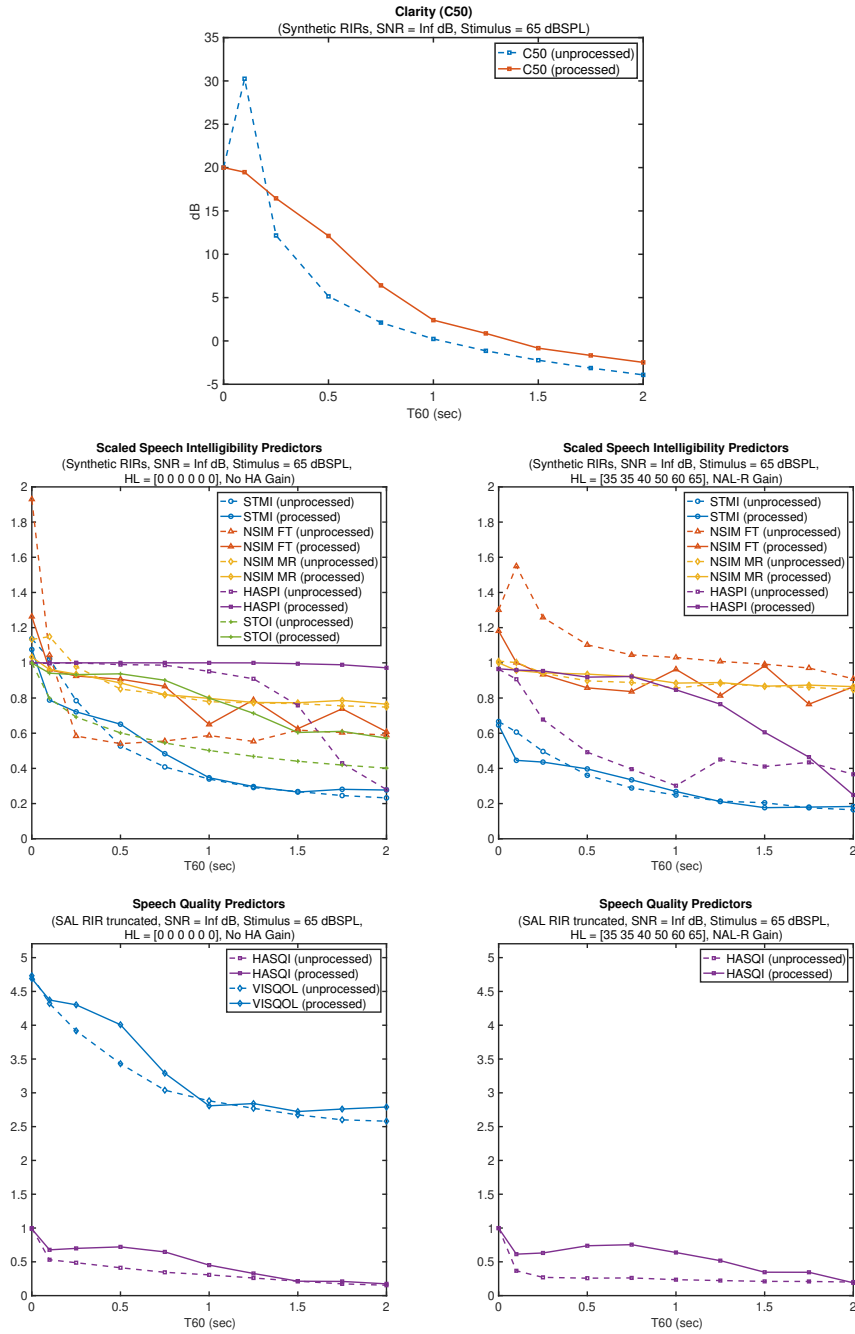


Figure 4.26: Evaluation of delay-and-predict dereverberation performance as a function of  $T_{60}$ . RIRs were synthetically generated by applying a variable decay-rate exponential window to sequences of uncorrelated Gaussian white noise.

## 4.4 Delay-and-Predict Dereverberation Evaluation with Realistic Reverberation

SI/SQ/Clarity v T60 w/ no noise

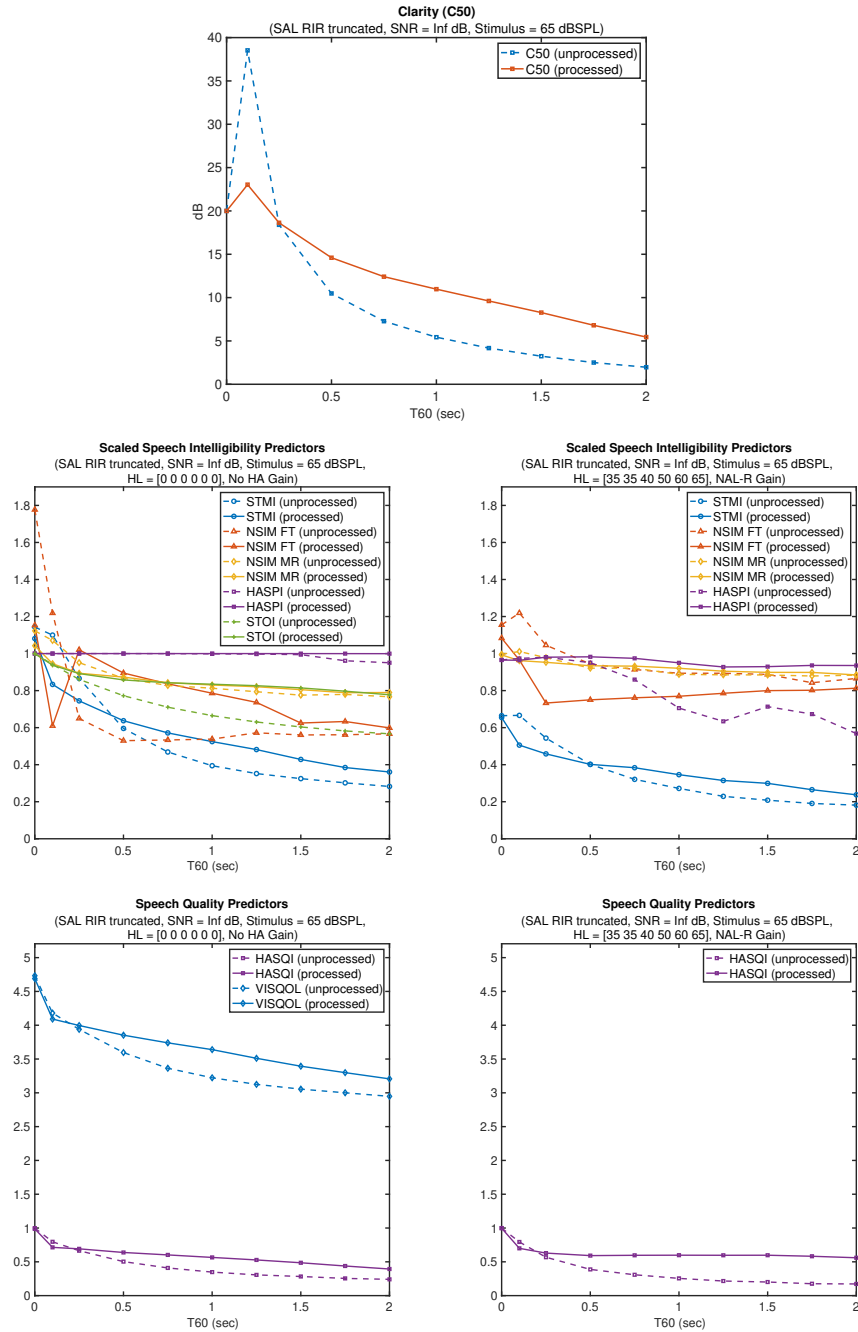


Figure 4.27: Evaluation of delay-and-predict dereverberation performance as a function of  $T_{60}$ . RIRs were generated by applying a variable decay-rate exponential window to a measured RIR (The SAL room from the MYRiAD database,  $T_{60} = 2.2$  sec) to control  $T_{60}$ .

## 4.5 Impact of Noise on Performance

NOTE: metrics computed on dereverberated speech with noise removed to neglect the impact of noise on perception (only looking at impacts of reverberation)

SI/SQ/Clarity v T60 w/ SNR = [0 or 12] dB depending on what's needed to show cost

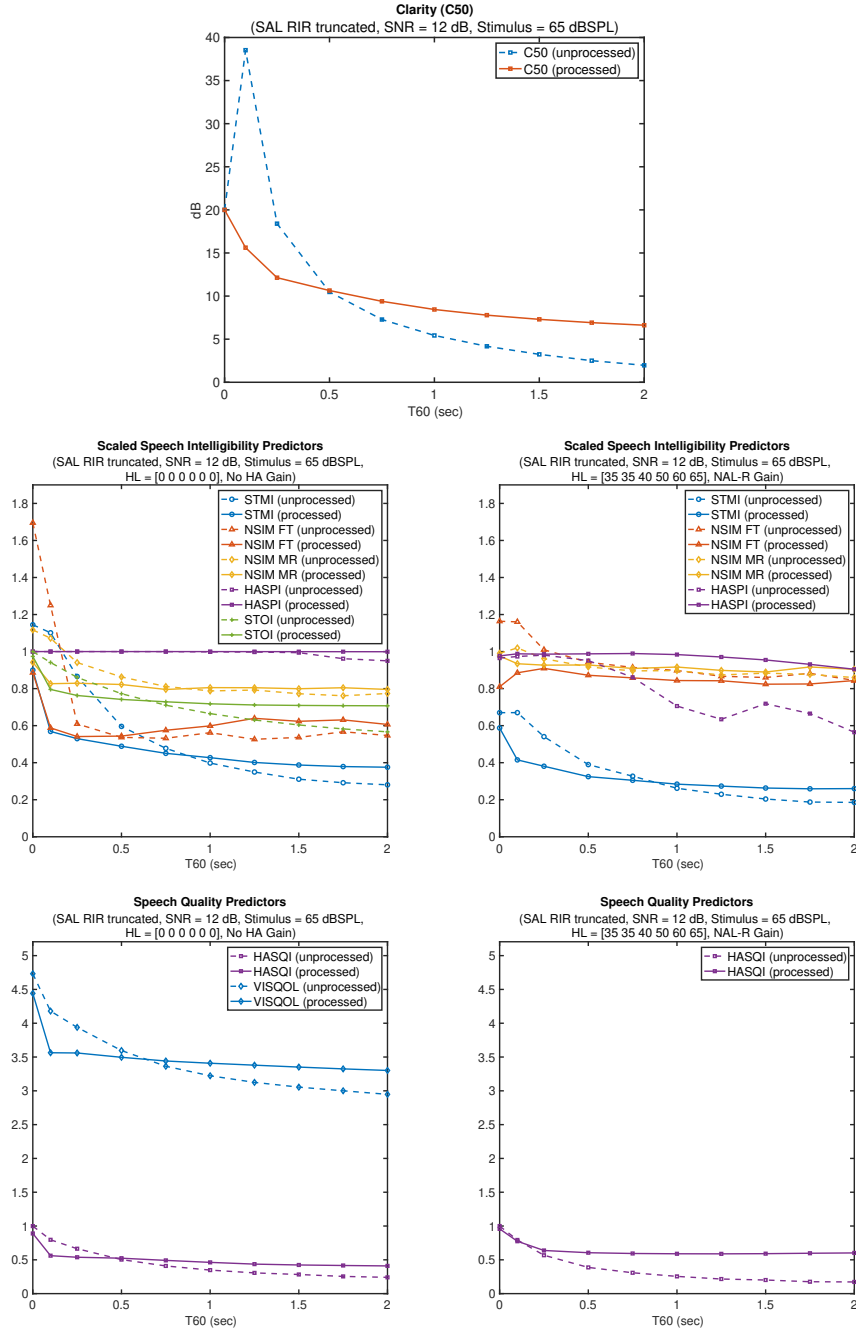


Figure 4.28: Evaluation of delay-and-predict dereverberation performance in the presence of noise as a function of T60. RIRs were generated by applying a variable decay-rate exponential window to a measured RIR (The SAL room from the MYRIAD database, T60 = 2.2 sec) to control T60. Noise was a multichannel recording of approximately stationary noise (Office ventilation noise from the HRIR database), and SNR was set to 12 dB.

**SI/SQ/Clarity v SNR w/ T60 = 1 second, stationary noise**

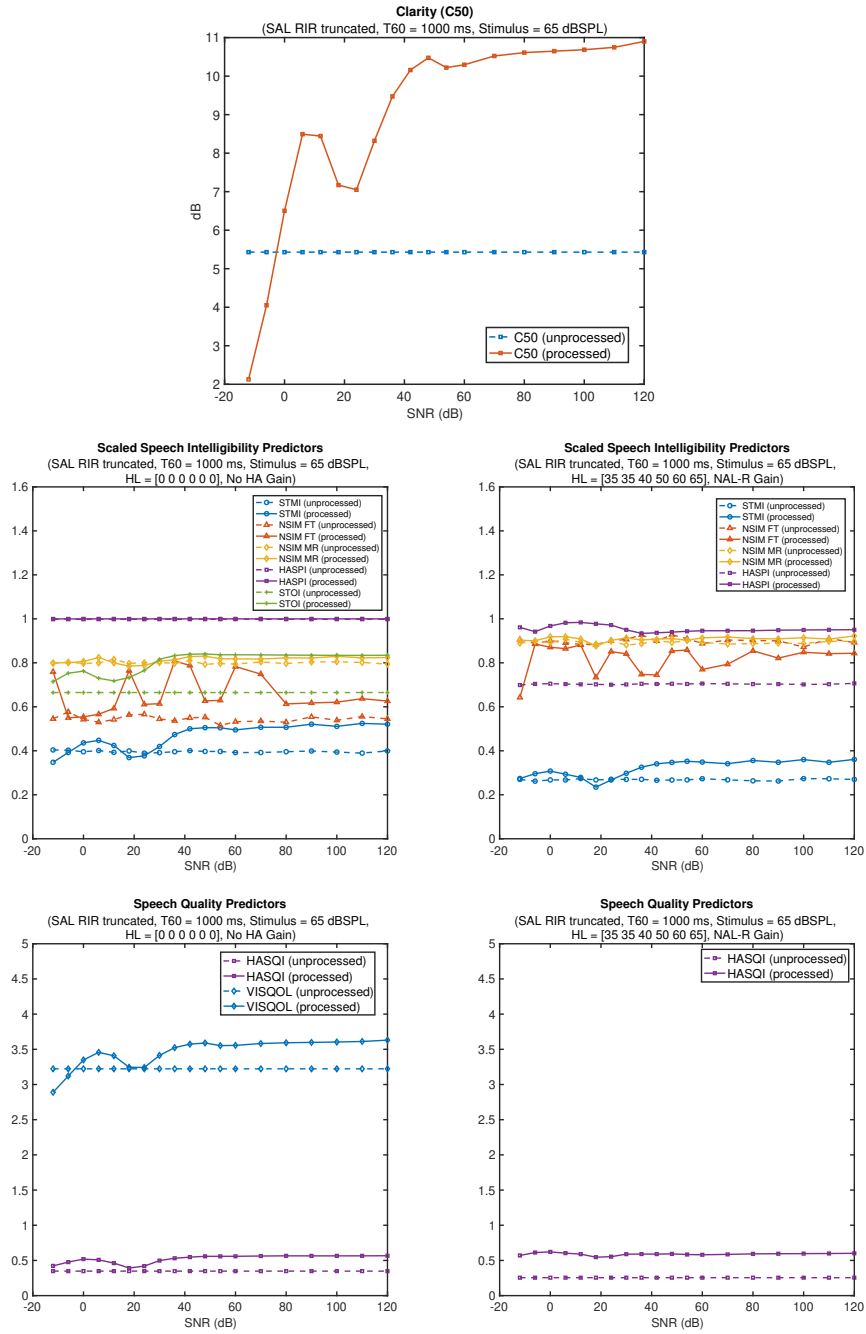


Figure 4.29: Evaluation of delay-and-predict dereverberation performance in the presence of noise as a function of SNR. RIRs were generated by applying a variable decay-rate exponential window to a measured RIR (The SAL room from the MYRIAD database,  $T60 = 2.2$  sec) to set  $T60 = 1$  second. Noise was a multichannel recording of approximately stationary noise (Office ventilation noise from the HRIR database).

**SI/SQ/Clarity v SNR w/ T60 = 1 second, Non-Stationary noise**

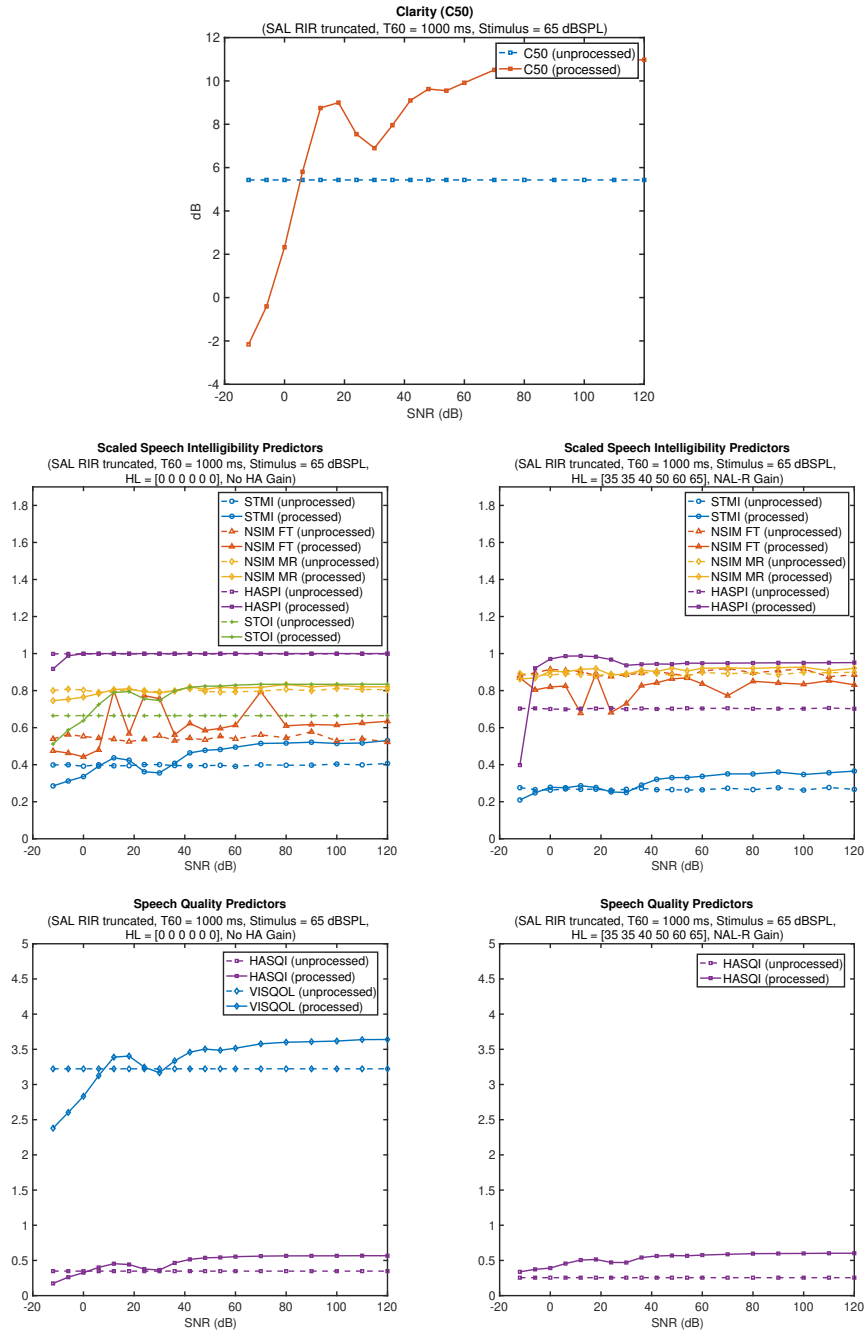


Figure 4.30: Evaluation of delay-and-predict dereverberation performance in the presence of noise as a function of SNR. RIRs were generated by applying a variable decay-rate exponential window to a measured RIR (The SAL room from the MYRIAD database,  $T_{60} = 2.2$  sec) to set  $T_{60} = 1$  second. Noise was a multichannel recording of non-stationary noise (Cafeteria babble noise from the HRIR database).

## 4.6 Impact of an Interfering Talker on Performance

NOTE: metrics computed on dereverberated speech with interfering talker removed to neglect the impact of interfering talker on perception (only looking at impacts of reverberation on primary talker)

SI/SQ/Clarity v T60 w/ SNR = [0 or 12] dB depending on what's needed to show cost

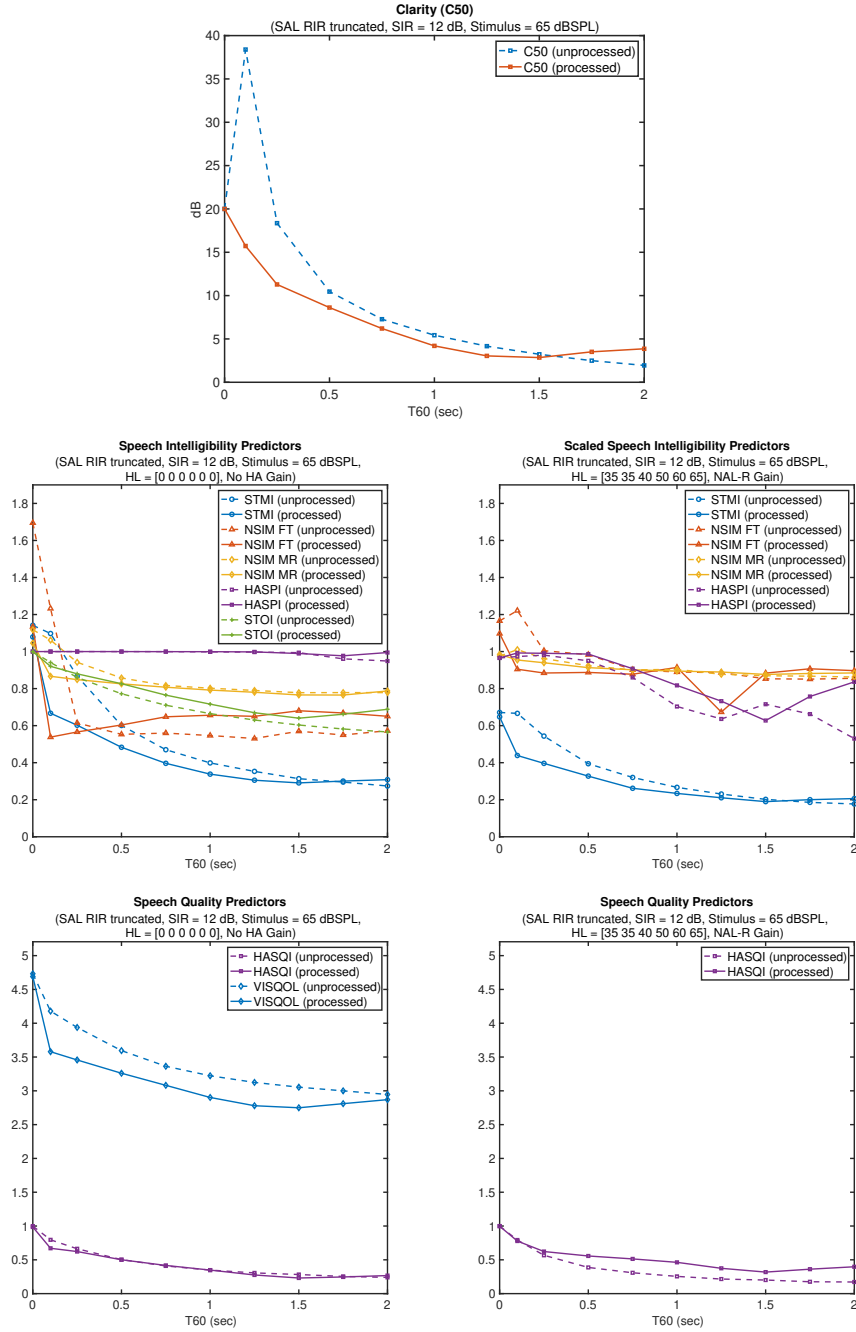


Figure 4.31: Evaluation of delay-and-predict dereverberation performance in the presence of an interfering talker, as a function of T60. RIRs were generated by applying a variable decay-rate exponential window to a measured RIR (The SAL room from the MYRiAD database,  $T60 = 2.2$  sec) to control T60. Similarly, a measured RIR from a different location in the room was exponentially windowed and used for the interfering talker. The primary-to-interfering talker ratio, i.e., signal-to-interference ratio, was set to  $SIR = 12$  dB.

# **Chapter 5**

## **Conclusions and Future Work**

# Bibliography

- Andersen, A. H., de Haan, J. M., Tan, Z.-H., and Jensen, J. (2018). Refinement and validation of the binaural short time objective intelligibility measure for spatially diverse conditions. *Speech Communication*, **102**, 1–13.
- ASA/ANSI S3.5-1997 (1997). Methods for Calculation of the Speech Intelligibility Index. Standard, American National Standards Institute, New York, NY.
- Atal, B. S. and Hanauer, S. L. (1971). Speech analysis and synthesis by linear prediction of the speech wave. *The journal of the acoustical society of America*, **50**(2B), 637–655.
- Atal, B. S. and Schroeder, M. R. (1970). Adaptive predictive coding of speech signals. *Bell System Technical Journal*, **49**(8), 1973–1986.
- Bean, C. and Craven, P. G. (1989). Loudspeaker and room correction using digital signal processing. In *Audio Engineering Society Convention 86*. Audio Engineering Society.
- Beranek, L. L. and Mellow, T. (2012). *Acoustics: sound fields and transducers*. Academic Press.

- Beutelmann, R. and Brand, T. (2006). Prediction of speech intelligibility in spatial noise and reverberation for normal-hearing and hearing-impaired listeners. *The Journal of the Acoustical Society of America*, **120**(1), 331–342.
- Brannmark, L.-J. and Ahlén, A. (2009). Spatially robust audio compensation based on simo feedforward control. *IEEE Transactions on Signal Processing*, **57**(5), 1689–1702.
- Bronkhorst, A. W. (2000). The cocktail party phenomenon: A review of research on speech intelligibility in multiple-talker conditions. *Acta acustica united with acustica*, **86**(1), 117–128.
- Bruce, I. C., Erfani, Y., and Zilany, M. S. (2018). A phenomenological model of the synapse between the inner hair cell and auditory nerve: Implications of limited neurotransmitter release sites. *Hearing research*, **360**, 40–54.
- Cherry, E. C. (1953). Some experiments on the recognition of speech, with one and with two ears. *The Journal of the acoustical society of America*, **25**(5), 975–979.
- Clarkson, P. M., Mourjopoulos, J., and Hammond, J. (1985). Spectral, phase, and transient equalization for audio systems. *Journal of the Audio Engineering Society*, **33**(3), 127–132.
- Ding, Z. and Li, Y. (2018). *Blind equalization and identification*. CRC press.
- Durlach, N. (1960). Note on the equalization and cancellation theory of binaural masking level differences. *The Journal of the Acoustical Society of America*, **32**(8), 1075–1076.

- Elliott, S. J. and Nelson, P. A. (1989). Multiple-point equalization in a room using adaptive digital filters. *Journal of the Audio Engineering Society*, **37**(11), 899–907.
- Farhang-Boroujeny, B. (2013). *Adaptive filters: theory and applications*. John wiley & sons.
- Ford, W. T. (1978). Optimum mixed delay spiking filters. *Geophysics*, **43**(1), 125–132.
- George, E. L., Goverts, S. T., Festen, J. M., and Houtgast, T. (2010). Measuring the effects of reverberation and noise on sentence intelligibility for hearing-impaired listeners.
- Godard, D. (1980). Self-recovering equalization and carrier tracking in two-dimensional data communication systems. *IEEE transactions on communications*, **28**(11), 1867–1875.
- Haas, H. (1951). Über den einfluß eines einfachechos auf die hörsamkeit von sprache. *Acta Acustica united with Acustica*, **1**(2), 49–58.
- Haneda, Y., Makino, S., and Kaneda, Y. (1997). Multiple-point equalization of room transfer functions by using common acoustical poles. *IEEE transactions on speech and audio processing*, **5**(4), 325–333.
- Hines, A. and Harte, N. (2010). Speech intelligibility from image processing. *Speech Communication*, **52**(9), 736–752.
- Hines, A. and Harte, N. (2012). Speech intelligibility prediction using a neurogram similarity index measure. *Speech Communication*, **54**(2), 306–320.

Hines, A., Skoglund, J., Kokaram, A., and Harte, N. (2013). Robustness of speech quality metrics to background noise and network degradations: Comparing visqol, pesq and polqa. In *2013 IEEE International Conference on Acoustics, Speech and Signal Processing*, pages 3697–3701. IEEE.

Hines, A., Skoglund, J., Kokaram, A. C., and Harte, N. (2015). Visqol: an objective speech quality model. *EURASIP Journal on Audio, Speech, and Music Processing*, **2015**, 1–18.

IEC 60268-16:2020 (2003). Sound system equipment—Part 16: Objective rating of speech intelligibility by speech transmission index. Standard, International Electrotechnical Commission.

ITU P.862 (2001). Perceptual evaluation of speech quality (PESQ): An objective method for end-to-end speech quality assessment of narrow-band telephone networks and speech codecs. Standard, International Telecommunication Union.

ITU P.863 (2011). Perceptual objective listening quality assessment . Standard, International Telecommunication Union.

Johansen, L. G. and Rubak, P. (1996). The excess phase in loudspeaker/room transfer functions: Can it be ignored in equalization tasks? In *Audio Engineering Society Convention 100*. Audio Engineering Society.

Karjalainen, M. and Paatero, T. (2006). Equalization of loudspeaker and room responses using kautz filters: Direct least squares design. *EURASIP Journal on Advances in Signal Processing*, **2007**, 1–13.

- Kates, J. M. and Arehart, K. H. (2022). An overview of the haspi and hasqi metrics for predicting speech intelligibility and speech quality for normal hearing, hearing loss, and hearing aids. *Hearing research*, **426**, 108608.
- Kirkeby, O., Nelson, P. A., Hamada, H., Orduna-Bustamante, F., and de Acustica, S. (1996). Fast deconvolution of multi-channel systems using regularisation. *PROCEEDINGS-INSTITUTE OF ACOUSTICS*, **18**, 2829–2832.
- Kormylo, J. and Jain, V. (1974). Two-pass recursive digital filter with zero phase shift. *IEEE Transactions on Acoustics, Speech, and Signal Processing*, **22**(5), 384–387.
- Kryter, K. D. (1962). Methods for the calculation and use of the articulation index. *The Journal of the Acoustical Society of America*, **34**(11), 1689–1697.
- Kulp, B. D. (1988). Digital equalization using fourier transform techniques. In *Audio Engineering Society Convention 85*. Audio Engineering Society.
- Kuttruff, H. (2016). *Room acoustics*. Crc Press.
- Lavandier, M., Kates, J., and Arehart, K. (2023). Towards a binaural hearing aid speech perception index (haspi): predictions of anechoic spatial release from masking for normal-hearing listeners.
- Leclere, T., Lavandier, M., and Culling, J. F. (2015). Speech intelligibility prediction in reverberation: Towards an integrated model of speech transmission, spatial unmasking, and binaural de-reverberation. *The Journal of the Acoustical Society of America*, **137**(6), 3335–3345.
- Lewicki, M. S. (2002). Efficient coding of natural sounds. *Nature Neuroscience*, **5**(4), 356–363.

- Litovsky, R. Y. (2012). Spatial release from masking. *Acoust. Today*, **8**(2), 18–25.
- Litovsky, R. Y., Colburn, H. S., Yost, W. A., and Guzman, S. J. (1999). The precedence effect. *The Journal of the Acoustical Society of America*, **106**(4), 1633–1654.
- Lucky, R. W. (1965). Automatic equalization for digital communication. *Bell System Technical Journal*, **44**(4), 547–588.
- Maamar, A., Kale, I., Krukowski, A., and Daoud, B. (2006). Partial equalization of non-minimum-phase impulse responses. *EURASIP Journal on Advances in Signal Processing*, **2006**, 1–8.
- Mei, T., Mertins, A., and Kallinger, M. (2009). Room impulse response reshaping/shortening based on least mean squares optimization with infinity norm constraint. In *2009 16th International Conference on Digital Signal Processing*, pages 1–6. IEEE.
- Miyoshi, M. and Kaneda, Y. (1986). Inverse control of room acoustics using multiple loudspeakers and/or microphones. In *ICASSP'86. IEEE International Conference on Acoustics, Speech, and Signal Processing*, volume 11, pages 917–920. IEEE.
- Miyoshi, M. and Kaneda, Y. (1988). Inverse filtering of room acoustics. *IEEE Transactions on acoustics, speech, and signal processing*, **36**(2), 145–152.
- Mourjopoulos, J. (1985). On the variation and invertibility of room impulse response functions. *Journal of Sound and Vibration*, **102**(2), 217–228.
- Mourjopoulos, J. and Paraskevas, M. (1991). Pole and zero modeling of room transfer functions. *Journal of Sound and Vibration*, **146**(2), 281–302.

- Mourjopoulos, J., Clarkson, P., and Hammond, J. (1982). A comparative study of least-squares and homomorphic techniques for the inversion of mixed phase signals. In *ICASSP'82. IEEE International Conference on Acoustics, Speech, and Signal Processing*, volume 7, pages 1858–1861. IEEE.
- Nakajima, H., Miyoshi, M., and Tohyama, M. (1997). Sound field control by indefinite mint filters. *IEICE transactions on fundamentals of electronics, communications and computer sciences*, **80**(5), 821–824.
- Neely, S. T. and Allen, J. B. (1979). Invertibility of a room impulse response. *The Journal of the Acoustical Society of America*, **66**(1), 165–169.
- Ohlenforst, B., Zekveld, A. A., Jansma, E. P., Wang, Y., Naylor, G., Lorens, A., Lunner, T., and Kramer, S. E. (2017). Effects of hearing impairment and hearing aid amplification on listening effort: A systematic review. *Ear and hearing*, **38**(3), 267–281.
- Omura, M., Yada, M., Saruwatari, H., Kajita, S., Takeda, K., and Itakura, F. (1999). Compensating of room acoustic transfer functions affected by change of room temperature. In *1999 IEEE International Conference on Acoustics, Speech, and Signal Processing. Proceedings. ICASSP99 (Cat. No. 99CH36258)*, volume 2, pages 941–944. IEEE.
- Pickles, J. O. (2013). *An introduction to the physiology of hearing*. Brill, Leiden ; Boston.
- Quatieri, T. F. (2002). *Discrete-time speech signal processing: principles and practice*. Pearson Education India.

- Radlovic, B. D. and Kennedy, R. A. (2000). Nonminimum-phase equalization and its subjective importance in room acoustics. *IEEE Transactions on Speech and Audio Processing*, **8**(6), 728–737.
- Reinhart, P. N. and Souza, P. E. (2018). Listener factors associated with individual susceptibility to reverberation. *Journal of the American Academy of Audiology*, **29**(01), 073–082.
- Rennies, J., Röttges, S., Huber, R., Hauth, C. F., and Brand, T. (2022a). A joint framework for blind prediction of binaural speech intelligibility and perceived listening effort. *Hearing Research*, **426**, 108598.
- Rennies, J., Warzybok, A., Kollmeier, B., and Brand, T. (2022b). Spatio-temporal integration of speech reflections in hearing-impaired listeners. *Trends in Hearing*, **26**, 23312165221143901.
- Risoud, M., Hanson, J.-N., Gauvrit, F., Renard, C., Lemesre, P.-E., Bonne, N.-X., and Vincent, C. (2018). Sound source localization. *European annals of otorhinolaryngology, head and neck diseases*, **135**(4), 259–264.
- Roberts, R. A., Koehnke, J., and Besing, J. (2003). Effects of noise and reverberation on the precedence effect in listeners with normal hearing and impaired hearing.
- Sabine, W. C. (1922). *Collected papers on acoustics*. Harvard university press.
- Saito, S., Itakura, F., *et al.* (1967). Theoretical consideration of the statistical optimum recognition of the spectral density of speech. *J. Acoust. Soc. Japan*.
- Sato, Y. (1975). A method of self-recovering equalization for multilevel amplitude-modulation systems. *IEEE Transactions on communications*, **23**(6), 679–682.

- Schepker, H., Haeder, K., Rennies, J., and Holube, I. (2016). Perceived listening effort and speech intelligibility in reverberation and noise for hearing-impaired listeners. *International journal of audiology*, **55**(12), 738–747.
- Schroeder, M. R. and Kuttruff, K. (1962). On frequency response curves in rooms. comparison of experimental, theoretical, and monte carlo results for the average frequency spacing between maxima. *The Journal of the Acoustical Society of America*, **34**(1), 76–80.
- Shapiro, S. B., Noij, K. S., Naples, J. G., and Samy, R. N. (2021). Hearing loss and tinnitus. *Medical Clinics*, **105**(5), 799–811.
- Shields, C., Sladen, M., Bruce, I. A., Kluk, K., and Nichani, J. (2023). Exploring the correlations between measures of listening effort in adults and children: a systematic review with narrative synthesis. *Trends in Hearing*, **27**, 23312165221137116.
- Srinivasan, N. K., Stansell, M., and Gallun, F. J. (2017). The role of early and late reflections on spatial release from masking: Effects of age and hearing loss. *The Journal of the Acoustical Society of America*, **141**(3), EL185–EL191.
- Taal, C. H., Hendriks, R. C., Heusdens, R., and Jensen, J. (2010). A short-time objective intelligibility measure for time-frequency weighted noisy speech. In *2010 IEEE international conference on acoustics, speech and signal processing*, pages 4214–4217. IEEE.
- Toole, F. E. and Olive, S. E. (1988). The modification of timbre by resonances: Perception and measurement. *Journal of the Audio Engineering Society*, **36**(3), 122–142.

- Torcoli, M., Kastner, T., and Herre, J. (2021). Objective measures of perceptual audio quality reviewed: An evaluation of their application domain dependence. *IEEE/ACM Transactions on Audio, Speech, and Language Processing*, **29**, 1530–1541.
- Treitel, S. and Robinson, E. (1966). The design of high-resolution digital filters. *IEEE Transactions on Geoscience Electronics*, **4**(1), 25–38.
- Tsironis, A., Vlahou, E., Kontou, P., Bagos, P., and Kopčo, N. (2024). Adaptation to reverberation for speech perception: A systematic review. *Trends in Hearing*, **28**, 23312165241273399.
- van Wijngaarden, S. J. and Drullman, R. (2008). Binaural intelligibility prediction based on the speech transmission index. *The Journal of the Acoustical Society of America*, **123**(6), 4514–4523.
- Wallach, H., Newman, E. B., and Rosenzweig, M. R. (1949). A precedence effect in sound localization. *The Journal of the Acoustical Society of America*, **21**(4 Supplement), 468–468.
- Wiener, N. (1949). *Extrapolation, interpolation, and smoothing of stationary time series: with engineering applications*. The MIT press.
- Winn, M. B. and Teece, K. H. (2021). Listening effort is not the same as speech intelligibility score. *Trends in Hearing*, **25**, 23312165211027688.
- Wirtzfeld, M. R., Ibrahim, R. A., and Bruce, I. C. (2017). Predictions of speech chimaera intelligibility using auditory nerve mean-rate and spike-timing neural cues. *Journal of the Association for Research in Otolaryngology*, **18**, 687–710.

Xia, J., Xu, B., Pentony, S., Xu, J., and Swaminathan, J. (2018). Effects of reverberation and noise on speech intelligibility in normal-hearing and aided hearing-impaired listeners. *The Journal of the Acoustical Society of America*, **143**(3), 1523–1533.

Zilany, M. S. and Bruce, I. C. (2007). Predictions of speech intelligibility with a model of the normal and impaired auditory-periphery. In *2007 3rd International IEEE/EMBS Conference on Neural Engineering*, pages 481–485. IEEE.

Zilany, M. S., Bruce, I. C., and Carney, L. H. (2014). Updated parameters and expanded simulation options for a model of the auditory periphery. *The Journal of the Acoustical Society of America*, **135**(1), 283–286.